ANALYSIS OF CRACKS IN TRANSVERSELY ISOTROPIC, LINEAR ELASTIC HALF-SPACE BY WEAKLY SINGULAR BOUNDARY INTEGRAL EQUATION METHOD

Mr. Tien Ngoc Pham

A Dissertation Submitted in Partial Fulfillment of the Requirements
for the Degree of Doctor of Philosophy Program in Civil Engineering
Department of Civil Engineering
Faculty of Engineering
Chulalongkorn University
Academic Year 2015

การวิเคราะห์รอยร้าวในตัวกลางกึ่งปริภูมิยืดหยุ่นเชิงเส้นที่มีคุณสมบัติเหมือนกันตามขวาง โดยระเบียบวิธีสมการปริพันธ์ขอบเขตเอกฐานต่ำ

นายเทียน งอค พัม

วิทยานิพนธ์นี้เป็นส่วนหนึ่งของการศึกษาตามหลักสูตรปริญญาวิศวกรรมศาสตรดุษฎีบัณฑิต
สาขาวิชาวิศวกรรมโยธา ภาควิชาวิศวกรรมโยธา
คณะวิศวกรรมศาสตร์ จุฬาลงกรณ์มหาวิทยาลัย
ปีการศึกษา 2558

Thesis Title	ANALYSIS OF CRACKS IN TRANSVERSELY ISOTROPIC, LINEAR ELASTIC HALF-SPACE BY WEAKLY SINGULAR BOUNDARY INTEGRAL EQUATION METHOD
By	Mr. Tien Ngoc Pham
Field of Study	Civil Engineering
Thesis Advisor	Associate Professor Jaroon Rungamornrat, Ph.D.
Thesis Co-Advisor	Assistant Professor Withit Pansuk, Ph.D.
	Associate Professor Yasuhiko Sato, D.Eng.

Accepted by the Faculty of Engineering, Chulalongkorn University in Partial Fulfillment of the Requirements for the Doctoral Degree

.....Dean of the Faculty of Engineering
(Professor Bundhit Eua-arporn, Ph.D.)

THESIS COMMITTEE

.....Chairman
(Professor Teerapong Senjuntichai, Ph.D.)
.....Thesis Advisor
(Associate Professor Jaroon Rungamornrat, Ph.D.)
.....Thesis Co-Advisor
(Assistant Professor Withit Pansuk, Ph.D.)
.....Thesis Co-Advisor
(Associate Professor Yasuhiko Sato, D.Eng.)
.....Examiner
(Associate Professor Akhrawat Lenwari, Ph.D.)
.....Examiner
(Assistant Professor Watanachai Smittakorn, Ph.D.)
.....External Examiner
(Professor Pruettha Nanakorn, D.Eng.)

เทียน งอค พัม : การวิเคราะห์รอยร้าวในตัวกลางกึ่งปริภูมิยืดหยุ่นเชิงเส้นที่มีคุณสมบัติเหมือนกันตามขวาง โดยระเบียบวิธีสมการปริพันธ์ขอบเขตเอกฐานต่ำ (ANALYSIS OF CRACKS IN TRANSVERSELY ISOTROPIC, LINEAR ELASTIC HALF-SPACE BY WEAKLY SINGULAR BOUNDARY INTEGRAL EQUATION METHOD) อ.ที่ปรึกษาวิทยานิพนธ์หลัก: รศ. ดร. จรูญ รุ่งอมรรัตน์, อ.ที่ปรึกษาวิทยานิพนธ์ร่วม: ผศ. ดร. วิทิต ปานสุข, ยาสุฮิโกะ ซาโต้, 111 หน้า.

วิทยานิพนธ์นี้นำเสนอระเบียบวิธีเชิงตัวเลขที่มีประสิทธิภาพสำหรับวิเคราะห์หาค่าตัวประกอบความเข้มของความเค้นและองค์ประกอบหน่วยแรงทีสำหรับรอยร้าวรูปร่างใดๆในตัวกลางกึ่งปริภูมิยืดหยุ่นเชิงเส้นเนื้อเดียวภายใต้เงื่อนไขขอบเขตบนผิวอิสระแบบต่างๆกัน สมการกำกับหลักถูกพัฒนาให้อยู่ในรูปแบบของสมการเชิงปริพันธ์พื้นผิวเชิงเอกฐานต่ำที่เกี่ยวข้องกับผลต่างและผลรวมของการขจัดบนผิวรอยร้าว ระเบียบวิธีการลดความเป็นเอกฐานของสมการปริพันธ์ซึ่งอ้างอิงจากการหาปริพันธ์แบบแยกส่วนและการแยกส่วนของเคอร์เนลที่มีความเป็นเอกฐานถูกนำมาใช้ในการพัฒนาสมการปริพันธ์พื้นผิวที่เกี่ยวข้องเฉพาะเคอร์เนลที่มีความเป็นเอกฐานต่ำ และต้องการเพียงความต่อเนื่องของข้อมูลที่ผิวของรอยร้าวเท่านั้น นอกเหนือจากผลกระทบโดยตรงจากความเป็นเอกฐานต่ำ สมการกำกับเชิงปริพันธ์ยังมีจุดเด่นอื่นๆ อาทิเช่น ไม่จำเป็นต้องพิจารณาพื้นผิวอิสระในขั้นตอนการประมาณผลเฉลย และสามารถประยุกต์ใช้กับกรณีของวัสดุที่มีคุณสมบัติขึ้นอยู่กับทิศทาง รอยร้าวที่ไม่ใช่รอยร้าวแบบระนาบ และแรงกระทำบนผิวรอยร้าวแบบทั่วไป ระเบียบวิธีบาวดารีเอลิเมนต์แบบสมมาตรกาเลอคินเชิงเอกฐานต่ำพร้อมด้วยการประมาณผลเฉลยบริเวณใกล้ขอบรอยร้าวแบบพิเศษถูกนำมาใช้ในการแก้สมการเชิงปริพันธ์ของแรงที่ผิวรอยร้าว เพื่อหาผลต่างของการขจัดบนผิวรอยร้าว ส่วนผลรวมของการขจัดบนผิวรอยร้าวสามารถหาได้โดยการแก้สมการปริพันธ์การขจัดด้วยระเบียบวิธีมาตราฐานของการ์เลอคิน ตัวประกอบความเข้มของความเค้นและองค์ประกอบหน่วยแรงทีสามารถคำนวณได้โดยตรงจากข้อมูลผลต่างและผลรวมของการขจัดบนผิวรอยร้าวบริเวณใกล้ขอบรอยร้าว ผลเฉลยเชิงตัวเลขที่ได้สำหรับกรณีต่างๆแสดงให้เห็นถึง ความถูกต้อง การลู่เข้าของผลเฉลย และความสามารถของระเบียบวิธีที่นำเสนอ

ภาควิชา	วิศวกรรมโยธา	ลายมือชื่อนิสิต .....
สาขาวิชา	วิศวกรรมโยธา	ลายมือชื่อ อ.ที่ปรึกษาหลัก .....
ปีการศึกษา	2558	ลายมือชื่อ อ.ที่ปรึกษาร่วม .....
		ลายมือชื่อ อ.ที่ปรึกษาร่วม .....

5571441621 : MAJOR CIVIL ENGINEERING
KEYWORDS: ELASTIC HALF-SPACE, SGBEM, STRESS INTENSITY FACTORS, T-STRESS, WEAKLY SINGULAR

TIEN NGOC PHAM: ANALYSIS OF CRACKS IN TRANSVERSELY ISOTROPIC, LINEAR ELASTIC HALF-SPACE BY WEAKLY SINGULAR BOUNDARY INTEGRAL EQUATION METHOD. ADVISOR: ASSOC. PROF. JAROON RUNGAMORNRAT, Ph.D., CO-ADVISOR: ASST. PROF. WITHIT PANSUK, Ph.D., ASSOC. PROF. YASUHIKO SATO, D.Eng., 111 pp.

This dissertation presents an efficient numerical technique for the analysis of stress intensity factors and T-stress components for arbitrary-shaped cracks in a homogeneous, linear elastic half-space under various conditions on the free surface. The key governing equations are established in a form of weakly singular boundary integral equations involving both unknown relative and sum of the crack-face displacements. A systematic regularization technique based on the integration by parts and special decompositions of singular kernels is adopted to regularize all involved strongly singular and hyper-singular integrals to those containing only weakly singular kernels and requiring only continuous crack-face data for their validity. Besides the direct consequence of the weakly singular nature, the governing integral equations also possess several positive features such as no requirement of free-surface discretization and the capability to treat material anisotropy, non-planar crack geometry and general crack-face loading conditions. In numerical implementations, a weakly singular, symmetric Galerkin boundary element method along with the special near-front approximation is employed to solve the traction integral equation for the relative crack-face displacement. The sum of the crack-face displacement is then obtained by solving the displacement integral equation via standard Galerkin method. The stress intensity factors and the T-stress components along the crack are extracted directly from the near-front relative and sum of the crack-face displacement data. Obtained numerical results for various scenarios clearly demonstrate the accuracy, convergence and capability of the proposed technique.

Department:	Civil Engineering	Student's Signature	.....
Field of Study:	Civil Engineering	Advisor's Signature	.....
Academic Year:	2015	Co-Advisor's Signature	.....
		Co-Advisor's Signature	.....

ACKNOWLEDGEMENTS

I would like to express the most sincere gratitude to my advisor, Associate Professor Dr. Jaroon Rungamornrat and co-advisor, Assistant Professor Dr. Withit Pansuk for their valuable instruction and encouragement on my research. I also wish to express my deepest appreciation to my co-advisor, Associate Professor Dr. Yasuhiko Sato at Hokkaido University, Japan, for his kindness and warm support during my stay in Hokkaido, Japan. Without these people willing to cooperate, I could not have accomplished my dissertation in fulfillment.

Besides my advisor and co-advisors, I would like to thank the rest of my dissertation committee, namely, Professor Dr. Teerapong Senjuntichai, Professor Dr. Pruettha Nanakorn, Associate Professor Dr. Akhrawat Lenwari, and Assistant Professor Dr. Watanachai Smittakorn for their encouragement and insightful comments on my work.

I would also like to offer my sincere gratitude to AUN/SEED-Net Project for providing financial support during the time of my study. In addition, I would like to extend my thanks to the International School of Engineering and Civil Engineering Department at Chulalongkorn University for their supporting programs. Further, I express my gratitude to Chulalongkorn University for offering education standards of friendly environment and quality.

I would also like to extend my thanks to all my lab mates and friends for their friendship and help in the last three years.

My special thanks go to my parents and parents-in-law for their continuous encouragement, support, and sharing difficulties in my life. Finally, I wish to express my appreciation to my wife, Loan Minh Tran, for her love, encouragement and sacrifices.

CONTENTS

Page

Page

LIST OF ABBREVIATIONS

a	crack radius or semi-major axis;
$\boldsymbol{a},\boldsymbol{b}$	orthonormal vectors;
b	semi-minor axis;
BC	boundary condition;
BIEM	boundary integral equation method;
$\boldsymbol{B},\bar{\boldsymbol{B}},\boldsymbol{C}$	coefficient matrices;
$\mathcal{B},\mathcal{C},\mathcal{G},\mathcal{H},\mathcal{U}$	linear integral operators;
$c(\boldsymbol{y})$	modified coefficient;
$C_{mj}^{tk},\ \hat{C}_{mj}^{tk}$	weakly singular kernel of order $\mathcal{O}(1/r)$;
d	distance between the center of a crack and the x_3 - axis
$D_t(.)$	surface operator;
$\boldsymbol{D},\boldsymbol{G},\bar{\boldsymbol{G}}$	coefficient matrices;
E_{ijkl}	linearly elastic constants;
$\{\boldsymbol{e}_1, \boldsymbol{e}_2, \boldsymbol{e}_3\}$	orthonormal base vector associated with Cartesian coordinate system;
FEM	finite element method;
FDM	finite different method;
$G_{mj}^{p},\ \hat{G}_{mj}^{p}$	weakly singular kernel of order $\mathcal{O}(1/r)$;
h	distance from the half-space surface to crack surface, or to the center of a crack, or to the top of a spherical cap crack;
H_{mj}^{p}	singular kernel of order $\mathcal{O}(1/r^2)$;
$\boldsymbol{H},\bar{\boldsymbol{H}}$	coefficient matrices;
i, j	Latin subscripts denoting field quantities associated with the bulk take the values 1, 2, 3;
K_I, K_{II}, K_{III}	stress intensity factors associated with crack opening modes I, II, III, respectively;
$M_{mj},\ N_{mj}, P_{mj}$	Papkovich-Neuber potentials;
N	number of nodal points;

$\boldsymbol{n}^+$, $\boldsymbol{n}^-$	unit normal vectors of positive and negative crack surfaces, respectively;
(r,θ)	polar coordinates;
SGBEM	symmetric Galerkin boundary element method;
S_c^+	positive crack surface;
S_c^-	negative crack surface;
S_{ij}^p	stress fundamental solution;
T_{11}, T_{13}, T_{33}	unknown T-stress components;
$\boldsymbol{t}^{0+}$, $\boldsymbol{t}^{0-}$	tractions applied on the positive and negative crack surfaces, respectively;
$\tilde{\boldsymbol{t}}$	test function;
U_j^p	displacement fundamental solution;
$\boldsymbol{u}$	displacement field;
$\boldsymbol{x}$	source point;
$\bar{\boldsymbol{x}}$	image point of $\boldsymbol{x}$;
$\boldsymbol{z}$	unit vector;
α, β	Greek index takes values 1 and 2;
δ_{ij}	standard Kronecker-delta symbol;
$\bar{\delta}_{ij}$	constant tensor;
$\Delta\boldsymbol{T}$, $\Sigma\boldsymbol{T}$	prescribed jump in nodal tractions, prescribed sum of nodal tractions, respectively;
$\Delta\tilde{\boldsymbol{u}}$	test function;
$\Delta\boldsymbol{U}$, $\Sigma\boldsymbol{U}$	unknown nodal quantity;
ε_{ijk}	standard alternating symbol;
$\boldsymbol{\varepsilon}$	strain field;
Λ_α	constants;
μ, λ	Lame's constants;
ν	Poisson's ratio;
$\boldsymbol{\xi}$	field point;
$\bar{\boldsymbol{\xi}}$	image point of $\boldsymbol{\xi}$;
$\boldsymbol{\sigma}$	stress field;

Σ_{ij}^{lk}	hyper-singular kernel;
φ_i, ψ_i	standard nodal basis functions;
ϕ_i	selected nodal basis function;
Ω	half-space's domain.

LIST OF FIGURES

LIST OF TABLES

CHAPTER 1
INTRODUCTION

For the past several decades, designing demands of multi-functional, high performance materials in various disciplines such as aircraft and aerospace industries, nautical structures, and engineering applications have increased remarkably (see examples in Figure 1.1). In general, this requirement is to ensure that all involved components must be made from stiffer, lighter and stronger materials. At the same time, use of such complex materials generally poses nontrivial challenges in the analysis and design procedure to ascertain the integrity and safety throughout the lifespan of those components. The major cause of partial damage and ultimate failure of components is from various sources such as uncertainties in the loading, pre-existing flaws and defects in materials, and load-induced cracks occurring during applications. As the direct consequence, the investigation of flaws and defects in engineering components, devices and parts is of primary interest of many researchers because information gained from those studies can be potentially used to assess their failure mechanism, usage lifespan and performance. Mathematical modeling and analysis is one of the most commonly used tools to achieve those essential tasks.

There are many situations encountered in practices where damages and flaws are induced in a region relatively near the surface and their sizes are sufficiently small when compared with the characteristic dimensions of components and parts. A half-space containing near-surface cracks, when supplied by a set of proper governing physics, is one of the most commonly used mathematical models and is found adequate for approximating those situations (see Figure 1.2). Such idealization significantly simplifies the overall actual geometry, reduces the computational effort, and also yields the reasonably accurate prediction relative to the full analysis of the whole body. However, performing the stress analysis of such idealized body by conventional domain-based numerical techniques such as the finite different method (FDM) and the finite element method (FEM) is not computationally efficient as a result of the unbounded nature of the domain and the irregularity induced in a localized region around the cracks. Methods based upon boundary integral equations (BIEs) have been well-known, for several decades, as alternative, efficient numerical techniques for modeling crack problems especially when the involved medium is unbounded (e.g., Cruse, 1988; Katsikadelis, 2002). This is due to that the key governing equations only contain unknowns on the boundary and crack surfaces; as a result, it only requires the solution discretization over a domain of reduced spatial dimensions.

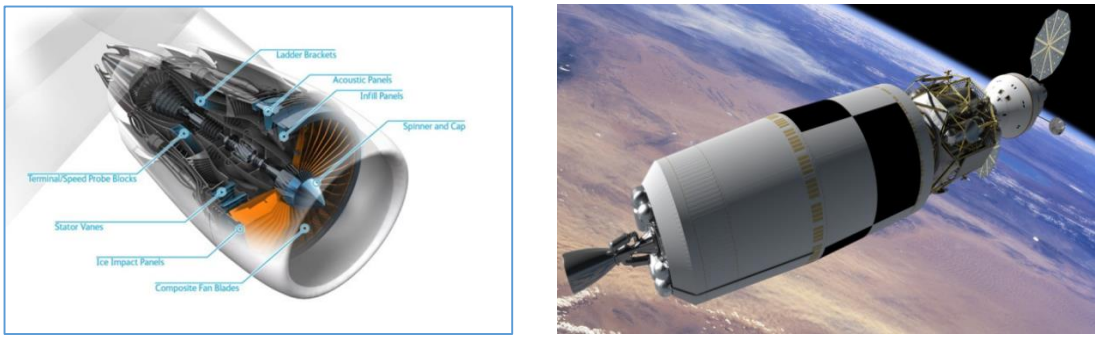

(a) (b)

(c) (d)

Figure 1.1: (a) Aircraft engine components[1], (b) an orion crew exploration vehicle[2], (c) a luxury yacht project[3], and (d) a composite structure[4].

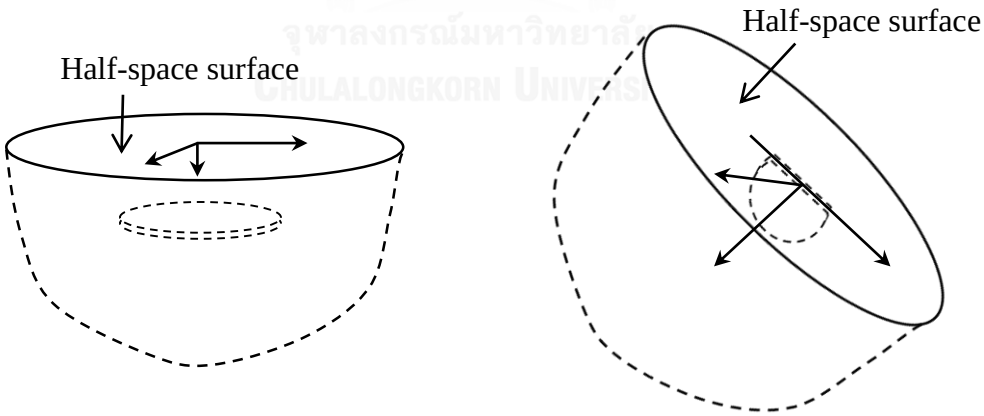

(a) (b)

Figure 1.2: Schematics of (a) interior elliptical crack and (b) surface-breaking crack.

1 http://www.cobham.com/about-cobham/communications-and-connectivity/about-us/composites/composite-engine-components.aspx
2 http://www.nasa.gov/mission_pages/constellation/altair/altair_concept_artwork.html
3 http://www.helicesnews.com/News/Monocoque-a-moteur/Couach-Couach-launches-a-new-26-metre-model-and-enters-the-realm-of-80-foot-boats
4 https://compositebuild.wordpress.com/category/architecture/

Various boundary integral equation techniques have been developed to solve cracks in an elastic half-space (e.g., Lo, 1979; Martin *et al.*, 1993; Khaj and Sushko, 1994; Sushko and Khaj, 1996; Hrylyts'kyi *et al.*, 2003; Gordeliy and Detournay, 2011). It should be remarked however that most of existing techniques were developed specifically to treat planar cracks and a half space made from isotropic materials. In addition, the key formulation was generally based either on strongly singular or hypersingular integral equations. The former limitation renders various practical cases cannot be treated; for instance, components made from hexagonal crystal materials and fiber-reinforced composites whose behavior is anisotropic in nature (see Figure 1.3) and non-planar geometry of the crack surface which commonly occurs during the propagation. For the latter, use of integral equations containing strongly singular and/or hypersingular kernels generally poses both theoretical and computational difficulties such as the interpretation and evaluation of values of singular integrals and constraints on solution space in the discretization.

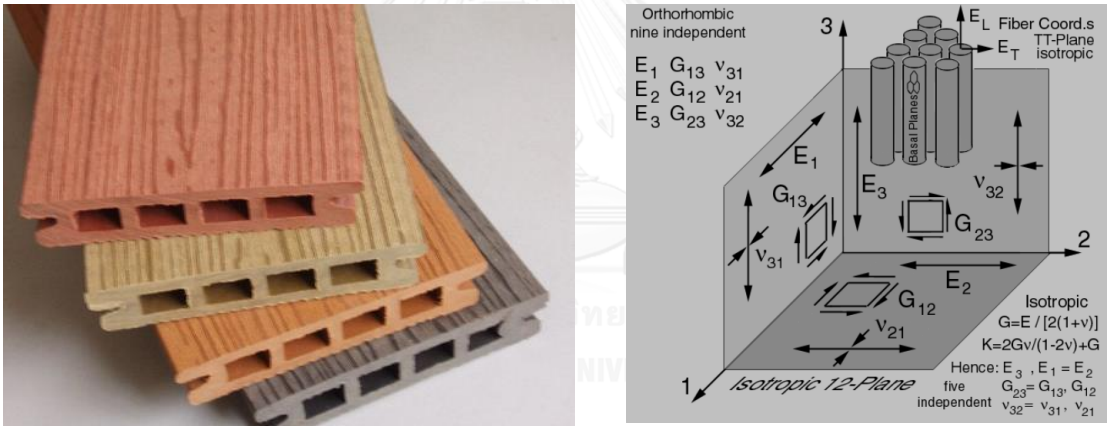

(a) (b)

Figure 1.3: (a) Composite materials[5] and (b) Transversely isotropic carbon fibers and their composites[6].

Li (1996) successfully derived a pair of singularity-reduced integral equations involving only weakly singular kernels for cracks in a linearly elastic half-space under several types of boundary conditions on its surface. However, the formulation is limited to the case of isotropic materials and the implementation of those integral equations to solve crack problems has not been found. The regularization technique proposed by Li

[5] http://iceland.balticnordic.com/jiangsu-jiajing-composite-materials-co-nanjing/company.html
[6] http://www.jwave.vt.edu/crcd/kriz/lectures/OnePageLect.html

(1996) was later enhanced and utilized by Li and Mear (1998), Li *et al.* (1998), Rungamornrat and Mear (2008a) in the derivation of the weakly singular boundary integral equations for cracks in both isotropic and anisotropic, linear elastic infinite and finite media. However, the similar nontrivial extension to treat material anisotropy for cracks in a linearly elastic half-space has not been recognized in the literature. In addition, the implementation of those weakly singular boundary integral equations to solve cracked half-spaces for essential fracture data such as the stress intensity factors and the T-stress components has also not been found. This significant gap of knowledge motivates the current study.

1.1 Objectives

The current investigation aims mainly to (i) develop a set of singularity-reduced integral relations and equations for cracks in a generally anisotropic, linearly elastic half-space, (ii) develop an accurate and computationally efficient numerical procedure, based on the boundary element method, for solving cracks in a linearly elastic half-space under various types conditions on the free surface, and (iii) investigate the computational performance of the developed numerical technique such as the accuracy, convergence behavior, and capability to treat general boundary value problems.

1.2 Scope of Work

The present study only applies to following situations: (i) a half-space that is made of a homogeneous, generally anisotropic, linear elastic material with its material-symmetry plane parallel to the free surface; (ii) a half-space that is free of the body force and remote loading; (iii) tractions on the crack surface that are fully prescribed; (iv) the crack surface that is sufficiently smooth; (v) the free surface of the half-space subjected to one of the following four boundary conditions (i.e., symmetrical boundary condition (BC-type-1), anti-symmetrical boundary condition (BC-type-2), traction-free boundary condition (BC-type-3), and fully rigid boundary condition (BC-type-4)) in which the last two boundary conditions are considered only for isotropic materials; and (vi) only the stress intensity factors and the T-stress components along the fracture front being of primary interest.

1.3 Methodology

A set of regularized boundary integral relations and equations for an elastic half-space containing cracks established in the present study is the non-trivial generalization of results presented by Li (1996) by taking the material anisotropy into account. A

systematic regularization procedure proposed by Rungamornrat and Mear (2008a) is adopted along with techniques used by Li (1996) in handling the symmetrical and anti-symmetrical boundary conditions to obtain the completely regularized boundary integral relations and equations. A well-known weakly singular, symmetric Galerkin boundary element method (SGBEM), utilized by Li *et al.* (1998) and Rungamornrat and Mear (2008b), and a standard Galerkin technique are selected to solve the associated boundary value problem. The underlying theories, proposed methodology and research procedure can be clearly outlined as follows.

(1) A classical theory of linear elasticity is adopted, along with the concept of linear elastic fracture mechanics, to form basic field equations governing responses of the cracked elastic half-space such as equilibrium equations, constitutive relations, and strain-displacement relations.

(2) Fundamental solutions for an un-cracked elastic half-space under BC-type-1 and BC-type-2 are established by using the superposition technique along with existing fundamental solutions for an un-cracked elastic whole space and the proper use of symmetrical and anti-symmetrical conditions with respect to the free surface of the half-space.

(3) Conventional boundary integral relations for displacements and stresses within the cracked elastic half-space under BC-type-1 and BC-type-2 are established by using the reciprocal theorem along with the established fundamental solutions for an un-cracked half space with the same type of boundary conditions.

(4) Singularity-reduced boundary integral relations and weakly singular boundary integral equations for the cracked elastic half-space under BC-type-1 and BC-type-2 are obtained by applying a systematic regularization procedure proposed by Rungamornrat and Mear (2008a) to the obtained standard integral relations. Specifically, special decompositions of both strongly singular and hypersingular kernels are first established using existing results for the elastic whole space and the symmetrical and anti-symmetrical conditions along the free surface of the half-space. Such special decompositions are then employed along with the integration by parts to transfer the derivative of involved kernels appearing in the decompositions to the boundary data via Stokes' theorem.

(5) The singularity-reduced boundary integral relations/equations for the cracked half-space made of isotropic materials and subjected either to BC-type-3 or BC-type-4 on the its free surface are obtained directly by applying a superposition technique to combine results of the first two boundary

conditions and the correction terms derived by Li (1996). The boundary value problem associated with the un-cracked half-space subjected to either the normal or shear traction on the free surface was solved using the potential-theory-based approach and solution representations. Again, a similar regularization procedure as that employed for BC-type-1 and BC-type-2 is employed to construct the final singularity-reduced boundary integral relations/equations.

(6) A weakly singular SGBEM is adopted to construct numerical solutions of the weak-form traction boundary integral equation. In the solution discretization, special crack-tip elements developed by Li *et al.* (1998) and Rungamornrat and Mear (2008b) are employed along the crack boundary to enhance the approximation of the near-front relative crack-face displacement and, in addition, to embed special degrees of freedom along the crack boundary which are related to the gradient of the crack-face displacement.

(7) Once the relative crack-face displacement is fully determined, the sum of the crack-face displacement is determined from the regularized weak-form displacement boundary integral equation using standard Galerkin technique.

(8) Special numerical quadrature based on the integrand regularization via a family of variable transformations including both the triangular polar transformations and the logarithmic transformations is utilized to numerically evaluate the nearly singular and weakly singular double surface integrals arising from the discretization of the crack surface.

(9) An interpolation technique proposed by Rungamornrat and Mear (2008b) is employed to evaluate weakly singular kernels for generally anisotropic materials in order to reduce the computational effort corresponding to the direct computation of the closed contour integral for every pair of field and source points.

(10) A selected indirect linear solver such as the conjugate gradient method with and without pre-conditioning is utilized to solve the two systems of linear algebraic equations.

(11) Explicit formula proposed by Rungamornrat and Mear (2008b) and Subsathaphol (2014) are implemented to compute the stress intensity factors and the T-stress components along the crack boundary in terms of the solved jump in and sum of the crack-face displacement, respectively.

1.4 Significance

The present study offers an accurate and computationally efficient numerical technique for modeling shallow, near surface, and surface breaking cracks within a bulk of material. The key formulation is established in a general three-dimensional context integrating both material anisotropy and various types of boundary conditions and this should enhance the capability to perform stress analysis of cracked bodies made of a broader class of materials such as composites and rocks. Since the governing equations are established in terms of the boundary integral equations and all types of conditions at the half-space surface are directly incorporated in the development of fundamental solutions, the discretization of the entire half-space and its surface is not required. This should significantly lessen the computational resources associated with the reduction in the number of unknowns and, in addition, provide an attractive computational tool for simulating crack advances where the adaptation of meshes is required during the simulations. Besides its direct applications to mathematically model a variety of engineering problems involving cracks (e.g., machine components, structural components, devices, geo-engineering and pressure vessels containing defects and flaws near their free surface), the developed methodology and procedure can be conveyed and generalized to investigate cracks in bi-material domains.

1.6 Outline of Dissertation

In this dissertation, a set of regularized boundary integral relations and equations for an elastic half-space containing cracks and subjected to various types of boundary conditions on the free surface is derived. In addition, the solution procedure based upon the regularized boundary element method and standard Galerkin technique is also established. The key motivation, research objective and scope of work, the brief methodology and significance of work are presented in Chapter 1 whereas the remaining portion of this dissertation is organized as follows.

In Chapter 2, a brief review of previous studies concerning the modeling and analysis of cracks in an elastic half-space is provided. Various existing solution techniques applied to solve cracked elastic half-space problems are summarized. Besides, the recent advances of boundary integral equation methods relevant to the present investigation are also briefly discussed.

Chapter 3 contains the problem description, basic field equations from a classical theory of linear elasticity, fundamental solutions of the displacement and stress for an un-cracked elastic half-space under symmetrical and anti-symmetrical boundary conditions, standard integral relations for stress and displacement within an elastic half-

space containing cracks, special representations of both hyper-singular and strongly singular functions, and the development of completely regularized integral equations essential for formulating the governing equations of cracks within the half-space.

Chapter 4 mainly presents components essential for the development of a computational procedure for determining the unknown crack-face data such as the sum of and jump in the crack-face displacement and the post-process for the mixed-mode stress intensity factors and the T-stress components. A formulation of the boundary value problem based upon the regularized integral equations established in the previous chapter is obtained first and, then, the discretization procedure following Galerkin technique is briefly outlined. Essential ingredients to enhance the computational efficiency and accuracy such as the approximation of the near-front behavior, the numerical integration, and the evaluations of kernels for anisotropic materials are also discussed. Finally, explicit formulae for extracting the stress intensity factors and the T-stress components along the crack front are proposed.

Extensive results for cracks in a linearly elastic half-space under various scenarios are reported in Chapter 5 to demonstrate the capability and accuracy of the developed numerical procedure. In particular, results for a particular class of boundary value problems are generated first and compared with reliable benchmark solutions to verify both the derivation of integral equations and the implementations. Then, more complicated problems associated with multiple and non-flat cracks are investigated and obtained results are reported to prove the versatility and robustness of the developed procedure.

The last chapter summarizes the essential finding associated with both the integral formulations and implemented numerical procedure. Besides, the extension of the present work to general types of boundary conditions and multi-field materials is also included.

CHAPTER 2
BACKGROUND AND REVIEW

This chapter reports results from an extensive review of literatures related to the theoretical modeling and analysis of cracks in an elastic half-space. Various existing solution methodologies are briefly summarized including their pros and cons. In addition, the background and recent advances of the boundary integral equation methods relevant to the current investigation is also briefly discussed.

2.1 Modeling of Cracked Half-Space

A half-space containing a surface of discontinuities is one of mathematical domains commonly used to represent a physical body in the simulation of localized, near-surface flaws, defects, and impurities if their sizes are sufficiently small when compared with the characteristic dimensions of the body. Such idealization significantly simplifies the real geometry, reduces the computational effort, and also yields the reasonably accurate prediction relative to the full analysis of the whole body. To perform such theoretical simulations, solution techniques have played a crucial role in the solution accuracy and computational performance and they must be properly selected to suit each involved scenario. Many investigations based upon the conventional theories of linear elasticity and linear elastic fracture mechanics have been well recognized in the literature and various techniques including analytical and semi-analytical approaches, conventional domain-based numerical techniques, and boundary-based approaches have been proposed to construct solutions of mathematical models of cracked half-spaces. In particular, those existing solution techniques were based on integral-transform-based and series-representation method (e.g., Srivastava and Singh, 1969; Feng *et al.*, 2007; Monastyrskyy and Kaczyński, 2010; Bogdanov, 2011; Eskandari-Ghadi *et al.*, 2013), the body force method (e.g., Murakami, 1985; Noguchi and Smith, 1995; Noguchi *et al.*, 1997), the iterative-based alternating method (e.g., Smith and Alavi, 1971; Shah and Kobayashi, 1973; Dhondt, 1995), the inverse method (e.g., Keat *et al.*, 1998), the standard finite element technique (e.g., Ghajar and Alizadeh, 2013) and the boundary integral equation methods (e.g., Lo, 1979; Hayashi and Abé, 1980; Mayrhoffer and Fischer, 1989; Martin *et al.*, 1993; Khaj and Sushko, 1994; Khaj and Sushko, 1996; Sushko and Khaj, 1996; Movchan and Willis, 2000; Kit *et al.*, 2000; Hrylyts'kyi *et al.*, 2003; Gordeliy and Detournay, 2011; Skalsky *et al.*, 2013).

Analytical and semi-analytical techniques based on integral transforms, dual integral equation theories, and series representations were successfully established in the investigation of the near-front elastic field and the stress intensity factors of some cracks with relatively simple geometry (e.g., a penny-shaped crack) in an isotropic, linearly elastic half-space (e.g., Srivastava and Singh, 1969; Feng *et al.*, 2007; Bogdanov, 2011). While those methodologies can yield very accurate results comparable to the exact solution, their capability has been found very limited and they cannot be applied to treat various practical scenarios due to the high complexity posed by the general prescribed information such as crack geometries, material behavior, boundary and loading conditions.

To further enhance and broaden the capability for modeling elastic cracked half-spaces, a variety of numerical procedures have continuously been developed in the past several decades. Based on the linear feature of the elastic field and a standard superposition technique, the body force method was exploited by several investigators to perform the stress analysis and estimate the stress intensity factors along the boundary of planar cracks contained in an elastic half-space (e.g., Murakami, 1985; Noguchi and Smith, 1995; Noguchi *et al.*, 1997). Although fully mixed-mode problems have been included in the work of Murakami (1985), it was still limited to planar cracks, the traction-free surface and isotropic materials. Other approaches such as the alternating techniques, which are based on an iterative solution procedure to remove the fictitious residual stress, were also established to solve cracked half-space problems (e.g., Smith and Alavi, 1971; Shah and Kobayashi, 1973; Dhondt, 1995). Due to the nature of the solution strategy, the alternating technique was found yielding results of relatively low accuracy (e.g., Mayrhoffer and Fischer, 1989). An experimental approach was also proposed by Keat *et al.* (1998) in which the algorithm of inversion for identifying embedded crack geometries and locations in a half-space from field measurements of the surface displacement was presented. Nonetheless, this technique can only be applied for simple cases of crack configurations and loading conditions. Recently, a standard finite element technique was also developed to investigate cracked half-space problems (e.g., Ghajar and Alizadeh, 2013); however, it has been found that substantially fine mesh is required in the discretization especially in the near-front zone and the truncation of the domain must be properly considered to treat the unbounded dimensions. It should also be remarked that all studies indicated above were still limited to certain crack configurations, isotropic materials, and determination of stress intensity factors. The analysis for nonsingular terms such as the T-stress components and the treatment of material anisotropy were still not addressed. The consideration of material anisotropy was found in the work of Monastyrskyy and Kaczyński (2010). In their

study, the material is assumed transversely isotropic and possessing the axis of material symmetry normal to the free surface and only a crack of penny-shape oriented horizontally is modeled. A technique of Hankel integral transforms along with a selected numerical procedure was adopted to determine the stress intensity factors along the crack front. Recently, Eskandari-Ghadi *et al.* (2013) applied the method of integral transform to analytically solve a horizontal, penny-shaped crack in a transversely isotropic, linearly elastic half-space under time-harmonic asymmetric tractions.

Among various existing solution techniques, ones based upon boundary integral equations have been extensively employed in the analysis procedure due to their simplicity to treat the unbounded geometry. With the proper incorporation of fundamental solutions to satisfy the boundary conditions on the free surface of the half-space, the key governing integral equations simply involve unknowns only on the crack surface and this, as a result, significantly reduces the number of degrees of freedom resulting from the discretization. In 1979, Lo applied Mindlin's point force solution to derive the strongly singular integral equation for an embedded planar crack oriented parallel to the surface of an isotropic, linearly elastic half-space. While the integral equation was successfully obtained, the implementation to solve cracked half-space problem was not found in this study. Hayashi and Abé (1980) developed the collocation technique based on a strongly singular traction boundary integral equation to determine the pure mode-I stress intensity factors of a uniformly pressurized, vertical, semi-elliptical, surface-breaking crack in an isotropic, linearly elastic half-space with the traction-free surface. Martin *et al.* (1993) employed Mindlin's fundamental solution to obtain a system of singular boundary integral equations for a pressurized crack oriented perpendicular to the free surface of an isotropic elastic half-space with the stress-free surface. Although the implementation of those equations was not included in their study, the solvability and the regularity of solutions of the developed integral equations were proven. Later, Khaj and Sushko (1994) investigated the interaction of two identical, near-surface, coplanar, circular cracks in an isotropic, linearly elastic, half-space with the stress-free surface and loaded by forces perpendicular to the crack surface. In the analysis, the opening of the cracks was determined by solving a system of hypersingular boundary integral equations and those results were employed to extract the stress intensity factors. Sushko and Khaj (1996) developed a system of hypersingular integro-differential equations governing the opening displacement of a planar surface-breaking crack in an isotropic, linearly elastic, half-space. Such equations were solved numerically for the special case of cracks with their geometry is a part of a circle. In the same year, Khaj and Sushko (1996) employed a conformal mapping along with a semi-analytical technique to solve a system of hypersingular

boundary integral equations in the investigation of the influence of the depth and orientation of a planar crack with the shape of a limacon of Pascal. Later, Kit *et al.* (2000) generalized the work of Khaj and Sushko (1994) to investigate the interaction of multiple, planar, surface-breaking cracks of arbitrary shapes and orientations. The solution procedure was based primary on solving a system of boundary integral equations for the relative crack-face displacement and used that data to post-process for the stress intensity factors. Movchan and Willis (2000) extended the work of Martin *et al.* (1993) to further explore the corner singularity at locations where the crack intersects the free boundary. In their analysis, a hypersingular integral equation formulated in terms of the relative crack-face displacement is employed. Later, Hrylyts'kyi *et al.* (2003) implemented a hypersingular boundary integral equation method to study the interaction of planar cracks in an isotropic elastic half-space with rigidly restrained surface. The potential method was employed to derive boundary integral equations in terms of unknown relative crack-face displacement. The stress intensity factors were also calculated for a circular crack perpendicular to rigid surface. Gordeliy and Detournay (2011) developed the displacement discontinuity technique to model axisymmetric cracks in an isotropic, linearly elastic, half-space. Their key formulation was based primarily on the hypersingular integral equations involving the displacement jump across the crack surface and the combined numerical integration scheme and recursive procedure was adopted to directly integrate involved hyper and Cauchy singular integrals. In addition, the tip-elements were also employed to enhance the accuracy of the near-front approximation. Recently, Skalsky *et al.* (2013) investigated an axisymmetric crack problem involving the mode-III loading condition for an isotropic, linearly elastic half-space. The displacement-field functions were numerically determined by the frequency-domain boundary integral equations. Still, this particular work focuses only a boundary value problem concerning a penny-shaped crack under the action of torsion loading. It should be remarked that, among various existing studies described above, the key formulations were still based primarily on strongly and/or hypersingular integral equations with limitation to isotropic materials and such equations were implemented mainly to treat planar cracks under simple crack-faced loading and determine the stress intensity factors.

It is well known that the displacement boundary integral equation derived directly from Somigliana's identity is insufficient for solving cracked bodies within the context of a single-domain-based formulation (e.g., Cruse, 1988). An alternative means to circumvent such difficulty besides inefficient multi-domain techniques is to employ, in addition, the traction boundary integral equation to treat cracks. Unfortunately, the conventional traction boundary integral equation established directly from the stress

boundary integral relation involves both hyper-singular and strongly singular kernels and their treatment requires special care (e.g., Guiggiani *et al.*, 1991). In addition, the smoothness requirement of the jump in crack-face displacement data for the validity of the hyper-singular boundary integral equation implies the need of C^1-elements in the solution discretization (e.g., Gray *et al.*, 1990, Martin and Rizzo, 1996). To further alleviate such requirement and facilitate the numerical treatment of involved integrals, a regularization technique was proposed by Li (1996) to derive the regularized boundary integral equations for displacement discontinuities embedded in a three-dimensional, isotropic, linearly elastic half-space under various boundary conditions. Such technique was later enhanced and utilized by Li and Mear (1998), Li *et al.* (1998), Rungamornrat and Mear (2008a) in the derivation of the weakly singular, weak-form boundary integral equations for cracks in both isotropic and anisotropic, linear elastic infinite and finite media. However, the similar nontrivial extension to treat material anisotropy for cracks in a linearly elastic half-space has not been recognized in the literature. In addition, the implementation of those weakly singular boundary integral equations to solve cracked half-spaces for essential fracture data such as the stress intensity factors and the T-stress components has also not been found.

2.2 Regularized BIEMs

Various regularization techniques have been continuously proposed to construct singularity-reduced integral equations with the primary objective to reduce the smoothness requirement in solution discretization. Within the context of the stress analysis of cracked elastic media, a set of regularized boundary integral equations has been recognized for past several decades and some of those relevant investigations are briefly presented here to indicate the recent advances in the area. Bui (1977) and Weaver (1977) simultaneously developed the singularity-reduced traction boundary integral equation for mode-I planar cracks contained in an infinite elastic medium. In their work, all hypersingular integrals were regularized with the final integrands containing only Cauchy-singular kernels. Later, Sládek and Sládek (1982) generalized the work of Bui (1977) and Weaver (1977) to treat non-flat cracks under general loading conditions. The key component used to establish the singularity-reduced traction integral equation indicated above was the derivative transferring between the hypersingular kernels and the crack-face data via the integration by parts. It should be remarked that the obtained strongly singular traction integral equation still require the continuity of the relative crack-face displacement for its validity and, in the numerical

implementation perspective, the computational cost associated with the use of C^1-interpolation functions is still significant (see also the work of Bonnet and Bui, 1993).

In past several decades, efforts have been invested to develop the completely regularized boundary integral equations involving only weakly singular kernels instead of ones involving Cauchy singular integrals. This is due mainly to the simplicity associated with the interpretation and numerical calculation of singular integrals and the low smoothness requirement of data. Within the context of linear elasticity applications, the work of Gu and Yew (1988) was recognized as the first derivation of weakly singular integral equations for crack problems. However, their formulation was still restricted to the case of isolated, planar cracks in an isotropic elastic whole space under the pure mode-I loading condition. Later Xu and Ortiz (1993) extended the work of Gu and Yew (1988) to treat non-planar cracks and mixed-mode loading conditions. In their work, the relative crack-face displacements were represented as the continuous distribution of the dislocation loops.

To allow the treatment of cracks of arbitrary shapes in an isotropic elastic half-space under different types of boundary conditions on the free surface, Li (1996) proposed a systematic regularization technique based upon the special representations of singular kernels and the integration by parts via Stokes' theorem. It is remarked that the formulation was limited to isotropic materials and the implementation of those integral equations to solve crack problems was not considered. Li and Mear (1998), and Li *et al.* (1998) generalized the work of Li (1996) to the case of arbitrary cracks in isotropic, linearly elastic, unbounded and finite media. The implementation of those equations based on the regularized SGBEM was also successfully implemented to model crack problems under various scenarios. Later, Xu (2000) employed the dislocation theory to establish the weak singular traction boundary integral equation for cracks in a medium made from generally anisotropic materials. While his formulation is applicable to treat arbitrary-shaped cracks and general loading conditions, it was still restricted to cracks in the whole space. The treatment of general material anisotropy in the development of boundary integral equations and the implementation of numerical procedure via the weakly singular SGBEM was also investigated by Rungamornrat and Mear (2008a) and Rungamornrat and Mear (2008b) for cracks in both unbounded and finite media. While various regularization procedures have been proposed in the literature, work concerning cracks in an anisotropic, linear elastic half-space has not been recognized. In addition, the development of weakly singular SGBEM for the special case of cracks in an isotropic, linearly elastic half-space under various conditions on the free surface is also not available in the literature.

In the present study, the systematic regularization procedure proposed by Li and Mear (1998); Li *et al.* (1998); Rungamornrat and Mear (2008a); Rungamornrat and Mear (2008b); Rungamornrat and Senjuntichai (2009) is further extended to derive a set of regularized integral relations for a half-space containing cracks and made of anisotropic materials possessing a plane of material symmetry parallel to the free surface. In addition, the implementation of the derived equations in the context of weakly singular SGBEM and standard Galerkin technique is also established. The proposed work is carried out within a general framework allowing the treatment of arbitrary shaped cracks and half-spaces under various conditions on the half-space surface and the determination of both the stress intensity factors and the T-stress components along the crack front.

CHAPTER 3
FORMULATION

This chapter summarizes the clear problem description, basic field equations from a classical theory of linear elasticity, fundamental solutions of the displacement and stress within an un-cracked elastic half-space under symmetrical and anti-symmetrical boundary conditions, standard integral relations for both stress and displacement within an elastic half-space containing cracks, special representations of hyper-singular and strongly singular functions, and the development of completely regularized integral equations essential for modeling cracks within the half-space.

3.1 Problem Description

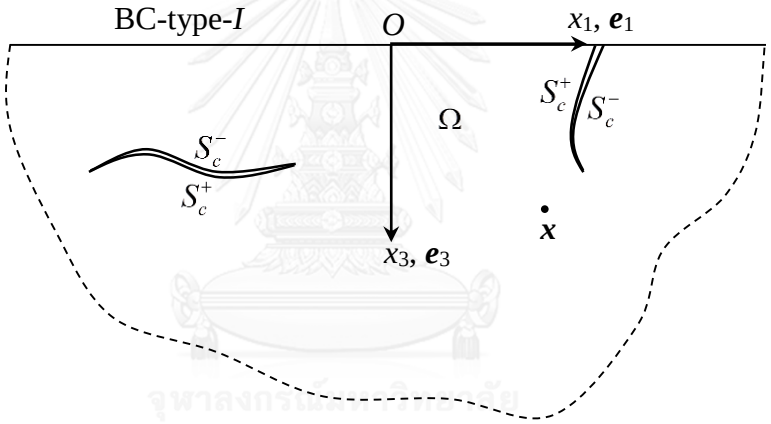

Figure 3.1: Schematic of elastic half-space containing isolated cracks and subjected to BC-type-*I* boundary conditions on the free surface.

Let us consider an elastic half-space Ω containing an embedded crack and a surface breaking crack as clearly illustrated in Figure 3.1. For convenience in further development, a reference Cartesian coordinate system $\{\boldsymbol{O}; x_1, x_2, x_3\}$ with the orthonormal base vectors $\{\boldsymbol{e}_1, \boldsymbol{e}_2, \boldsymbol{e}_3\}$ is taken such that the origin $\boldsymbol{O}$ is located on the half-space surface; the x_3-axis directs downward; and the x_1- and x_2-axes follow the right hand rule. The body is made from a homogeneous, anisotropic, linearly elastic material with the elastic constants E_{ijkl} referring to the selected coordinate system and possessing $x_3 = 0$ as the plane of material symmetry. The crack surfaces in the reference or undeformed state can be represented by two geometrically identical

surfaces S_c^+ and S_c^- (see Figure 3.1). The outward unit normal vectors at a smooth point $\boldsymbol{\xi}^+ \in S_c^+$ and its coincident point $\boldsymbol{\xi}^- \in S_c^-$ are denoted, respectively, by $\boldsymbol{n}^+$ and $\boldsymbol{n}^-$ and they clearly satisfy $\boldsymbol{n}^+ = -\boldsymbol{n}^-$. On both crack surfaces S_c^+ and S_c^-, the traction data is fully prescribed (i.e., $\boldsymbol{t}(\mathbf{x}) = \boldsymbol{t}^{0+}(\boldsymbol{x})\ \forall \boldsymbol{x} \in S_c^+$ and $\boldsymbol{t}(\mathbf{x}) = \boldsymbol{t}^{0-}(\boldsymbol{x})\ \forall \boldsymbol{x} \in S_c^-$ where $\boldsymbol{t}^{0+}$ and $\boldsymbol{t}^{0-}$ are known functions) whereas, on the surface $x_3 = 0$, one of the following four types of boundary conditions, termed BC-type-*I* for *I* = 1, 2, 3 and 4, is assumed. For the BC-type-1, the normal component of the displacement and the shear tractions vanish identically (i.e., $u_3 = 0, \sigma_{13} = \sigma_{23} = 0$); for the BC-type-2, the tangential components of the displacement and the normal traction vanish (i.e., $u_1 = u_2 = 0, \sigma_{33} = 0$); for the BC-type-3, all components of the traction vanish (i.e., $\sigma_{13} = \sigma_{23} = \sigma_{33} = 0$); and for the BC-type-4, all components of the displacement vanish (i.e., $u_1 = u_2 = u_3 = 0$). In the current investigation, the crack surfaces S_c^+ and S_c^- are assumed piecewise smooth (i.e., the unit normal vector is piecewise well-defined) and the remote loading and body force are absent.

The statement of the current research problem is to determine the complete elastic field (including the displacement and stress fields) of the cracked elastic half-space Ω and the fracture data including the relative crack-face displacement, the stress intensity factors, and the T-stress components along the crack front.

3.2 Basic Field Equations

Mechanical responses of the given half-space Ω (including the displacement, stress, and strain fields) under external excitation are mathematically modeled by a classical theory of linear elasticity and the concept of linear elastic fracture mechanics. All involved field quantities and associated field equations are introduced and listed below.

From the conservation of linear and angular momentum and, in the absence of the body force field, the stress tensor $\boldsymbol{\sigma}$ (with its components referring to the reference Cartesian coordinate system $\{\boldsymbol{O}; x_1, x_2, x_3\}$ denoted by σ_{ij}) must be symmetric (i.e., $\sigma_{ij} = \sigma_{ji}$) and divergence free everywhere, i.e.,

$$\sigma_{ij,j} = 0 \tag{3.1}$$

where $f_{,j}$ stands for the partial derivative of a function f with respect to the coordinate x_j. Here and in what follows, all standard Latin indices take the values from 1 to 3 and

repeated indices imply the summation over their range. For a body made of linear elastic materials, the stress tensor $\boldsymbol{\sigma}$ is related to the strain tensor $\boldsymbol{\varepsilon}$ (with its components denoted by ε_{ij}) via the generalized Hooke's law, i.e.,

$$\sigma_{ij} = E_{ijkl}\varepsilon_{kl} \tag{3.2}$$

where E_{ijkl} are prescribed constant elastic moduli satisfying following symmetries: $E_{ijkl} = E_{ijlk} = E_{jikl} = E_{klij}$. For isotropic materials, the elastic moduli involve only two independent material parameters and take a simple form

$$E_{ijkl} = \mu(\delta_{ik}\delta_{jl} + \delta_{il}\delta_{jk}) + \lambda\delta_{ij}\delta_{kl} \tag{3.3}$$

where μ and λ are Lame's constants and δ_{ij} denotes a standard Kronecker-delta symbol. The relation between the displacement vector $\boldsymbol{u}$ and the strain tensor $\boldsymbol{\varepsilon}$ are given by

$$\varepsilon_{ij} = \frac{1}{2}\left(u_{i,j} + u_{j,i}\right) \tag{3.4}$$

where u_i denotes components of the displacement vector $\boldsymbol{u}$. In addition, the traction vector $\boldsymbol{t}$ at any point on a smooth surface can be obtained in terms of the stress tensor at the same point by

$$t_i = \sigma_{ij}n_j \tag{3.5}$$

where t_i and n_i are components of the traction vector $\boldsymbol{t}$ and a unit normal vector $\boldsymbol{n}$, respectively. The relations (3.1), (3.2) and (3.4) form the basic field equations governing all unknown elastic fields $\boldsymbol{u} = \boldsymbol{u}(\boldsymbol{x})$, $\boldsymbol{\varepsilon} = \boldsymbol{\varepsilon}(\boldsymbol{x})$ and $\boldsymbol{\sigma} = \boldsymbol{\sigma}(\boldsymbol{x})$.

3.3 Fundamental Solutions of Half-Space under BC-type-1 and BC-type-2

To construct fundamental solutions for the displacement and stress of an un-cracked, linearly elastic half-space subjected to boundary conditions of BC-type-1 and BC-type-2, the existing fundamental solutions of an un-cracked elastic whole space (e.g., Ting and Lee, 1997; Wang, 1997) can be used along with the symmetrical and anti-symmetrical conditions as indicated below. It should be remarked that results presented here are restricted only to the case that the material constituting the half-space is

homogeneous and linearly elastic, and possesses $x_3 = 0$ as a plane of material symmetry.

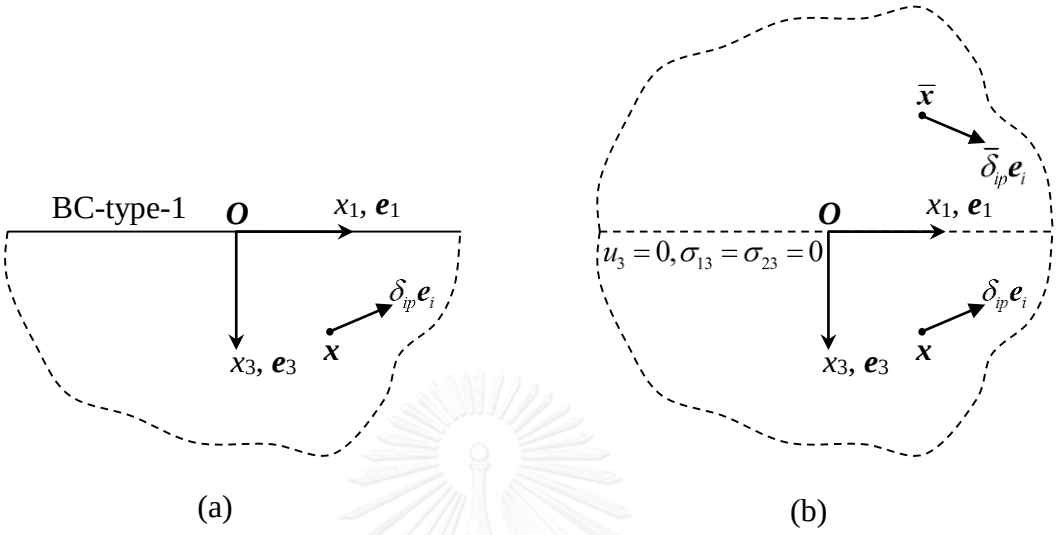

(a) (b)

Figure 3.2: Schematic of (a) un-cracked elastic half-space with boundary condition of BC-type-1 and subjected to unit concentrated force at point $\boldsymbol{x}$ and (b) un-cracked elastic whole space subjected to a pair of symmetrical unit concentrated forces at a point $\boldsymbol{x}$ and its image point $\bar{\boldsymbol{x}}$ with respect to the surface $x_3 = 0$.

First, consider the un-cracked elastic half-space with the boundary condition of BC-type-1 and subjected to a unit concentrated force $\delta_{ip}\boldsymbol{e}_i$ at a source point $\boldsymbol{x} = x_k\boldsymbol{e}_k$ as illustrated in Figure 3.2(a). It can readily be verified that an elastic field of this elastic half-space is identical to that of the bottom half of an elastic whole space subjected to a unit concentrated force $\delta_{ip}\boldsymbol{e}_i$ acting at a point $\boldsymbol{x} = x_k\boldsymbol{e}_k$ and a unit concentrated force $\bar{\delta}_{ip}\boldsymbol{e}_i$ (where $\bar{\delta}_{ip}$ is a constant tensor defined by $\bar{\delta}_{11} = \bar{\delta}_{22} = -\bar{\delta}_{33} = 1$, $\bar{\delta}_{ij} = 0$ for $i \neq j$) acting at a point $\bar{\boldsymbol{x}} = \bar{x}_k\boldsymbol{e}_k$ with $\bar{x}_k = \bar{\delta}_{kp}x_p$ as indicated in Figure 3.2(b). Note, in particular, that the loading condition of the elastic whole space is clearly symmetrical with respect to the plane $x_3 = 0$ and, as a result, the conditions $u_3 = 0, \sigma_{13} = \sigma_{23} = 0$ are automatically satisfied. Upon using the symmetry, the displacement and stress at any field point $\boldsymbol{\xi}$ within the half-space, denoted respectively by $U_j^{1p}(\boldsymbol{\xi}, \boldsymbol{x})$ and $S_{ij}^{1p}(\boldsymbol{\xi}, \boldsymbol{x})$, can therefore be obtained as

$$U_j^{1p}(\boldsymbol{\xi}, \boldsymbol{x}) = U_j^p(\boldsymbol{\xi} - \boldsymbol{x}) + \bar{\delta}_{pk}U_j^k(\boldsymbol{\xi} - \bar{\boldsymbol{x}}) \tag{3.6}$$

$$S_{ij}^{1p}(\boldsymbol{\xi},\boldsymbol{x}) = S_{ij}^{p}(\boldsymbol{\xi}-\boldsymbol{x}) + \bar{\delta}_{pk} S_{ij}^{k}(\boldsymbol{\xi}-\bar{\boldsymbol{x}}) \tag{3.7}$$

where the superscript "1" is utilized to emphasize that the fundamental solutions correspond to the boundary condition of BC-type-1 and $U_j^p(\boldsymbol{\xi}-\boldsymbol{x})$ and $S_{ij}^p(\boldsymbol{\xi}-\boldsymbol{x})$ denote the displacement and stress at any point $\boldsymbol{\xi}$ of the elastic whole space subjected to a unit concentrated force $\delta_{ip}\boldsymbol{e}_i$ at a point $\boldsymbol{x} = x_k\boldsymbol{e}_k$. The explicit form of the displacement and stress fundamental solutions $U_j^p(\boldsymbol{\xi}-\boldsymbol{x})$ and $S_{ij}^p(\boldsymbol{\xi}-\boldsymbol{x})$ for generally anisotropic, linearly elastic materials is given by (see details in the work of Rungamornrat and Mear, 2008a)

$$U_j^p(\boldsymbol{\xi}-\boldsymbol{x}) = \frac{1}{8\pi^2 r}\oint_{\mathbf{z}\cdot\mathbf{r}=0} (z,z)_{jp}^{-1} ds(z) \tag{3.8}$$

$$S_{ij}^p(\boldsymbol{\xi}-\boldsymbol{x}) = E_{ijkl}\frac{\partial U_k^p(\boldsymbol{\xi}-\boldsymbol{x})}{\partial \xi_l} \tag{3.9}$$

where $(\mathbf{z},\mathbf{z})_{kl} = z_i E_{iklj} z_j$, $\boldsymbol{r} = \boldsymbol{\xi}-\boldsymbol{x}$, $r = \|\boldsymbol{r}\|$ and the line integral is taken over a unit circle $\|\mathbf{z}\| = 1$ on a particular plane $\mathbf{z}\cdot\boldsymbol{r} = 0$. It is apparent from (3.6)-(3.7) and the properties of the fundamental solutions $U_j^p(\boldsymbol{\xi}-\boldsymbol{x})$ and $S_{ij}^p(\boldsymbol{\xi}-\boldsymbol{x})$ that $U_j^{1p}(\boldsymbol{\xi},\boldsymbol{x})$ and $S_{ij}^{1p}(\boldsymbol{\xi},\boldsymbol{x})$ are singular only at $\boldsymbol{\xi} = \boldsymbol{x}$ of $\mathcal{O}(1/r)$ and $\mathcal{O}(1/r^2)$, respectively. Explicit form of the fundamental solutions for the isotropic case can be found in available literatures (e.g., Xiao, 1998).

Let us consider, next, the elastic half-space with the boundary condition of BC-type-2 and subjected to a unit concentrated force $\delta_{ip}\boldsymbol{e}_i$ at a source point $\boldsymbol{x} = x_k\boldsymbol{e}_k$ as shown in Figure 3.3(a). With the same analogy as the previous case, the elastic solution of the half-space is identical to that of the bottom half of an elastic whole space subjected to a unit concentrated force $\delta_{ip}\boldsymbol{e}_i$ acting at a point $\boldsymbol{x} = x_k\boldsymbol{e}_k$ and a unit concentrated force $-\bar{\delta}_{ip}\boldsymbol{e}_i$ acting at the image point $\bar{\boldsymbol{x}} = \bar{x}_k\boldsymbol{e}_k$ as indicated in Figure 3.3(b). For this particular case, the elastic whole space apparently subjected to anti-symmetrical loading conditions with respect to the plane $x_3 = 0$. As a result, the displacement and stress at any field point $\boldsymbol{\xi}$ of the half-space, denoted respectively by $U_j^{2p}(\boldsymbol{\xi},\boldsymbol{x})$ and $S_{ij}^{2p}(\boldsymbol{\xi},\boldsymbol{x})$, are given, in terms of $U_j^p(\boldsymbol{\xi}-\boldsymbol{x})$ and $S_{ij}^p(\boldsymbol{\xi}-\boldsymbol{x})$, by

$$U_j^{2p}(\boldsymbol{\xi},\boldsymbol{x}) = U_j^p(\boldsymbol{\xi}-\boldsymbol{x}) - \bar{\delta}_{pk} U_j^k(\boldsymbol{\xi}-\bar{\boldsymbol{x}}) \tag{3.10}$$

$$S_{ij}^{2p}(\boldsymbol{\xi},\boldsymbol{x}) = S_{ij}^{p}(\boldsymbol{\xi}-\boldsymbol{x}) - \bar{\delta}_{pk} S_{ij}^{k}(\boldsymbol{\xi}-\bar{\boldsymbol{x}}) \tag{3.11}$$

where the superscript "2" is introduced to clearly indicate that the fundamental solutions belong to the half-space with the boundary condition of BC-type-2. Similar to the previous case, the singularity behavior of the fundamental solutions $U_j^{2p}(\boldsymbol{\xi},\boldsymbol{x})$ and $S_{ij}^{2p}(\boldsymbol{\xi},\boldsymbol{x})$ follows directly that of $U_j^{p}(\boldsymbol{\xi}-\boldsymbol{x})$ and $U_j^{p}(\boldsymbol{\xi}-\boldsymbol{x})$.

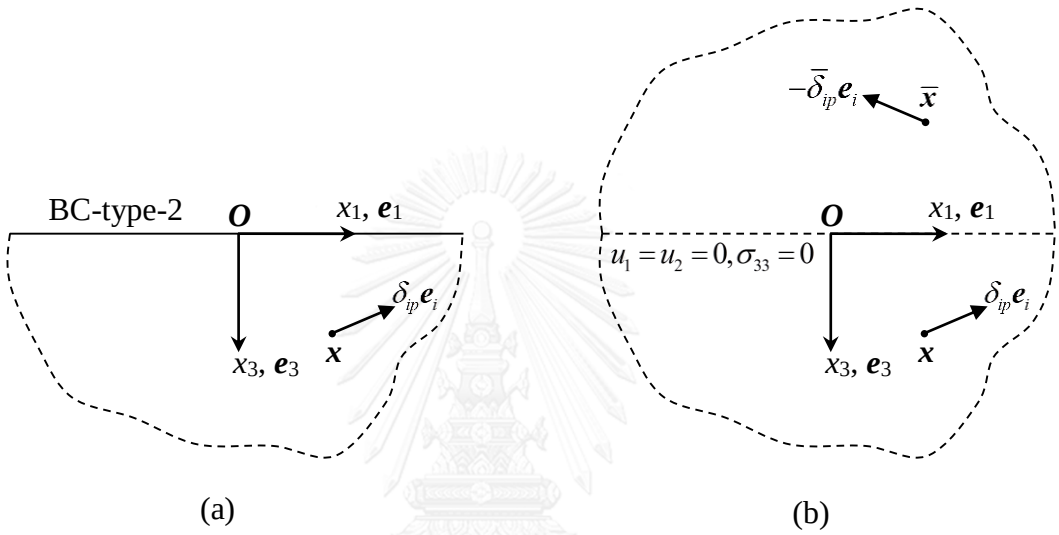

Figure 3.3: Schematic of (a) un-cracked elastic half-space with boundary condition of BC-type-2 and subjected to unit concentrated force at point $\boldsymbol{x}$ and (b) un-cracked elastic whole space subjected to a pair of anti-symmetrical unit concentrated forces at a point $\boldsymbol{x}$ and its image point $\bar{\boldsymbol{x}}$ with respect to the surface $x_3 = 0$.

3.4 Standard Integral Relations for Cracked Half-Space under BC-type-1 and BC-type-2

By applying the reciprocal theorem to an elastic half-space Ω containing cracks and subjected to the boundary condition of BC-type-α (α = 1 or 2) as shown in Figure 3.1 along with another elastic state associated with a fundamental problem of the half-space with the same boundary condition of BC-type-α (constructed in section 3.3), it leads to the displacement boundary integral relation for the cracked half-space with the boundary condition of BC-type-α:

$$u_p^{\alpha}(\boldsymbol{x}) = \int_{S_c^+} U_j^{\alpha p}(\boldsymbol{\xi},\boldsymbol{x}) \Sigma t_j^0(\boldsymbol{\xi}) dA(\boldsymbol{\xi}) - \int_{S_c^+} S_{ij}^{\alpha p}(\boldsymbol{\xi},\boldsymbol{x}) n_i^+(\boldsymbol{\xi}) \Delta u_j^{\alpha}(\boldsymbol{\xi}) dA(\boldsymbol{\xi}) \tag{3.12}$$

where $\Sigma t_j^0(\boldsymbol{\xi}) = t_j^{0+}(\boldsymbol{\xi}) + t_j^{0-}(\boldsymbol{\xi})$ denotes the sum of tractions on both crack surfaces; $\Delta u_j^{\alpha}(\boldsymbol{\xi}) = u_j^{\alpha+}(\boldsymbol{\xi}) - u_j^{\alpha-}(\boldsymbol{\xi})$ denotes the jump in the crack-face displacements; and the fundamental solutions $U_j^{\alpha p}(\boldsymbol{\xi}, \boldsymbol{x})$ and $S_{ij}^{\alpha p}(\boldsymbol{\xi}, \boldsymbol{x})$ are given in terms of $U_j^p(\boldsymbol{\xi} - \boldsymbol{x})$ and $S_{ij}^p(\boldsymbol{\xi} - \boldsymbol{x})$ in a concise form as

$$U_j^{\alpha p}(\boldsymbol{\xi}, \boldsymbol{x}) = \Gamma_\alpha U_j^p(\boldsymbol{\xi} - \boldsymbol{x}) + \Lambda_\alpha \bar{\delta}_{pk} U_j^k(\boldsymbol{\xi} - \bar{\boldsymbol{x}}) \tag{3.13}$$

$$S_{ij}^{\alpha p}(\boldsymbol{\xi}, \boldsymbol{x}) = \Gamma_\alpha S_{ij}^p(\boldsymbol{\xi} - \boldsymbol{x}) + \Lambda_\alpha \bar{\delta}_{pk} S_{ij}^k(\boldsymbol{\xi} - \bar{\boldsymbol{x}}) \tag{3.14}$$

where Γ_α and Λ_α are constants defined by $\Gamma_1 = \Gamma_2 = 1$, $\Lambda_1 = 1$ and $\Lambda_2 = -1$. Here and in what follows, the Greek index α takes the values 1 and 2 and the summation does not apply to the repeated α. It is important to remark that the reduction to integrals over a single crack surface S_c^+ results directly from the continuity of the fundamental solutions $U_j^{\alpha p}(\boldsymbol{\xi}, \boldsymbol{x})$ and $S_{ij}^{\alpha p}(\boldsymbol{\xi}, \boldsymbol{x})$.

By taking spatial derivative of (3.12) along with the relation (3.4) to obtain the strain tensor and then employing the constitutive law (3.2), it yields an integral relation for the stress at an interior point $\boldsymbol{x}$ of the cracked elastic half-space under the boundary condition of BC-type- α:

$$\sigma_{lk}^{\alpha}(\boldsymbol{x}) = \int_{S_c^+} E_{lkpq} \frac{\partial U_j^{\alpha p}(\boldsymbol{\xi}, \boldsymbol{x})}{\partial x_q} \Sigma t_j^0(\boldsymbol{\xi}) dA(\boldsymbol{\xi}) - \int_{S_c^+} E_{lkpq} \frac{\partial S_{ij}^{\alpha p}(\boldsymbol{\xi}, \boldsymbol{x})}{\partial x_q} n_i^+(\boldsymbol{\xi}) \Delta u_j^{\alpha}(\boldsymbol{\xi}) dA(\boldsymbol{\xi}) \tag{3.15}$$

From the relations (3.13) along with (3.9), the kernel $E_{lkpq} \partial U_j^{\alpha p}(\boldsymbol{\xi}, \boldsymbol{x}) / \partial x_q$ can be obtained explicitly in terms of the stress fundamental solution $S_{ij}^p(\boldsymbol{\xi} - \boldsymbol{x})$ for the un-cracked elastic whole space as follows:

$$\begin{aligned} E_{lkpq} \frac{\partial U_j^{\alpha p}(\boldsymbol{\xi}, \boldsymbol{x})}{\partial x_q} &= \Gamma_\alpha E_{lkpq} \frac{\partial U_j^p(\boldsymbol{\xi} - \boldsymbol{x})}{\partial x_q} + \Lambda_\alpha \bar{\delta}_{pm} E_{lkpq} \frac{\partial U_j^m(\boldsymbol{\xi} - \bar{\boldsymbol{x}})}{\partial x_q} \\ &= -\Gamma_\alpha E_{lkpq} \frac{\partial U_p^j(\boldsymbol{\xi} - \boldsymbol{x})}{\partial \xi_q} + \Lambda_\alpha \bar{\delta}_{pm} \bar{\delta}_{ma} \bar{\delta}_{jb} E_{lkpq} \frac{\partial U_b^a(\bar{\boldsymbol{\xi}} - \boldsymbol{x})}{\partial x_q} \\ &= -\Gamma_\alpha E_{lkpq} \frac{\partial U_p^j(\boldsymbol{\xi} - \boldsymbol{x})}{\partial \xi_q} + \Lambda_\alpha \bar{\delta}_{jb} E_{lkpq} \frac{\partial U_p^b(\boldsymbol{x} - \bar{\boldsymbol{\xi}})}{\partial x_q} \end{aligned}$$

$$= -\Gamma_\alpha S_{lk}^{j}(\boldsymbol{\xi}-\boldsymbol{x}) + \Lambda_\alpha \bar{\delta}_{jb} S_{lk}^{b}(\boldsymbol{x}-\bar{\boldsymbol{\xi}}) \tag{3.16}$$

where the following crucial properties have been used:

$$U_j^p(\boldsymbol{\xi}-\boldsymbol{x}) = U_p^j(\boldsymbol{\xi}-\boldsymbol{x}) \tag{3.17}$$

$$U_j^m(\boldsymbol{\xi}-\bar{\boldsymbol{x}}) = \bar{\delta}_{ma}\bar{\delta}_{jb} U_b^a(\bar{\boldsymbol{\xi}}-\boldsymbol{x}) \tag{3.18}$$

$$\partial U_p^j(\boldsymbol{\xi}-\boldsymbol{x})/\partial x_q = -\partial U_p^j(\boldsymbol{\xi}-\boldsymbol{x})/\partial \xi_q \tag{3.19}$$

$$\bar{\delta}_{ia}\bar{\delta}_{aj} = \delta_{ij} \tag{3.20}$$

It should be evident from (3.16) that the kernel $E_{lkpq}\partial U_j^{\alpha p}(\boldsymbol{\xi},\boldsymbol{x})/\partial x_q$ is singular only at $\boldsymbol{\xi}=\boldsymbol{x}$ of $\mathcal{O}(1/r^2)$. From (3.14), the kernel $E_{lkpq}\partial S_{ij}^{\alpha p}(\boldsymbol{\xi},\boldsymbol{x})/\partial x_q$ in (3.15) can be further simplified, in a similar fashion, to

$$\begin{aligned}
E_{lkpq}\frac{\partial S_{ij}^{\alpha p}(\boldsymbol{\xi},\boldsymbol{x})}{\partial x_q} &= \Gamma_\alpha E_{lkpq}\frac{\partial S_{ij}^{p}(\boldsymbol{\xi}-\boldsymbol{x})}{\partial x_q} + \Lambda_\alpha \bar{\delta}_{pm} E_{lkpq}\frac{\partial S_{ij}^{m}(\boldsymbol{\xi}-\bar{\boldsymbol{x}})}{\partial x_q} \\
&= -\Gamma_\alpha E_{lkpq}\frac{\partial S_{ij}^{p}(\boldsymbol{\xi}-\boldsymbol{x})}{\partial \xi_q} + \Lambda_\alpha \bar{\delta}_{pm}\bar{\delta}_{ia}\bar{\delta}_{jb}\bar{\delta}_{mc} E_{lkpq}\frac{\partial S_{ab}^{c}(\bar{\boldsymbol{\xi}}-\boldsymbol{x})}{\partial x_q} \\
&= -\Gamma_\alpha E_{lkpq}\frac{\partial S_{ij}^{p}(\boldsymbol{\xi}-\boldsymbol{x})}{\partial \xi_q} - \Lambda_\alpha \bar{\delta}_{ia}\bar{\delta}_{jb} E_{lkpq}\frac{\partial S_{ab}^{p}(\boldsymbol{x}-\bar{\boldsymbol{\xi}})}{\partial x_q} \\
&= -\Gamma_\alpha \Sigma_{ij}^{lk}(\boldsymbol{\xi}-\boldsymbol{x}) - \Lambda_\alpha \bar{\delta}_{ia}\bar{\delta}_{jb}\Sigma_{ab}^{lk}(\boldsymbol{x}-\bar{\boldsymbol{\xi}})
\end{aligned} \tag{3.21}$$

where the function $\Sigma_{ij}^{lk}(\boldsymbol{\xi}-\boldsymbol{x})$ can be given in terms of the stress fundamental solution $S_{ij}^{p}(\boldsymbol{\xi}-\boldsymbol{x})$ of the un-cracked elastic whole space by

$$\Sigma_{ij}^{lk}(\boldsymbol{\xi}-\boldsymbol{x}) = E_{lkpq}\frac{\partial S_{ij}^{p}(\boldsymbol{\xi}-\boldsymbol{x})}{\partial \xi_q} \tag{3.22}$$

In addition, to obtain the final expression (3.21), the relation (3.20) and the following properties have also been employed:

$$\partial S_{ij}^{p}(\boldsymbol{\xi}-\boldsymbol{x})/\partial x_q = -\partial S_{ij}^{p}(\boldsymbol{\xi}-\boldsymbol{x})/\partial \xi_q \tag{3.23}$$

$$S_{ij}^{m}(\boldsymbol{\xi}-\bar{\boldsymbol{x}}) = \bar{\delta}_{ia}\bar{\delta}_{jb}\bar{\delta}_{mc} S_{ab}^{c}(\bar{\boldsymbol{\xi}}-\boldsymbol{x}) \tag{3.24}$$

$$S_{ab}^{c}(\bar{\boldsymbol{\xi}}-\boldsymbol{x}) = -S_{ab}^{c}(\boldsymbol{x}-\bar{\boldsymbol{\xi}}) \tag{3.25}$$

From (3.21), (3.22) and the singularity behavior of the fundamental solution $S_{ij}^{p}(\boldsymbol{\xi}-\boldsymbol{x})$, the kernel $E_{lkpq}\partial S_{ij}^{\alpha p}(\boldsymbol{\xi},\boldsymbol{x})/\partial x_q$ is singular only at $\boldsymbol{\xi}=\boldsymbol{x}$ of $\mathcal{O}(1/r^3)$. It should be noted that the boundary integral relations (3.12) and (3.15) can be used to compute the displacements and stresses at any interior point $\boldsymbol{x}$ provided that all unknown crack-face data is completely known. By taking an appropriate limit process of the boundary integral relation (3.12) to a point on the crack face, it yield the conventional integral equation for the sum of the crack-face displacement. However, such the displacement integral equation is mathematically degenerate and not sufficient for solving the key unknowns on the crack face. This is due to the coincidence of the crack surfaces S_c^+ and S_c^- that renders the final displacement boundary integral equation containing incomplete, crack-face traction data (i.e., it involves only the sum of the crack-face tractions). To overcome this mathematical difficulty, the integral equation of the jump in the traction across the crack surfaces is additionally required in the formulation of the governing equation. Such the integral equation can readily be constructed from the boundary integral relation for the stress (3.15) by taking the appropriate limit to any point on the crack surface S_c^+. Although the conventional traction boundary integral equation is sufficient for performing the stress analysis of cracked bodies, it still contains both the strongly singular kernels $S_{ij}^{\alpha p}(\boldsymbol{\xi},\boldsymbol{x})$ and $E_{lkpq}\partial U_j^{\alpha p}(\boldsymbol{\xi},\boldsymbol{x})/\partial x_q$ of order $\mathcal{O}(1/r^2)$ and the hyper-singular kernel $E_{lkpq}\partial S_{ij}^{\alpha p}(\boldsymbol{\xi},\boldsymbol{x})/\partial x_q$ of order $\mathcal{O}(1/r^3)$ that render the involved integrals difficult to be interpreted theoretically and treated numerically.

3.5 Decompositions of Strongly Singular and Hypersingular Kernels

To aid the regularization procedure of the boundary integral relations (3.12) and (3.15), the strongly singular kernels $S_{ij}^{\alpha p}(\boldsymbol{\xi},\boldsymbol{x})$ and $E_{lkpq}\partial U_j^{\alpha p}(\boldsymbol{\xi},\boldsymbol{x})/\partial x_q$ and the hypersingular kernel $E_{lkpq}\partial S_{ij}^{\alpha p}(\boldsymbol{\xi},\boldsymbol{x})/\partial x_q$ are, first, decomposed into a form suiting the integration by parts through well-known Stokes' theorem described in the next section. The key component to achieve such crucial task is based on the special decompositions of the strongly singular kernel $S_{ij}^{p}(\boldsymbol{\xi}-\boldsymbol{x})$ and the hypersingular kernel $\Sigma_{ij}^{lk}(\boldsymbol{\xi}-\boldsymbol{x})$ associated with the un-cracked elastic whole space proposed by Rungamornrat and Mear (2008a):

$$S_{ij}^{p}(\boldsymbol{\xi}-\boldsymbol{x}) = H_{ij}^{p}(\boldsymbol{\xi}-\boldsymbol{x}) + \varepsilon_{ism}\frac{\partial}{\partial \xi_s}G_{mj}^{p}(\boldsymbol{\xi}-\boldsymbol{x}) \tag{3.26}$$

$$\Sigma_{ij}^{lk}(\boldsymbol{\xi}-\boldsymbol{x}) = -E_{ijkl}\delta(\boldsymbol{\xi}-\boldsymbol{x}) + \varepsilon_{ism}\frac{\partial}{\partial \xi_s}\varepsilon_{lrt}\frac{\partial}{\partial \xi_r}C_{mj}^{tk}(\boldsymbol{\xi}-\boldsymbol{x}) \tag{3.27}$$

where ε_{ism} is an alternating symbol, $\delta(\boldsymbol{\xi}-\boldsymbol{x})$ denote the Dirac-delta function with the center at a point $\boldsymbol{x}$, and the functions $H_{ij}^{p}(\boldsymbol{\xi}-\boldsymbol{x})$, $G_{mj}^{p}(\boldsymbol{\xi}-\boldsymbol{x})$ and $C_{mj}^{tk}(\boldsymbol{\xi}-\boldsymbol{x})$ are defined by

$$H_{ij}^{p}(\boldsymbol{\xi}-\boldsymbol{x}) = -\delta_{jp}\frac{\xi_i - x_i}{4\pi r^3} \tag{3.28}$$

$$G_{mj}^{p}(\boldsymbol{\xi}-\boldsymbol{x}) = \frac{\varepsilon_{mqa}E_{qjkl}}{8\pi^2 r}\oint_{\mathbf{z}\cdot\mathbf{r}=0}(z,z)_{kp}^{-1}z_a z_l ds(z) \tag{3.29}$$

$$C_{mj}^{tk}(\boldsymbol{\xi}-\boldsymbol{x}) = \frac{A_{mtsl}^{kjap}}{8\pi^2 r}\oint_{\mathbf{z}\cdot\mathbf{r}=0}(z,z)_{ap}^{-1}z_s z_l ds(z),\ A_{mtsl}^{kjap} = \varepsilon_{ptd}\varepsilon_{pmq}\left\{E_{djpl}E_{qkms} - \frac{1}{3}E_{lmps}E_{djkq}\right\} \tag{3.30}$$

For isotropic materials, the functions $G_{mj}^{p}(\boldsymbol{\xi}-\boldsymbol{x})$ and $C_{mj}^{tk}(\boldsymbol{\xi}-\boldsymbol{x})$ are provided in a closed form (see the work of Li, 1996)

$$G_{mj}^{p}(\boldsymbol{\xi}-\boldsymbol{x}) = \frac{1}{8\pi(1-\nu)r}\left[(1-2\nu)\varepsilon_{mpj} + \varepsilon_{ijm}\frac{(\xi_i - x_i)(\xi_p - x_p)}{r^2}\right] \tag{3.31}$$

$$C_{mj}^{tk}(\boldsymbol{\xi}-\boldsymbol{x}) = \frac{\mu}{4\pi(1-\nu)r}\left[(1-\nu)\delta_{tk}\delta_{mj} + 2\nu\delta_{tj}\delta_{km} - \delta_{tm}\delta_{kj} - \delta_{tm}\frac{(\xi_k - x_k)(\xi_j - x_j)}{r^2}\right] \tag{3.32}$$

Note, in addition, that the kernel $H_{ij}^{p}(\boldsymbol{\xi}-\boldsymbol{x})$ is clearly independent of material constants and is singular only at $\boldsymbol{\xi}=\boldsymbol{x}$ of $\mathcal{O}(1/r^2)$ whereas $G_{mj}^{p}(\boldsymbol{\xi}-\boldsymbol{x})$ and $C_{mj}^{tk}(\boldsymbol{\xi}-\boldsymbol{x})$ depends primarily on material properties and are singular only at $\boldsymbol{\xi}=\boldsymbol{x}$ of $\mathcal{O}(1/r)$.

By using the decomposition (3.26) along with the relation (3.14), it leads to the decomposition of the strongly singular kernel $S_{ij}^{\alpha p}(\boldsymbol{\xi},\boldsymbol{x})$:

$$S_{ij}^{\alpha p}(\boldsymbol{\xi},\boldsymbol{x}) = H_{ij}^{\alpha p}(\boldsymbol{\xi},\boldsymbol{x}) + \varepsilon_{ism}\frac{\partial}{\partial \xi_s}G_{mj}^{\alpha p}(\boldsymbol{\xi},\boldsymbol{x}) \tag{3.33}$$

where the functions $H_{ij}^{\alpha p}(\boldsymbol{\xi},\boldsymbol{x})$ and $G_{mj}^{\alpha p}(\boldsymbol{\xi},\boldsymbol{x})$ are defined by

$$H_{ij}^{\alpha p}(\boldsymbol{\xi},\boldsymbol{x}) = \Gamma_\alpha H_{ij}^{p}(\boldsymbol{\xi}-\boldsymbol{x}) + \Lambda_\alpha\bar{\delta}_{pk}H_{ij}^{k}(\boldsymbol{\xi}-\bar{\boldsymbol{x}}) \tag{3.34}$$

$$G_{mj}^{\alpha p}(\boldsymbol{\xi},\boldsymbol{x}) = \Gamma_\alpha G_{mj}^{p}(\boldsymbol{\xi}-\boldsymbol{x}) + \Lambda_\alpha\bar{\delta}_{pk}G_{mj}^{k}(\boldsymbol{\xi}-\bar{\boldsymbol{x}}) \tag{3.35}$$

Similarly, by using again the decomposition (3.26) along with the expression (3.16), it results in

$$E_{lkpq}\frac{\partial U_j^{\alpha p}(\boldsymbol{\xi},\boldsymbol{x})}{\partial x_q} = H_{lk}^{\alpha j}(\boldsymbol{x},\boldsymbol{\xi}) + \varepsilon_{lrt}\frac{\partial}{\partial x_r}G_{tk}^{\alpha j}(\boldsymbol{x},\boldsymbol{\xi}) \tag{3.36}$$

in which the fact that $H_{lk}^{j}(\boldsymbol{\xi}-\boldsymbol{x})$ and $G_{mj}^{p}(\boldsymbol{\xi}-\boldsymbol{x})$ are odd and even functions, respectively, has been utilized. Finally, by applying the decomposition (3.27) along with the relation (3.21), it yields the decomposition of the hypersingular kernel $E_{lkpq}\partial S_{ij}^{\alpha p}(\boldsymbol{\xi},\boldsymbol{x})/\partial x_q$:

$$E_{lkpq}\frac{\partial S_{ij}^{\alpha p}(\boldsymbol{\xi},\boldsymbol{x})}{\partial x_q} = \Gamma_\alpha E_{ijkl}\delta(\boldsymbol{\xi}-\boldsymbol{x}) - \Lambda_\alpha \bar{\delta}_{ia}\bar{\delta}_{jb}E_{abkl}\delta(\boldsymbol{x}-\bar{\boldsymbol{\xi}}) + \varepsilon_{ism}\frac{\partial}{\partial \xi_s}\varepsilon_{lrt}\frac{\partial}{\partial x_r}C_{mj}^{\alpha tk}(\boldsymbol{\xi},\boldsymbol{x}) \tag{3.37}$$

where the kernel $C_{mj}^{\alpha tk}(\boldsymbol{\xi},\boldsymbol{x})$ is given by

$$C_{mj}^{\alpha tk}(\boldsymbol{\xi},\boldsymbol{x}) = \Gamma_\alpha C_{mj}^{tk}(\boldsymbol{\xi}-\boldsymbol{x}) - \Lambda_\alpha \bar{\delta}_{am}\bar{\delta}_{bj}C_{ab}^{tk}(\boldsymbol{x}-\bar{\boldsymbol{\xi}}) \tag{3.38}$$

and following important properties have been employed:

$$\partial C_{mj}^{tk}(\boldsymbol{\xi}-\boldsymbol{x})/\partial \xi_q = -\partial C_{mj}^{tk}(\boldsymbol{\xi}-\boldsymbol{x})/\partial x_q \tag{3.39}$$

$$\partial C_{mj}^{tk}(\boldsymbol{x}-\bar{\boldsymbol{\xi}})/\partial x_q = -\partial C_{mj}^{tk}(\boldsymbol{x}-\bar{\boldsymbol{\xi}})/\partial \bar{\xi}_q \tag{3.40}$$

$$\partial(\cdot)/\partial \bar{\xi}_q = \bar{\delta}_{mq}\partial(\cdot)/\partial \xi_q \tag{3.41}$$

$$\varepsilon_{ijk} = -\bar{\delta}_{ia}\bar{\delta}_{jb}\bar{\delta}_{kc}\varepsilon_{abc} \tag{3.42}$$

3.6 Weakly Singular Integral Equation for BC-type-1 and BC-type-2

In this particular section, a pair of regularized boundary integral equations, one for the crack-face displacement and the other for the crack-face traction, is established. The special decompositions (3.33), (3.36) and (3.37) are employed along with Stokes' theorem to carry out the integration by parts of both hypersingular and strongly singular integrals in order to shift the derivatives from involved kernels to the crack-face data. This regularization procedure is similar to that used by Rungamornrat and Mear (2008a) and Rungamornrat and Senjuntichai (2009).

3.6.1 Weakly Singular Integral Equation for Displacement

To establish the regularized boundary integral relation for the displacement at any interior point $\boldsymbol{x} \in \Omega$, the special decomposition (3.33) is first substituted into the integral relation (3.12) to obtain

$$u_p^{\alpha}(\boldsymbol{x}) = \int_{S_c^+} U_j^{\alpha p}(\boldsymbol{\xi}, \boldsymbol{x}) \Sigma t_j^0(\boldsymbol{\xi}) dA(\boldsymbol{\xi}) - \int_{S_c^+} H_{ij}^{\alpha p}(\boldsymbol{\xi}, \boldsymbol{x}) n_i^+(\boldsymbol{\xi}) \Delta u_j^{\alpha}(\boldsymbol{\xi}) dA(\boldsymbol{\xi}) - \int_{S_c^+} \Delta u_j^{\alpha}(\boldsymbol{\xi}) D_m G_{mj}^{\alpha p}(\boldsymbol{\xi}, \boldsymbol{x}) dA(\boldsymbol{\xi}) \tag{3.43}$$

where $D_m(\cdot)$ denotes the surface differential operator given by

$$D_m(\cdot) = n_i \varepsilon_{ism} \frac{\partial(\cdot)}{\partial \xi_s} \tag{3.44}$$

Upon performing the integration by parts of a term containing curl of the function $G_{mj}^p(\boldsymbol{\xi} - \boldsymbol{x})$ via Stokes' theorem and then using the property that the jump in the crack-face displacement Δu_j^{α} identically vanishes along the crack front (i.e., $\Delta u_j^{\alpha} = 0$ on ∂S_c^+), it finally yields

$$u_p^{\alpha}(\boldsymbol{x}) = \int_{S_c^+} U_j^{\alpha p}(\boldsymbol{\xi}, \boldsymbol{x}) \Sigma t_j^0(\boldsymbol{\xi}) dA(\boldsymbol{\xi}) - \int_{S_c^+} H_{ij}^{\alpha p}(\boldsymbol{\xi}, \boldsymbol{x}) n_i^+(\boldsymbol{\xi}) \Delta u_j^{\alpha}(\boldsymbol{\xi}) dA(\boldsymbol{\xi}) + \int_{S_c^+} G_{mj}^{\alpha p}(\boldsymbol{\xi}, \boldsymbol{x}) D_m \Delta u_j^{\alpha}(\boldsymbol{\xi}) dA(\boldsymbol{\xi}) \tag{3.45}$$

By taking limit $\boldsymbol{x} \to \boldsymbol{y} \in S_c^+$ of (3.45), we then obtain the integral equation of the sum of the crack-face displacements as

$$c(\boldsymbol{y}) \Sigma u_p^{\alpha}(\boldsymbol{y}) = \int_{S_c^+} U_j^{\alpha p}(\boldsymbol{\xi}, \boldsymbol{y}) \Sigma t_j^0(\boldsymbol{\xi}) dA(\boldsymbol{\xi}) - \int_{S_c^+} H_{ij}^{\alpha p}(\boldsymbol{\xi}, \boldsymbol{y}) n_i^+(\boldsymbol{\xi}) \Delta u_j^{\alpha}(\boldsymbol{\xi}) dA(\boldsymbol{\xi}) + \int_{S_c^+} G_{mj}^{\alpha p}(\boldsymbol{\xi}, \boldsymbol{y}) D_m \Delta u_j^{\alpha}(\boldsymbol{\xi}) dA(\boldsymbol{\xi}) \tag{3.46}$$

where *c* is a function defined such that $c(\boldsymbol{y}) = 1/2$ if the surface is smooth at a point $\boldsymbol{y}$ (i.e., the unit normal vector $\boldsymbol{n}$ at $\boldsymbol{y}$ is well-defined), otherwise $c(\boldsymbol{y}) \in (0, 1)$ and $\Sigma u_p^{\alpha}(\boldsymbol{y}) = u_p^{\alpha+}(\boldsymbol{y}) + u_p^{\alpha-}(\boldsymbol{y})$ denotes the sum of the crack-face displacement. By multiplying (3.46) with a sufficiently smooth test function $\tilde{t}_p(\boldsymbol{y})$ and then integrating

the product over the whole crack surface S_c^+, it finally leads to a weakly-singular, weak-form integral equation for the crack-face displacement as

$$\begin{aligned}\frac{1}{2}\int_{S_c^+}\tilde{t}_p(\boldsymbol{y})\Sigma u_p^{\alpha}(\boldsymbol{y})dA(\boldsymbol{y}) &= \int_{S_c^+}\tilde{t}_p(\boldsymbol{y})\int_{S_c^+}U_j^{\alpha p}(\boldsymbol{\xi},\boldsymbol{y})\Sigma t_j^0(\boldsymbol{\xi})dA(\boldsymbol{\xi})dA(\boldsymbol{y}) \\ &+\int_{S_c^+}\tilde{t}_p(\boldsymbol{y})\int_{S_c^+}G_{mj}^{\alpha p}(\boldsymbol{\xi},\boldsymbol{y})D_m\Delta u_j^{\alpha}(\boldsymbol{\xi})dA(\boldsymbol{\xi})dS(\boldsymbol{y}) \\ &-\int_{S_c^+}\tilde{t}_p(\boldsymbol{y})\int_{S_c^+}H_{ij}^{\alpha p}(\boldsymbol{\xi},\boldsymbol{y})n_i^+(\boldsymbol{\xi})\Delta u_j^{\alpha}(\boldsymbol{\xi})dA(\boldsymbol{\xi})dS(\boldsymbol{y})\end{aligned} \tag{3.47}$$

Note that the function $c = c(\boldsymbol{y})$ simply reduces to 1/2 since the crack face is assumed piecewise smooth (i.e., a set of all points $\boldsymbol{y}$ that the unit normal vector $\boldsymbol{n}$ is not defined is of measure zero). It should be remarked that the weak-form boundary integral equation (3.47) contains only weakly singular kernels $U_j^{\alpha p}(\boldsymbol{\xi},\boldsymbol{y})$, $G_{mj}^{\alpha p}(\boldsymbol{\xi},\boldsymbol{y})$ and $H_{ij}^{\alpha p}(\boldsymbol{\xi},\boldsymbol{y})n_i^+(\boldsymbol{\xi})$ of $\mathcal{O}(1/r)$.

3.6.2 Weakly Singular Integral Equation for Traction

To establish a weakly singular, weak-form integral equation for the crack-face traction, a similar procedure as described in the previous subsection is employed. First, the special decompositions (3.36) and (3.37) are substituted into the integral relation for the stress (3.15) to obtain

$$\begin{aligned}\sigma_{lk}^{\alpha}(\boldsymbol{x}) &= \int_{S_c^+}H_{lk}^{\alpha j}(\boldsymbol{x},\boldsymbol{\xi})\Sigma t_j^0(\boldsymbol{\xi})dA(\boldsymbol{\xi}) + \varepsilon_{lrt}\frac{\partial}{\partial x_r}\left\{\int_{S_c^+}G_{tk}^{\alpha j}(\boldsymbol{x},\boldsymbol{\xi})\Sigma t_j^0(\boldsymbol{\xi})dA(\boldsymbol{\xi})\right\} \\ &-\int_{S_c^+}D_m\left\{\varepsilon_{lrt}\frac{\partial}{\partial x_r}C_{mj}^{\alpha tk}(\boldsymbol{\xi},\boldsymbol{x})\right\}\Delta u_j^{\alpha}(\boldsymbol{\xi})dA(\boldsymbol{\xi})\end{aligned} \tag{3.48}$$

By, again, carrying out the integration by parts of the third integral on the right hand side using Stokes' theorem, it gives rise to the regularized boundary integral relation for the stress at any interior point $\boldsymbol{x}\in\Omega$:

$$\begin{aligned}\sigma_{lk}^{\alpha}(\boldsymbol{x}) &= \varepsilon_{lrt}\frac{\partial}{\partial x_r}\left\{\int_{S_c^+}G_{tk}^{\alpha j}(\boldsymbol{x},\boldsymbol{\xi})\Sigma t_j^0(\boldsymbol{\xi})dA(\boldsymbol{\xi}) + \int_{S_c^+}C_{mj}^{\alpha tk}(\boldsymbol{\xi},\boldsymbol{x})D_m\Delta u_j^{\alpha}(\boldsymbol{\xi})dA(\boldsymbol{\xi})\right\} \\ &+\int_{S_c^+}H_{lk}^{\alpha j}(\boldsymbol{x},\boldsymbol{\xi})\Sigma t_j^0(\boldsymbol{\xi})dA(\boldsymbol{\xi})\end{aligned} \tag{3.49}$$

It is noted that the boundary integral relation for the stress (3.49) still contains strongly singular kernels of $\mathcal{O}(1/r^2)$. By further forming the product $n_l^+(\boldsymbol{y})\sigma_{lk}^{\alpha}(\boldsymbol{x})$ where $\boldsymbol{y} \in S_c^+$ and then taking appropriate limit $\boldsymbol{x} \to \boldsymbol{y}$, it leads to an integral equation for the jump in the crack-face traction as

$$\begin{aligned}\rho(\boldsymbol{y})\Delta t_k^0(\boldsymbol{y}) = D_t \left\{ \int_{S_c^+} G_{tk}^{\alpha j}(\boldsymbol{y},\boldsymbol{\xi})\Sigma t_j^0(\boldsymbol{\xi})dA(\boldsymbol{\xi}) + \int_{S_c^+} C_{mj}^{\alpha tk}(\boldsymbol{\xi},\boldsymbol{y})D_m \Delta u_j^{\alpha}(\boldsymbol{\xi})dA(\boldsymbol{\xi}) \right\} \\ + n_l^+(\boldsymbol{y}) \int_{S_c^+} H_{lk}^{\alpha j}(\boldsymbol{y},\boldsymbol{\xi})\Sigma t_j^0(\boldsymbol{\xi})dA(\boldsymbol{\xi})\end{aligned} \tag{3.50}$$

where ρ is a function defined such that $\rho(\boldsymbol{y})$ = 1/2 if the crack surface is smooth at point $\boldsymbol{y}$ otherwise $\rho(\boldsymbol{y}) \in (0, 1)$ and $\Delta t_k^0(\boldsymbol{\xi}) = t_k^{0+}(\boldsymbol{\xi}) - t_k^{0-}(\boldsymbol{\xi})$ represents the jump in the crack-face traction across the crack surface. Upon multiplying the boundary integral equation (3.50) by a smooth, well-defined test function $\Delta\tilde{u}_k(\boldsymbol{y})$, forming the integration of the product over the whole crack surface S_c^+, carrying out the integration by parts through Stokes' theorem, and using the fact that the test function $\Delta\tilde{u}_k(\boldsymbol{y})$ satisfies the homogeneous condition along the crack front, it finally yields a completely regularized weak-form boundary integral equation for the jump in the crack-face traction:

$$\begin{aligned}\frac{1}{2}\int_{S_c^+} \Delta\tilde{u}_k(\mathbf{y})\Delta t_k^0(\mathbf{y})dA(\mathbf{y}) = \int_{S_c^+} \Delta\tilde{u}_k(\mathbf{y}) \int_{S_c^+} H_{lk}^{\alpha j}(\mathbf{y},\boldsymbol{\xi}) n_l^+(\mathbf{y})\Sigma t_j^0(\boldsymbol{\xi})dA(\boldsymbol{\xi})dA(\mathbf{y}) \\ - \int_{S_c^+} D_t\Delta\tilde{u}_k(\mathbf{y}) \int_{S_c^+} G_{tk}^{\alpha j}(\mathbf{y},\boldsymbol{\xi})\Sigma t_j^0(\boldsymbol{\xi})dA(\boldsymbol{\xi})dA(\mathbf{y}) \\ - \int_{S_c^+} D_t\Delta\tilde{u}_k(\mathbf{y}) \int_{S_c^+} C_{mj}^{\alpha tk}(\boldsymbol{\xi},\mathbf{y})D_m\Delta u_j^{\alpha}(\boldsymbol{\xi})dA(\boldsymbol{\xi})dA(\mathbf{y})\end{aligned} \tag{3.51}$$

Again, from the assumption that the crack surface is piecewise smooth, the function $\rho(\boldsymbol{y})$ simply reduces to 1/2. It is remarked that the boundary integral equation (3.51) involves only weakly singular kernels $H_{lk}^{\alpha j}(\boldsymbol{y},\boldsymbol{\xi})n_l^+(\boldsymbol{y})$, $G_{tk}^{\alpha j}(\boldsymbol{y},\boldsymbol{\xi})$ and $C_{mj}^{\alpha tk}(\boldsymbol{\xi},\boldsymbol{y})$ of $\mathcal{O}(1/r)$.

While the two equations (3.47) and (3.51) form a sufficient system of governing integral equations for determining the crack-face unknown data, the two relations (3.45) and (3.49) can be utilized to compute the displacements and stresses at any interior point of the body once the crack-face unknowns are solved.

3.7 Treatment of Cracked Half-Space under BC-type-*I* (for *I* = 3, 4)

By applying the reciprocal theorem to the cracked elastic half-space Ω subjected to the boundary condition of BC-type-*I* (*I* = 1, 2, 3, 4) along with the elastic state associated with a fundamental problem of the un-cracked half-space under the same type of boundary conditions on the half-space surface, the standard integral relations for the displacement and stress at any interior point of the cracked half-space can be generalized to

$$u_p^I(\boldsymbol{x}) = \int_{S_c^+} U_j^{Ip}(\boldsymbol{\xi},\boldsymbol{x})\Sigma t_j^0(\boldsymbol{\xi})dA(\boldsymbol{\xi}) - \int_{S_c^+} S_{ij}^{Ip}(\boldsymbol{\xi},\boldsymbol{x})n_i^+(\boldsymbol{\xi})\Delta u_j^I(\boldsymbol{\xi})dA(\boldsymbol{\xi}) \tag{3.52}$$

$$\sigma_{lk}^I(\boldsymbol{x}) = \int_{S_c^+} E_{lkpq}\frac{\partial U_j^{Ip}(\boldsymbol{\xi},\boldsymbol{x})}{\partial x_q}\Sigma t_j^0(\boldsymbol{\xi})dA(\boldsymbol{\xi}) - \int_{S_c^+} E_{lkpq}\frac{\partial S_{ij}^{Ip}(\boldsymbol{\xi},\boldsymbol{x})}{\partial x_q}n_i^+(\boldsymbol{\xi})\Delta u_j^I(\boldsymbol{\xi})dA(\boldsymbol{\xi}) \tag{3.53}$$

where $U_j^{Ip}(\boldsymbol{\xi},\boldsymbol{x})$ and $S_{ij}^{Ip}(\boldsymbol{\xi},\boldsymbol{x})$ are the displacement and stress fundamental solutions of an un-cracked half space under BC-type-*I* and the summation does not apply to the repeated index *I*.

To completely regularize the boundary integral relations (3.52) and (3.53) for the two remaining boundary conditions BC-type-*I* (*I* = 3, 4), the same regularization procedure can be used and the special decompositions of the strongly singular kernels $S_{ij}^{Ip}(\boldsymbol{\xi},\boldsymbol{x})$ and $E_{lkpq}\partial U_j^{Ip}(\boldsymbol{\xi},\boldsymbol{x})/\partial x_q$ and the hypersingular kernel $E_{lkpq}\partial S_{ij}^{Ip}(\boldsymbol{\xi},\boldsymbol{x})/\partial x_q$ play an important role in such development. To derive those decompositions, the superposition technique similar to that employed by Li (1996) can be adopted. More specifically, the problem of a cracked half-space under BC-type-3 can be treated as a linear combination of two sub-problems, a sub-problem-1 associated with the original cracked half-space with the boundary condition BC-type-3 on the free surface being replaced by the boundary condition BC-type-1 and a sub-problem-2 corresponding to an un-cracked half-space subjected only to the normal traction opposite to that generated on the free surface of the sub-problem-1. Similarly, the problem of a cracked half-space under the boundary condition BC-type-4 can also be treated as a linear combination of two sub-problems: a sub-problem-1 associated with the original cracked half-space with the boundary condition BC-type-4 on the free surface being replaced by the boundary condition BC-type-2 and a sub-problem-2 corresponding to an un-cracked half-space subjected only to the shear traction opposite to that generated on the free surface of the sub-problem-2. Based on above linear combinations, the kernels

$S_{ij}^{Ip}(\boldsymbol{\xi},\boldsymbol{x})$, $E_{lkpq}\partial U_j^{Ip}(\boldsymbol{\xi},\boldsymbol{x})/\partial x_q$, and $E_{lkpq}\partial S_{ij}^{Ip}(\boldsymbol{\xi},\boldsymbol{x})/\partial x_q$ for I = 3 and 4 can be written in terms of the known results corresponding to BC-type-α and the correction terms as

$$S_{ij}^{3p}(\boldsymbol{\xi},\boldsymbol{x}) = S_{ij}^{1p}(\boldsymbol{\xi},\boldsymbol{x}) + \hat{S}_{ij}^{3p}(\boldsymbol{\xi},\boldsymbol{x}) \tag{3.54}$$

$$S_{ij}^{4p}(\boldsymbol{\xi},\boldsymbol{x}) = S_{ij}^{1p}(\boldsymbol{\xi},\boldsymbol{x}) + \hat{S}_{ij}^{4p}(\boldsymbol{\xi},\boldsymbol{x}) \tag{3.55}$$

$$E_{lkpq}\frac{\partial U_j^{3p}(\boldsymbol{\xi},\boldsymbol{x})}{\partial x_q} = E_{lkpq}\frac{\partial U_j^{1p}(\boldsymbol{\xi},\boldsymbol{x})}{\partial x_q} + E_{lkpq}\frac{\partial \hat{U}_j^{3p}(\boldsymbol{\xi},\boldsymbol{x})}{\partial x_q} \tag{3.56}$$

$$E_{lkpq}\frac{\partial U_j^{4p}(\boldsymbol{\xi},\boldsymbol{x})}{\partial x_q} = E_{lkpq}\frac{\partial U_j^{2p}(\boldsymbol{\xi},\boldsymbol{x})}{\partial x_q} + E_{lkpq}\frac{\partial \hat{U}_j^{4p}(\boldsymbol{\xi},\boldsymbol{x})}{\partial x_q} \tag{3.57}$$

$$E_{lkpq}\frac{\partial S_{ij}^{3p}(\boldsymbol{\xi},\boldsymbol{x})}{\partial x_q} = E_{lkpq}\frac{\partial S_{ij}^{1p}(\boldsymbol{\xi},\boldsymbol{x})}{\partial x_q} + E_{lkpq}\frac{\partial \hat{S}_{ij}^{3p}(\boldsymbol{\xi},\boldsymbol{x})}{\partial x_q} \tag{3.58}$$

$$E_{lkpq}\frac{\partial S_{ij}^{4p}(\boldsymbol{\xi},\boldsymbol{x})}{\partial x_q} = E_{lkpq}\frac{\partial S_{ij}^{2p}(\boldsymbol{\xi},\boldsymbol{x})}{\partial x_q} + E_{lkpq}\frac{\partial \hat{S}_{ij}^{4p}(\boldsymbol{\xi},\boldsymbol{x})}{\partial x_q} \tag{3.59}$$

where the correction terms $\hat{S}_{ij}^{Ip}(\boldsymbol{\xi},\boldsymbol{x})$, $E_{lkpq}\partial \hat{U}_j^{Ip}(\boldsymbol{\xi},\boldsymbol{x})/\partial x_q$, and $E_{lkpq}\partial \hat{S}_{ij}^{Ip}(\boldsymbol{\xi},\boldsymbol{x})/\partial x_q$ are obtained by solving the sub-problem-2 for each type of boundary conditions. From the regularity of the sub-problem-2, it can readily be verified from the divergence-free condition that all the functions $\hat{S}_{ij}^{Ip}(\boldsymbol{\xi},\boldsymbol{x})$, $E_{lkpq}\partial \hat{U}_j^{Ip}(\boldsymbol{\xi},\boldsymbol{x})/\partial x_q$ and $E_{lkpq}\partial \hat{S}_{ij}^{Ip}(\boldsymbol{\xi},\boldsymbol{x})/\partial x_q$ admit the following representations

$$\hat{S}_{ij}^{Ip}(\boldsymbol{\xi},\boldsymbol{x}) = \varepsilon_{ism}\frac{\partial}{\partial \xi_s}\hat{G}_{mj}^{Ip}(\boldsymbol{\xi},\boldsymbol{x}) \tag{3.60}$$

$$E_{lkpq}\frac{\partial \hat{U}_j^{Ip}(\boldsymbol{\xi},\boldsymbol{x})}{\partial x_q} = \varepsilon_{lrt}\frac{\partial}{\partial x_r}\hat{G}_{tk}^{Ij}(\boldsymbol{x},\boldsymbol{\xi}) \tag{3.61}$$

$$E_{lkpq}\frac{\partial \hat{S}_{ij}^{Ip}(\boldsymbol{\xi},\boldsymbol{x})}{\partial x_q} = \varepsilon_{ism}\frac{\partial}{\partial \xi_s}\varepsilon_{lrt}\frac{\partial}{\partial x_r}\hat{C}_{mj}^{Itk}(\boldsymbol{\xi},\boldsymbol{x}) \tag{3.62}$$

where $\hat{G}_{mj}^{Ip}(\boldsymbol{\xi},\boldsymbol{x})$ and $\hat{C}_{mj}^{Itk}(\boldsymbol{\xi},\boldsymbol{x})$ are functions that are singular only at a point $\boldsymbol{\xi} = \bar{\boldsymbol{x}}$ of $\mathcal{O}(1/r)$. While the existence of the representations (3.60)-(3.62) can be ensured, determination of both functions $\hat{G}_{mj}^{Ip}(\boldsymbol{\xi},\boldsymbol{x})$ and $\hat{C}_{mj}^{Itk}(\boldsymbol{\xi},\boldsymbol{x})$ is nontrivial and generally requires solving a system of linear partial differential equations.

For an isotropic elastic half-space, the functions $\hat{G}_{mj}^{Ip}(\boldsymbol{\xi},\boldsymbol{x})$ and $\hat{C}_{mj}^{Itk}(\boldsymbol{\xi},\boldsymbol{x})$ were successfully developed by Li (1996). In his study, the sub-problem-2 for both types of boundary conditions indicated above was solved first using the method of displacement representation in terms of Papovich-Neuber potentials and the functions $\hat{G}_{mj}^{Ip}(\boldsymbol{\xi},\boldsymbol{x})$ and $\hat{C}_{mj}^{Itk}(\boldsymbol{\xi},\boldsymbol{x})$ in the representations (3.60)-(3.62) were derived indirectly and equivalently using the method of stress functions. The explicit expressions for BC-type-3 are given by

$$\hat{G}_{mj}^{3p}(\boldsymbol{\xi},\boldsymbol{x})=\frac{1}{2\mu}[x_3\frac{\partial M_{mj}(\boldsymbol{\xi},\boldsymbol{x})}{\partial x_p}-(3-4\nu)\delta_{3p}M_{mj}(\boldsymbol{\xi},\boldsymbol{x})+\frac{\partial N_{mj}(\boldsymbol{\xi},\boldsymbol{x})}{\partial x_p}] \tag{3.63}$$

$$\hat{C}_{mj}^{3tk}(\boldsymbol{\xi},\boldsymbol{x})=\varepsilon_{tak}x_3\frac{\partial M_{mj}(\boldsymbol{\xi},\boldsymbol{x})}{\partial x_a}-\frac{1}{(1-2\nu)}\varepsilon_{ta\beta}\lambda_{ak}\frac{\partial N_{mj}(\boldsymbol{\xi},\boldsymbol{x})}{\partial x_\beta} \tag{3.64}$$

where $M_{mj}(\boldsymbol{\xi},\boldsymbol{x})$ and $N_{mj}(\boldsymbol{\xi},\boldsymbol{x})$ are Papkovich-Neuber potentials (see closed-form expressions in Li (1996) and Appendix A), and λ_{ak} denotes a constant tensor defined by

$$\lambda_{ak}=\begin{cases}(1-2\nu) & a=k=1,\,2\\ -1 & a=k=3\\ 0 & a\neq k\end{cases} \tag{3.65}$$

Similarly, the functions $\hat{G}_{mj}^{4p}(\boldsymbol{\xi},\boldsymbol{x})$ and $\hat{C}_{mj}^{4tk}(\boldsymbol{\xi},\boldsymbol{x})$ for BC-type-4 can also be obtained in a closed form as

$$\hat{G}_{mj}^{4p}(\boldsymbol{\xi},\boldsymbol{x})=\frac{1}{2\mu}[x_3\frac{\partial P_{mj}(\boldsymbol{\xi},\boldsymbol{x})}{\partial x_p}-(3-4\nu)\delta_{3p}P_{mj}(\boldsymbol{\xi},\boldsymbol{x})] \tag{3.66}$$

$$\hat{C}_{mj}^{4tk}(\boldsymbol{\xi},\boldsymbol{x})=(1-2\nu)\varepsilon_{tk3}P_{mj}(\boldsymbol{\xi},\boldsymbol{x})+\varepsilon_{tak}x_3\frac{\partial P_{mj}(\boldsymbol{\xi},\boldsymbol{x})}{\partial x_a}+2(1-\nu)\delta_{3k}\varepsilon_{3\gamma t}\frac{\partial Q_{mj}(\boldsymbol{\xi},\boldsymbol{x})}{\partial x_\gamma} \tag{3.67}$$

where $P_{mj}(\boldsymbol{\xi},\boldsymbol{x})$ is the Papkovich-Neuber potential and $Q_{mj}(\boldsymbol{\xi},\boldsymbol{x})$ is obtained directly by integrating the potential $P_{mj}(\boldsymbol{\xi},\boldsymbol{x})$. The closed-form expressions of $P_{mj}(\boldsymbol{\xi},\boldsymbol{x})$ and $Q_{mj}(\boldsymbol{\xi},\boldsymbol{x})$ can also be found in Li (1996) and Appendix B.

Now, based on the relations (3.54)-(3.59) and the representations (3.60)-(3.62), the decompositions (3.33), (3.36) and (3.37) can be now generalized to all types of boundary conditions on the half-space surface:

$$S_{ij}^{Ip}(\boldsymbol{\xi},\boldsymbol{x}) = H_{ij}^{Ip}(\boldsymbol{\xi},\boldsymbol{x}) + \varepsilon_{ism}\frac{\partial}{\partial \xi_s} G_{mj}^{Ip}(\boldsymbol{\xi},\boldsymbol{x}) \tag{3.68}$$

$$E_{lkpq}\frac{\partial U_j^{Ip}(\boldsymbol{\xi},\boldsymbol{x})}{\partial x_q} = H_{lk}^{Ij}(\boldsymbol{x},\boldsymbol{\xi}) + \varepsilon_{lrt}\frac{\partial}{\partial x_r} G_{tk}^{Ij}(\boldsymbol{x},\boldsymbol{\xi}) \tag{3.69}$$

$$E_{lkpq}\frac{\partial S_{ij}^{Ip}(\boldsymbol{\xi},\boldsymbol{x})}{\partial x_q} = \Gamma_I E_{ijkl}\delta(\boldsymbol{\xi}-\boldsymbol{x}) - \Lambda_I \bar{\delta}_{ia}\bar{\delta}_{jb}E_{abkl}\delta(\boldsymbol{x}-\bar{\boldsymbol{\xi}}) + \varepsilon_{ism}\frac{\partial}{\partial \xi_s}\varepsilon_{lrt}\frac{\partial}{\partial x_r} C_{mj}^{Itk}(\boldsymbol{\xi},\boldsymbol{x}) \tag{3.70}$$

where $\Gamma_3 = \Gamma_1$, $\Gamma_4 = \Gamma_2$, $\Lambda_3 = \Lambda_1$, $\Lambda_4 = \Lambda_2$ and the functions $H_{ij}^{Ip}(\boldsymbol{\xi},\boldsymbol{x})$, $G_{mj}^{Ip}(\boldsymbol{\xi},\boldsymbol{x})$ and $C_{mj}^{Itk}(\boldsymbol{\xi},\boldsymbol{x})$ for I = 3 and 4 are defined by

$$H_{ij}^{3p}(\boldsymbol{\xi},\boldsymbol{y}) = H_{ij}^{1p}(\boldsymbol{\xi},\boldsymbol{y}) \tag{3.71}$$

$$H_{ij}^{4p}(\boldsymbol{\xi},\boldsymbol{x}) = H_{ij}^{2p}(\boldsymbol{\xi},\boldsymbol{x}) \tag{3.72}$$

$$G_{mj}^{3p}(\boldsymbol{\xi},\boldsymbol{y}) = G_{mj}^{1p}(\boldsymbol{\xi},\boldsymbol{y}) + \hat{G}_{mj}^{3p}(\boldsymbol{\xi},\boldsymbol{y}) \tag{3.73}$$

$$G_{mj}^{4p}(\boldsymbol{\xi},\boldsymbol{x}) = G_{mj}^{2p}(\boldsymbol{\xi},\boldsymbol{x}) + \hat{G}_{mj}^{4p}(\boldsymbol{\xi},\boldsymbol{x}) \tag{3.74}$$

$$C_{mj}^{3tk}(\boldsymbol{\xi},\boldsymbol{y}) = C_{mj}^{1tk}(\boldsymbol{\xi},\boldsymbol{y}) + \hat{C}_{mj}^{3tk}(\boldsymbol{\xi},\boldsymbol{y}) \tag{3.75}$$

$$C_{mj}^{4tk}(\boldsymbol{\xi},\boldsymbol{x}) = C_{mj}^{2tk}(\boldsymbol{\xi},\boldsymbol{x}) + \hat{C}_{mj}^{4tk}(\boldsymbol{\xi},\boldsymbol{x}) \tag{3.76}$$

Upon using the decompositions (3.68)-(3.70) along with the regularization technique presented for BC-type-1 and BC-type-2, the regularized boundary integral relations for both displacements and stresses and the weakly singular, weak-form integral equations for both crack-face displacements and crack-face tractions of the cracked half-space under one of the four types of boundary conditions can also be obtained in the same form as

$$\begin{aligned} u_p^I(\boldsymbol{x}) = & \int_{S_c^+} U_j^{Ip}(\boldsymbol{\xi},\boldsymbol{x})\Sigma t_j^0(\boldsymbol{\xi})dA(\boldsymbol{\xi}) - \int_{S_c^+} H_{ij}^{Ip}(\boldsymbol{\xi},\boldsymbol{x})n_i^+(\boldsymbol{\xi})\Delta u_j^I(\boldsymbol{\xi})dA(\boldsymbol{\xi}) \\ & + \int_{S_c^+} G_{mj}^{Ip}(\boldsymbol{\xi},\boldsymbol{x})D_m\Delta u_j^I(\boldsymbol{\xi})dA(\boldsymbol{\xi}) \end{aligned} \tag{3.77}$$

$$\sigma_{lk}^{I}(\boldsymbol{x}) = \varepsilon_{lrt}\frac{\partial}{\partial x_r}\left\{\int_{S_c^+} G_{tk}^{Ij}(\boldsymbol{x},\boldsymbol{\xi})\Sigma t_j^0(\boldsymbol{\xi})dA(\boldsymbol{\xi}) + \int_{S_c^+} C_{mj}^{Itk}(\boldsymbol{\xi},\boldsymbol{x})D_m\Delta u_j^I(\boldsymbol{\xi})dA(\boldsymbol{\xi})\right\} + \int_{S_c^+} H_{lk}^{Ij}(\boldsymbol{x},\boldsymbol{\xi})\Sigma t_j^0(\boldsymbol{\xi})dA(\boldsymbol{\xi}) \tag{3.78}$$

$$\begin{aligned}\frac{1}{2}\int_{S_c^+}\tilde{t}_p(\boldsymbol{y})\Sigma u_p^I(\boldsymbol{y})dA(\boldsymbol{y}) &= \int_{S_c^+}\tilde{t}_p(\boldsymbol{y})\int_{S_c^+} U_j^{Ip}(\boldsymbol{\xi},\boldsymbol{y})\Sigma t_j^0(\boldsymbol{\xi})dA(\boldsymbol{\xi})dA(\boldsymbol{y}) \\ &+ \int_{S_c^+}\tilde{t}_p(\boldsymbol{y})\int_{S_c^+} G_{mj}^{Ip}(\boldsymbol{\xi},\boldsymbol{y})D_m\Delta u_j^I(\boldsymbol{\xi})dA(\boldsymbol{\xi})dS(\boldsymbol{y}) \\ &- \int_{S_c^+}\tilde{t}_p(\boldsymbol{y})\int_{S_c^+} H_{ij}^{Ip}(\boldsymbol{\xi},\boldsymbol{y})n_i^+(\boldsymbol{\xi})\Delta u_j^I(\boldsymbol{\xi})dA(\boldsymbol{\xi})dS(\boldsymbol{y})\end{aligned} \tag{3.79}$$

$$\begin{aligned}\frac{1}{2}\int_{S_c^+}\Delta\tilde{u}_k(\boldsymbol{y})\Delta t_k^0(\boldsymbol{y})dA(\boldsymbol{y}) &= \int_{S_c^+}\Delta\tilde{u}_k(\boldsymbol{y})\int_{S_c^+} H_{lk}^{Ij}(\boldsymbol{y},\boldsymbol{\xi})n_l^+(\boldsymbol{y})\Sigma t_j^0(\boldsymbol{\xi})dA(\boldsymbol{\xi})dA(\boldsymbol{y}) \\ &- \int_{S_c^+} D_t\Delta\tilde{u}_k(\boldsymbol{y})\int_{S_c^+} G_{tk}^{Ij}(\boldsymbol{y},\boldsymbol{\xi})\Sigma t_j^0(\boldsymbol{\xi})dA(\boldsymbol{\xi})dA(\boldsymbol{y}) \\ &- \int_{S_c^+} D_t\Delta\tilde{u}_k(\boldsymbol{y})\int_{S_c^+} C_{mj}^{Itk}(\boldsymbol{\xi},\boldsymbol{y})D_m\Delta u_j^I(\boldsymbol{\xi})dA(\boldsymbol{\xi})dA(\boldsymbol{y})\end{aligned} \tag{3.80}$$

The last two boundary integral equations form a sufficient set of governing integral equations for determining the unknown crack-face data whereas the first two relations can be utilized to compute the displacements and stresses at any interior point of the body once the crack-face unknown data is solved.

CHAPTER 4
SOLUTION METHODOLOGY

This chapter mainly presents an efficient and accurate numerical procedure for determining the unknown crack-face data and related fracture information such as the stress intensity factors and the T-stress components. A formulation of the boundary value problem based upon a pair of singularity-reduced, weak-form boundary integral equations established in the previous chapter is obtained first and, then, the solution procedure based on the weakly singular SGBEM and standard Galerkin method is briefly outlined. Essential ingredients to enhance the computational efficiency and accuracy such as the approximation of the near-front unknown relative crack-face displacement, the numerical integration, and the evaluations of kernels for generally anisotropic materials are also discussed. Finally, an explicit formula for extracting the stress intensity factors and the T-stress components along the crack boundary is presented.

4.1 Solution Procedure

To obtain the complete elastic field of the given problem described in section 3.1 (i.e., the displacement and stress fields), it is sufficient to determine the unknown crack-face data including the sum of and jump in the crack-face displacement. The displacement and stress at any interior point can be post-processed from a pair of regularized boundary integral relations (3.77) and (3.78).

In the present study, the weakly singular, weak-form integral equations for the crack-face displacement and crack-face traction (3.79) and (3.80) is exploited to form a complete set of equations governing the sum of and jump in the crack-face displacements. Those two equations can be written in a more concise form as

$$\mathcal{B}(\tilde{\boldsymbol{t}}, \Sigma \boldsymbol{u}^I) = \mathcal{U}(\tilde{\boldsymbol{t}}, \Sigma \boldsymbol{t}^0) + \mathcal{G}(\tilde{\boldsymbol{t}}, \Delta \boldsymbol{u}^I) + \mathcal{H}(\tilde{\boldsymbol{t}}, \Delta \boldsymbol{u}^I) \tag{4.1}$$

$$\mathcal{C}(\Delta \tilde{\boldsymbol{u}}, \Delta \boldsymbol{u}^I) = \mathcal{G}(\Sigma \boldsymbol{t}^0, \Delta \tilde{\boldsymbol{u}}) + \mathcal{H}(\Sigma \boldsymbol{t}^0, \Delta \tilde{\boldsymbol{u}}) + \mathcal{B}(\Delta \tilde{\boldsymbol{u}}, \Delta \boldsymbol{t}^0) \tag{4.2}$$

where the linear integral operator $\mathcal{B}, \mathcal{U}, \mathcal{G}, \mathcal{H}$ and $\mathcal{C}$ are defined by

$$\mathcal{B}(\boldsymbol{X}, \boldsymbol{Y}) = \frac{1}{2} \int_{S_c^+} X_p(\boldsymbol{y}) Y_p(\boldsymbol{y}) dS(\boldsymbol{y}) \tag{4.3}$$

$$\mathcal{U}(\boldsymbol{X}, \boldsymbol{Y}) = \int_{S_c^+} X_p(\boldsymbol{y}) \int_{S_c^+} U_j^{Ip}(\boldsymbol{\xi}, \boldsymbol{y}) Y_j(\boldsymbol{\xi}) dS(\boldsymbol{\xi}) dS(\boldsymbol{y}) \tag{4.4}$$

$$\mathcal{G}(\boldsymbol{X},\boldsymbol{Y}) = \int_{S_c^+} X_p(\boldsymbol{y}) \int_{S_c^+} G_{mj}^{Ip}(\boldsymbol{\xi},\boldsymbol{y}) D_m Y_j(\boldsymbol{\xi}) dS(\boldsymbol{\xi}) dS(\boldsymbol{y}) \tag{4.5}$$

$$\mathcal{H}(\boldsymbol{X},\boldsymbol{Y}) = -\int_{S_c^+} X_p(\boldsymbol{y}) \int_{S_c^+} H_{ij}^{Ip}(\boldsymbol{\xi},\boldsymbol{y}) n_i^+(\boldsymbol{\xi}) Y_j(\boldsymbol{\xi}) dS(\boldsymbol{\xi}) dS(\boldsymbol{y}) \tag{4.6}$$

$$\mathcal{C}(\boldsymbol{X},\boldsymbol{Y}) = -\int_{S_c^+} D_t X_k(\boldsymbol{y}) \int_{S_c^+} C_{mj}^{Itk}(\boldsymbol{\xi},\boldsymbol{y}) D_m Y_j(\boldsymbol{\xi}) dS(\boldsymbol{\xi}) dS(\boldsymbol{y}) \tag{4.7}$$

where $\boldsymbol{X}$ and $\boldsymbol{Y}$ are argument vectors and U_j^{Ip}, G_{mj}^{Ip}, $H_{ij}^{Ip} n_i^+$ and C_{mj}^{Itk} are weakly singular kernels associated with the elastic half-space under the boundary condition BC-type-*I* on the free surface. It should be evident from the symmetry of the kernel C_{mj}^{Itk} and the integral form of (4.3) and (4.7) that the linear integral operators $\mathcal{B}$ and $\mathcal{C}$ satisfy the relations $\mathcal{B}(\boldsymbol{X},\boldsymbol{Y}) = \mathcal{B}(\boldsymbol{Y},\boldsymbol{X})$ and $\mathcal{C}(\boldsymbol{X},\boldsymbol{Y}) = \mathcal{C}(\boldsymbol{Y},\boldsymbol{X})$. As a result, the boundary integral equations (4.1) and (4.2) are in a symmetric form with respect to the unknown sum of and jump in the crack-face displacements, respectively. Since the integral equation for the jump in the crack-face traction (4.2) is independent of the sum of the crack-face displacement, it can be solved first to obtain the jump in the crack-face displacement. Once $\Delta\boldsymbol{u}^I$ is fully determined on the entire crack face, the sum of the crack-face displacement $\Sigma\boldsymbol{u}^I$ can subsequently be obtained by solving the crack-face displacement integral equation (4.1).

To construct the numerical solution of the crack-face traction integral equation (4.2), a well-known, weakly singular, symmetric Galerkin boundary element method (SGBEM) is adopted (also see details in the work of Li *et al.*, 1998 and Rungamornrat and Mear, 2008b). Both the jump in the crack-face displacement $\Delta\boldsymbol{u}^I$ and the test function $\Delta\tilde{\boldsymbol{u}}$ on the entire crack face are approximated by

$$\Delta\boldsymbol{u}^I(\boldsymbol{\xi}) = \sum_{i=1}^{N} \Delta\boldsymbol{u}^{I(i)} \phi_i(\boldsymbol{\xi}) \tag{4.8}$$

$$\Delta\tilde{\boldsymbol{u}}(\boldsymbol{\xi}) = \sum_{i=1}^{N} \Delta\tilde{\boldsymbol{u}}^{(i)} \phi_i(\boldsymbol{\xi}) \tag{4.9}$$

where $\phi_i(\boldsymbol{\xi})$ is a selected nodal basis function; N is the number of nodes; $\Delta\boldsymbol{u}^{I(i)}$ denotes the unknown nodal quantities; and $\Delta\tilde{\boldsymbol{u}}^{(i)}$ are arbitrary nodal constants. In the current study, the basis function $\phi_i(\boldsymbol{\xi})$ is constructed locally in an element-wise fashion by using standard, two-dimensional, C^0-isoparametric elements on the majority of the crack face and special crack-tip elements on the remaining region adjacent to the crack boundary. The special crack-tip element was originally proposed by Li *et al.* (1998) to

properly integrate the square-root-type behavior into the shape functions in the modeling of cracks in an isotropic, linearly elastic medium and later modified by Rungamornrat and Mear (2008b) to model cracks in anisotropic bodies. It has been found in their study that use of those special crack-tip elements to model the near-front relative crack-face displacement can significantly enhance both the accuracy of numerical solutions and the computational efficiency regarding to the significant reduction of a level of mesh refinement. To allow the treatment of general prescribed traction data on the crack face, the sum of and the jump in the crack-face tractions are interpolated from

$$\Sigma \boldsymbol{t}^0(\boldsymbol{\xi}) = \sum_{i=1}^{N} \Sigma \boldsymbol{t}^{0(i)} \psi_i(\boldsymbol{\xi}) \tag{4.10}$$

$$\Delta \boldsymbol{t}^0(\boldsymbol{\xi}) = \sum_{i=1}^{N} \Delta \boldsymbol{t}^{0(i)} \psi_i(\boldsymbol{\xi}) \tag{4.11}$$

where $\psi_i(\boldsymbol{\xi})$ is a nodal basis function constructed by standard, two-dimensional, C^0-isoparametric elements for the entire crack front; $\Sigma \boldsymbol{t}^{0(i)}$ is the prescribed sum of the crack-face traction at the i^{th} node; and $\Delta \boldsymbol{t}^{0(i)}$ denotes the prescribed jump in the crack-face traction at the i^{th} node. By substituting (4.8)-(4.11) into (4.2) and then invoking the arbitrariness of the constant $\Delta \tilde{\boldsymbol{u}}^{(i)}$, it finally yields a system of linear algebraic equations:

$$\boldsymbol{C} \Delta \boldsymbol{U}^I = (\boldsymbol{G} + \boldsymbol{H}) \Sigma \boldsymbol{T}^0 + \boldsymbol{B} \Delta \boldsymbol{T}^0 \tag{4.12}$$

where $\Delta \boldsymbol{U}^I$ is a vector containing unknown nodal quantities $\Delta \boldsymbol{u}^{I(i)}$ with its entries given by $[\Delta \boldsymbol{U}^I]_{3(i-1)+k} = [\Delta \boldsymbol{u}^{I(i)}]_k$; $\Sigma \boldsymbol{T}^0$ is a vector containing prescribed sum of nodal tractions $\Sigma \boldsymbol{t}^{0(i)}$ with its entries given by $[\Sigma \boldsymbol{T}^0]_{3(i-1)+k} = [\Sigma \boldsymbol{t}^{0(i)}]_k$; $\Delta \boldsymbol{T}^0$ is a vector containing the prescribed jump in nodal tractions $\Delta \boldsymbol{t}^{0(i)}$ with its entries given by $[\Delta \boldsymbol{T}^0]_{3(i-1)+k} = [\Delta \boldsymbol{t}^{0(i)}]_k$; and $\boldsymbol{C}$, $\boldsymbol{G}$, $\boldsymbol{H}$ and $\boldsymbol{B}$ are known coefficient matrices associated with the linear integral operators $\mathcal{C}$, $\mathcal{G}$, $\mathcal{H}$ and $\mathcal{B}$, respectively, and their entries are given explicitly by

$$[\boldsymbol{C}]_{3(i-1)+k,3(j-1)+l} = -\int_{S_c^+} D_t \phi_i(\boldsymbol{y}) \int_{S_c^+} C_{ml}^{Itk}(\boldsymbol{\xi}, \boldsymbol{y}) D_m \phi_j(\boldsymbol{\xi}) dS(\boldsymbol{\xi}) dS(\boldsymbol{y}) \tag{4.13}$$

$$[\boldsymbol{G}]_{3(i-1)+k,3(j-1)+l} = -\int_{S_c^+} D_t \phi_i(\boldsymbol{y}) \int_{S_c^+} G_{tk}^{Il}(\boldsymbol{y}, \boldsymbol{\xi}) \psi_j(\boldsymbol{\xi}) dA(\boldsymbol{\xi}) dA(\boldsymbol{y}) \tag{4.14}$$

$$[\boldsymbol{H}]_{3(i-1)+k,3(j-1)+l} = \int_{S_c^+} \phi_i(\boldsymbol{y}) \int_{S_c^+} H_{mk}^{Il}(\boldsymbol{\xi}, \boldsymbol{y}) n_m^+(\boldsymbol{\xi}) \psi_j(\boldsymbol{\xi}) dS(\boldsymbol{\xi}) dS(\boldsymbol{y}) \tag{4.15}$$

$$[\boldsymbol{B}]_{3(i-1)+k,3(j-1)+l} = \frac{1}{2} \int_{S_c^+} \phi_i(\boldsymbol{y}) \psi_j(\boldsymbol{y}) \delta_{kl} dS(\boldsymbol{y}) \tag{4.16}$$

It is evident that terms on the right hand side of (4.12) are completely known and the coefficient matrix $\boldsymbol{C}$ is symmetric.

To discretize the weakly singular, weak-form, crack-face displacement boundary integral equation (4.1), a similar strategy following Galerkin approximation procedure is utilized. Specifically, the sum of the crack-face displacement $\Sigma \boldsymbol{u}^I$ and the test function $\tilde{t}$ are discretized by

$$\Sigma \boldsymbol{u}^I(\boldsymbol{\xi}) = \sum_{i=1}^{N} \Sigma \boldsymbol{u}^{I(i)} \psi_i(\boldsymbol{\xi}) \tag{4.17}$$

$$\tilde{\boldsymbol{t}}(\boldsymbol{\xi}) = \sum_{i=1}^{N} \tilde{\boldsymbol{t}}^{(i)} \psi_i(\boldsymbol{\xi}) \tag{4.18}$$

where $\Sigma \boldsymbol{u}^{I(i)}$ and $\tilde{\boldsymbol{t}}^{(i)}$ are the unknown sum of the crack-face displacements and an arbitrary constant vector at the i^{th} node, respectively. It is worth noting that the same nodal basis functions $\psi_i(\boldsymbol{\xi})$ as those employed in (4.10) and (4.11) are utilized in the discretization (4.17) and (4.18) since the unknown $\Sigma \boldsymbol{u}^I$ is well-behaved for the entire crack surface. By substituting (4.8), (4.10) and (4.17)-(4.18) into (4.1), it yields a system of linear algebraic equations

$$\bar{\boldsymbol{B}} \Sigma \boldsymbol{U}^I = \boldsymbol{D} \Sigma \boldsymbol{T}^0 + (\bar{\boldsymbol{G}} + \bar{\boldsymbol{H}}) \Delta \boldsymbol{U}^I \tag{4.19}$$

where $\Sigma \boldsymbol{U}^I$ is a vector containing the unknown nodal quantities $\Sigma \boldsymbol{u}^{I(i)}$ with its entries given by $[\Sigma \boldsymbol{U}^I]_{3(i-1)+k} = [\Sigma \boldsymbol{u}^{I(i)}]_k$ and $\bar{\boldsymbol{B}}$, $\boldsymbol{D}$, $\bar{\boldsymbol{G}}$ and $\bar{\boldsymbol{H}}$ are known matrices associated with the linear integral operators $\mathscr{B}$, $\mathscr{U}$, $\mathscr{G}$ and $\mathscr{H}$, respectively, and their entries are given explicitly by

$$[\bar{\boldsymbol{B}}]_{3(i-1)+k,3(j-1)+l} = \frac{1}{2} \int_{S_c^+} \psi_i(\boldsymbol{y}) \psi_j(\boldsymbol{y}) \delta_{kl} dS(\boldsymbol{y}) \tag{4.20}$$

$$[\boldsymbol{D}]_{3(i-1)+k,3(j-1)+l} = \int_{S_c^+} \psi_i(\boldsymbol{y}) \int_{S_c^+} U_l^{Ik}(\boldsymbol{\xi}, \boldsymbol{y}) \psi_j(\boldsymbol{\xi}) dS(\boldsymbol{\xi}) dS(\boldsymbol{y}) \tag{4.21}$$

$$[\bar{\boldsymbol{G}}]_{3(i-1)+k,3(j-1)+l} = \int_{S_c^+} \psi_i(\boldsymbol{y}) \int_{S_c^+} G_{tk}^{Il}(\boldsymbol{y}, \boldsymbol{\xi}) D_t \phi_j(\boldsymbol{\xi}) dA(\boldsymbol{\xi}) dA(\boldsymbol{y}) \tag{4.22}$$

$$[\bar{\boldsymbol{H}}]_{3(i-1)+k,3(j-1)+l} = -\int_{S_c^+} \psi_i(\boldsymbol{y}) \int_{S_c^+} H_{ml}^{Ik}(\boldsymbol{\xi}, \boldsymbol{y}) n_m^+(\boldsymbol{\xi}) \phi_j(\boldsymbol{\xi}) dS(\boldsymbol{\xi}) dS(\boldsymbol{y}) \tag{4.23}$$

It should be remarked that the matrix $\boldsymbol{B}$ is symmetric and, once the unknown $\Delta \boldsymbol{U}^I$ is obtained from (4.12), the system (4.19) can be subsequently solved for the unknown $\Sigma \boldsymbol{U}^I$.

4.2 Computation of Coefficient Matrices

To form the two systems of linear algebraic equations (4.12) and (4.19), the coefficient matrices $\boldsymbol{B}$, $\bar{\boldsymbol{B}}$, $\boldsymbol{C}$, $\boldsymbol{D}$, $\boldsymbol{G}$, $\bar{\boldsymbol{G}}$, $\boldsymbol{H}$ and $\bar{\boldsymbol{H}}$ are computed numerically as described below.

All entries of the matrices $\boldsymbol{B}$ and $\bar{\boldsymbol{B}}$ clearly involve the single surface integral of regular elementary functions and the numerical calculation of their value can be achieved efficiently using standard Gaussian quadrature. On the contrary, evaluation of all entries of matrices $\boldsymbol{C}$, $\boldsymbol{D}$, $\boldsymbol{G}$, $\bar{\boldsymbol{G}}$, $\boldsymbol{H}$ and $\bar{\boldsymbol{H}}$ is more computationally challenging since it requires to evaluate the double surface integrals containing weakly singular kernels. Resulting from the discretization, double surface integrals for a pair of finite elements can generally be separated into three groups depending mainly on the behavior of the integrand. A regular double surface integral for a pair of relatively remote elements can be efficiently integrated by standard Gaussian quadrature since the involved integrand is sufficiently well-behaved. For a weakly singular double surface integral over a pair of identical elements, a systematic numerical integration scheme based on a series of special variable transformations is employed to regularize the weakly singular integrand allowing the resulting integrals to be efficiently integrated by standard Gaussian quadrature. For a double surface integral over a pair of relatively close or adjacent elements, the integrand possesses a rapid variation behavior introduced by pairs of relatively close source and field points and, as a result, it cannot be integrated efficiently by standard Gaussian quadrature (see also the work of Xiao (1998)). In the present study, a family of logarithmic variable transformation is introduced to eliminate the nearly singular feature of the integrand and the final integral can be computed using standard Gaussian quadrature. Details of special numerical quadrature for both nearly and weakly singular integrals can be found in the work of Xiao (1998).

In addition to the numerical integration scheme described above, it still requires the efficient computation of all involved kernels $H_{ij}^{Ip}(\boldsymbol{\xi}, \boldsymbol{y})$, $U_j^{Ip}(\boldsymbol{\xi}, \boldsymbol{y})$, $G_{mj}^{Ip}(\boldsymbol{\xi}, \boldsymbol{y})$ and $C_{mj}^{Itk}(\boldsymbol{\xi}, \boldsymbol{y})$ for every pair of points $(\boldsymbol{\xi}, \boldsymbol{y})$. Since the kernel $H_{ij}^{Ip}(\boldsymbol{\xi}, \boldsymbol{y})$ involves only

elementary functions and is independent of the material properties, its value can readily and efficiently be obtained by a direct substitution. Unlike the kernel $H_{ij}^{Ip}(\boldsymbol{\xi},\boldsymbol{y})$, the kernels $U_j^{Ip}(\boldsymbol{\xi},\boldsymbol{y})$, $G_{mj}^{Ip}(\boldsymbol{\xi},\boldsymbol{y})$ and $C_{mj}^{Itk}(\boldsymbol{\xi},\boldsymbol{y})$ are expressed in terms of a line integral over a unit circle and the direct computation of such integral for every pair of field and source points $(\boldsymbol{\xi},\boldsymbol{y})$ can be computationally massive. In the present study, an interpolation scheme similar to that exploited by Rungamornrat and Mear (2008b) is adopted. In this technique, the direct calculation of the line integral is only required at interpolation grid points and this can be accomplished efficiently via standard Gaussian quadrature. Values of each kernel at any pair of field and siurce points $(\boldsymbol{\xi},\boldsymbol{y})$ within the interpolation grid can be approximated from their nodal-based interpolants. The accuracy of such approximation can be controlled by adjusting the number of grid points and the order of the interpolation functions employed.

4.3 Determination of Stress Intensity Factors and T-stress Components

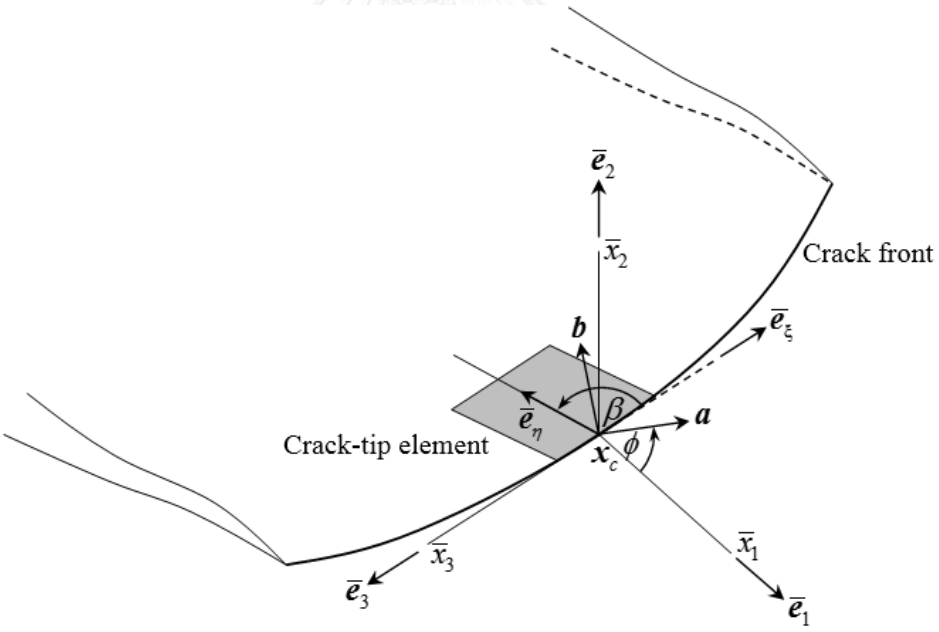

Figure 4.1: Local Cartesian coordinate system and all involved parameters for determining stress intensity factors and T-stress components.

Let $\boldsymbol{x}_c$ be a point on the crack front and $\{\boldsymbol{x}_c;\bar{x}_1,\bar{x}_2,\bar{x}_3\}$ be a local Cartesian coordinate system with the origin at $\boldsymbol{x}_c$ and the corresponding orthonormal base vectors $\{\bar{\boldsymbol{e}}_1,\bar{\boldsymbol{e}}_2,\bar{\boldsymbol{e}}_3\}$. In particular, the $\bar{x}_3$-axis is selected to be tangent to the crack boundary; the $\bar{x}_1$-axis

directs outward and perpendicular to the crack front such that $\bar{x}_1$-$\bar{x}_3$ plane forms a local tangent plane of the crack surface at $\boldsymbol{x}_c$; and $\bar{x}_2$-axis follows the right hand rule as depicted in Figure 4.1. From the asymptotic stress analysis, the near-front stress field in the neighborhood of the point $\boldsymbol{x}_c$ takes the form

$$\sigma_{ij}(\boldsymbol{x}_c;r,\theta)=\sum_{p=1}^{3}\frac{K_p(\boldsymbol{x}_c)}{\sqrt{r}}f_{ij}^{p}(\theta)+T_{ij}(\boldsymbol{x}_c)g^{ij}(\theta)+\sum_{m=1}^{\infty}r^{m/2}\hat{\sigma}_{ij}^{m}(\boldsymbol{x}_c;\theta) \tag{4.24}$$

where (r,θ) are polar coordinates of any point in the $\bar{x}_1$- $\bar{x}_2$ plane; K_I, K_{II} and K_{III} denote the mode-I, mode-II and mode-III stress intensity factors, respectively; T_{ij} denotes the T-stress tensor; and f_{ij}^{p}, g^{ij} and $\hat{\sigma}_{ij}^{m}$ are functions independent of the radial coordinate *r*. It is important to remark that the angular dependent function f_{ij}^{p} and g^{ij} can be fully determined from the eigen analysis of the near-front field and, as a result, the singular term and the first non-singular term of the near-front stress field are completely known once the stress intensity factors and the T-stress tensor are computed. Unlike the functions f_{ij}^{p} and g^{ij}, both K_p and T_{ij} cannot be obtained directly from the asymptotic analysis but still requires solving the full boundary value problem.

In the present study, an explicit formula proposed by Rungamornrat and Mear (2008b) for cracks in generally anisotropic infinite and finite media is employed to compute the mixed-mode stress intensity factors. This formula only requires the information of extra nodal degrees of freedom along the crack front as follows:

$$k_i(\boldsymbol{x}_c)=\sqrt{\frac{\pi}{2J_\eta\sin\beta}}B_{il}\left\{\hat{\boldsymbol{u}}(\boldsymbol{x}_c)\cdot\bar{\boldsymbol{e}}_l(\boldsymbol{x}_c)\right\} \tag{4.25}$$

where $k_1\equiv K_{II}$, $k_2\equiv K_I$ and $k_3\equiv K_{III}$; $J_\eta=\|\partial\boldsymbol{r}/\partial\eta(\xi_c,-1)\|$; $J_\xi=\|\partial\boldsymbol{r}/\partial\xi(\xi_c,-1)\|$; $\boldsymbol{r}=\boldsymbol{r}(\xi,\eta)=\boldsymbol{x}(\xi,\eta)-\boldsymbol{x}_c(\xi_c,-1)$; (ξ,η) denote the natural coordinates of a point $\boldsymbol{x}$ on the crack-tip element; $(\xi_c,-1)$ are natural coordinates of a point $\boldsymbol{x}_c$; β denotes an angle between the unit vectors $\bar{\boldsymbol{e}}_\eta=\{\partial\boldsymbol{r}/\partial\eta(\xi_c,-1)\}/J_\eta$ and $\bar{\boldsymbol{e}}_\xi=\{\partial\boldsymbol{r}/\partial\xi(\xi_c,-1)\}/J_\xi$; $\hat{\boldsymbol{u}}(\boldsymbol{x}_c)=\sum_i\Delta\boldsymbol{u}^{(i)}\varphi_i(\xi_c,-1)$ with $\Delta\boldsymbol{u}^{(i)}$ denoting the extra degree of freedom of the special crack-tip element obtained from equation (4.12), φ_i denoting the standard shape

functions, and the summation taken over all nodes along the crack front of the crack-tip element containing the point $\boldsymbol{x}_c$; and

$$B_{il} = \frac{-1}{2\pi}\int_0^{2\pi}\left[(\boldsymbol{a},\boldsymbol{b})_{im}(\boldsymbol{b},\boldsymbol{b})^{-1}_{mn}(\boldsymbol{b},\boldsymbol{a})_{nl} - (\boldsymbol{a},\boldsymbol{a})_{il}\right]d\phi \tag{4.26}$$

with $\boldsymbol{a}$ and $\boldsymbol{b}$ denoting orthonormal vectors in the plane $\bar{x}_3 = 0$, ϕ denoting the angle between $\boldsymbol{a}$ and the unit vector $\bar{\boldsymbol{e}}_3$ as indicated in Figure 4.1, $(\boldsymbol{a}, \boldsymbol{b})_{ij} = a_m E_{imnj} b_n$, and $(\boldsymbol{b},\boldsymbol{b})^{-1}$ denoting the inverse of $(\boldsymbol{b},\boldsymbol{b})$.

The unknown T-stress components along the crack front can also be extracted from the sum of the crack-face displacement as described below. First, components of the T-stress tensor at $\boldsymbol{x}_c$ are related to the non-singular part of the strain at the same point via the following linear constitutive relation

$$T_{ij}(\boldsymbol{x}_c) = \bar{E}_{ijkl}(\boldsymbol{x}_c)\bar{\varepsilon}_{kl}(\boldsymbol{x}_c) \tag{4.27}$$

where $\bar{E}_{ijkl}(\boldsymbol{x}_c)$ and $\bar{\varepsilon}_{kl}(\boldsymbol{x}_c)$ are elastic constants and components of the finite part of the strain tensor relative to the local coordinate system at $\boldsymbol{x}_c$. It can readily be verified from the continuity of the tensor $T_{ij}(\boldsymbol{x}_c)$ that the three components T_{12}, T_{22}, and T_{23} are known and equal, respectively, to the $\bar{x}_1$-, $\bar{x}_2$-, and $\bar{x}_3$-components of the applied crack-face traction at the limiting point of $\boldsymbol{x}_c$. The finite strain components $\bar{\varepsilon}_{11}$, $\bar{\varepsilon}_{33}$ and $\bar{\varepsilon}_{13}$ at $\boldsymbol{x}_c$ can also be calculated from the sum of the crack-face displacement in the neighborhood of $\boldsymbol{x}_c$ through the following expressions

$$\bar{\varepsilon}_{11}(\boldsymbol{x}_c) = \frac{1}{2}\frac{\partial \Sigma u_1^{\gamma}(\boldsymbol{x}_c)}{\partial \bar{x}_1} \tag{4.28}$$

$$\bar{\varepsilon}_{33}(\boldsymbol{x}_c) = \frac{1}{2}\frac{\partial u_3^{\gamma}(\boldsymbol{x}_c)}{\partial \bar{x}_3} \tag{4.29}$$

$$\bar{\varepsilon}_{13}(\boldsymbol{x}_c) = \frac{1}{4}\left(\frac{\partial \Sigma u_1^{\gamma}(\boldsymbol{x}_c)}{\partial \bar{x}_3} + \frac{\partial \Sigma u_3^{\gamma}(\boldsymbol{x}_c)}{\partial \bar{x}_1}\right) \tag{4.30}$$

The derivatives involved in the expressions (4.28)-(4.30) can be carried out directly within elements along the crack front. From the prescribed information of T_{12}, T_{22}, and T_{23} and the computed strain components $\bar{\varepsilon}_{11}$, $\bar{\varepsilon}_{33}$ and $\bar{\varepsilon}_{13}$, the unknown components T_{11}, T_{13} and T_{33} at any point $\boldsymbol{x}_c$ along the crack front, commonly termed the *T-stress*

components, can now be obtained by solving a system of six independent linear algebraic equations (4.27).

CHAPTER 5
NUMERICAL RESULTS

In this chapter, a selected set of boundary value problems involving cracks in an elastic half-space under various scenarios is analyzed by the implemented solution procedure. First, the proposed technique and the underlying integral formulation is fully validated by comparing computed numerical results with existing reliable reference solutions for both an isotropic cracked half-space under all four types of boundary conditions and an anisotropic cracked half-space under symmetrical and anti-symmetrical boundary conditions on the free surface. Then, more complex boundary value problems involving multiple and non-flat cracks are also investigated to clarify the capability and robustness of the proposed numerical procedure.

In the numerical simulations, both isotropic and transversely isotropic linearly elastic materials with the elastic constants given in Table 5.1 are considered. For the transversely isotropic cracked half-space, the axis of material symmetry is taken to direct normal to the half-space surface. Other classes of anisotropic materials, such as cubic and orthotropic materials, are also treated to illustrate the capability of the current method and results are reported in Appendix C. To additionally explore the convergence behavior of numerical solutions, a series of meshes with different levels of refinement is adopted in the analysis. Special 9-node crack-tip elements are adopted along the crack boundary whereas standard 8-node quadrilateral elements and 6-node triangular elements are used to discretize the majority of the crack surface.

Table 5.1: Elastic constants for isotropic material (associated with Poisson's ratio v = 0.3 and E = 2.6GPa) and transversely isotropic material with the axis of material symmetry normal to half-space surface (Kassir and Sih, 1975).

Materials	Elastic constants (GPa)				
	E_{1111}	E_{1122}	E_{1133}	E_{2222}	E_{1313}
Isotropic material	3.500	1.500	1.500	3.500	1.000
Transversely isotropic material	16.090	3.350	5.010	6.100	3.830

5.1 Verification

This section aims to verify the integral formulation and the implemented numerical scheme. Results for both isotropic and anisotropic cracked half-space under various conditions on the free surface are reported and compared with the benchmark solutions. Both interior cracks and surface breaking cracks under mode-I and mixed-mode conditions are investigated.

5.1.1 Isotropic Cracked Half-Space under BC-type-I

In this particular sub-section, the proposed technique is validated for the case of an isotropic cracked half-space under all four types of boundary conditions on the free surface (i.e., BC-type-1: symmetrical boundary condition; BC-type-2: anti-symmetrical boundary condition; BC-type-3: traction-free boundary condition; and BC-type-4: rigidly-fixed boundary condition).

a. Horizontal penny-shaped crack

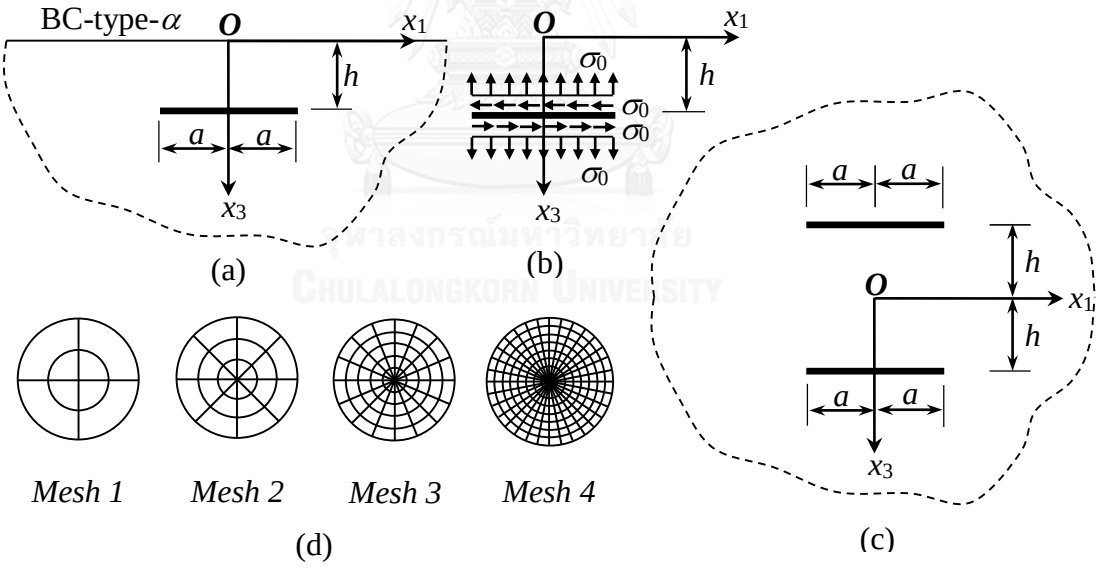

Figure 5.1: (a) Schematic of horizontal penny-shaped crack contained in half-space under BC-type-1 or BC-type-2, (b) tractions acting on crack surfaces, (c) equivalent whole space problem, and (d) four meshes adopted in the analysis.

Consider a penny-shaped crack contained in a half-space with the depth h and the crack surface parallel to the free surface as shown in Figure 5.1(a). The crack radius is denoted by a and the crack front is parameterized by $x_1 = a\cos\beta,\ \ x_2 = -a\sin\beta,\ \ x_3 = h$ for

$\beta \in [0, 2\pi]$. The crack surface is subjected only to a self-equilibrated, uniform traction $t_1^+ = -t_1^+ = \sigma_0$, $t_2^+ = -t_2^+ = 0$, $t_3^+ = -t_3^+ = \sigma_0$ (see Figure 5.1(b)) whereas the half-space surface is under the boundary conditions BC-type-1 and BC-type-2. In the analysis, four meshes are utilized as indicated in Figure 5.1(d) and the normalized depth h/a = 0.5 is considered.

Computed results for the stress intensity factors and the T-stress components at $\beta = \{0^0, 90^0, 180^0\}$ of both boundary conditions are normalized by the reference solution and reported in Table 5.2 and Table 5.3, respectively. It is remarked that the reference solution is taken as the solution of an equivalent whole space containing a pair of symmetric penny-shaped cracks about the surface $x_3 = 0$ shown in Figure 5.1(c), which is generated by the SGBEM proposed by Rungamornrat and Mear (2008b) with use of the Mesh 4. As can be seen from results in Table 5.2, numerical solutions display the excellent agreement with the reference solution for the first three meshes and they are weakly dependent on the level of refinement. In particular, the discrepancy between the stress intensity factors generated by the coarsest and intermediate meshes and the reference solution is less than 2.4% and 0.2%, respectively, whereas results generated from the Mesh 3 are nearly identical to the reference solution. The high quality of the numerical solutions, while employing relatively coarse meshes, is the direct consequence of using special crack-tip elements to enhance the approximation of the near-front relative crack-face displacement.

Table 5.2: Normalized stress intensity factors at $\beta = 0^0$, 90^0 and 180^0 for horizontal penny-shaped crack embedded in half-space under BC-type-1 or BC-type-2 and $h / a = 0.5$.

β	Mesh	BC-type-1			BC-type-2		
		K_I / K_I^{ref}	K_{II} / K_{II}^{ref}	K_{III} / K_{III}^{ref}	K_I / K_I^{ref}	K_{II} / K_{II}^{ref}	K_{III} / K_{III}^{ref}
0^0	1	0.9949	0.9896	-	0.9844	0.9806	-
	2	1.0004	1.0001	-	0.9987	0.9987	-
	3	1.0003	1.0002	-	0.9999	1.0001	-
90^0	1	0.9935	1.0011	0.9817	0.9861	0.9901	0.9947
	2	1.0002	1.0016	0.9990	0.9988	0.9998	1.0007
	3	1.0003	1.0004	1.0000	0.9999	1.0001	1.0002
180^0	1	0.9916	0.9911	-	0.9874	0.9761	-
	2	1.0000	1.0003	-	0.9990	0.9982	-
	3	1.0002	1.0002	-	1.0000	1.0000	-

Similar convergence behavior can also be observed for results of the T-stress components shown in Table 5.3; however, it is evident that the difference between the computed solutions T_{13} from the Mesh 1 and Mesh 2 and the benchmark solutions is larger than the case of the stress intensity factors. The reduction in the accuracy results directly from the fact that the derivatives of the sum of the crack-face displacement are required in the calculation of the T-stress components.

Table 5.3: Normalized T-stress components at $\beta = 0^0$, 90^0 and 180^0 for horizontal penny-shaped crack contained in half-space under BC-type-1 or BC-type-2 and $h/a = 0.5$.

β	Mesh	BC-type-1			BC-type-2		
		T_{11}/T_{11}^{ref}	T_{33}/T_{33}^{ref}	T_{13}/T_{13}^{ref}	T_{11}/T_{11}^{ref}	T_{33}/T_{33}^{ref}	T_{13}/T_{13}^{ref}
0^0	1	1.0359	1.0252	-	0.9322	0.9593	-
	2	1.0186	1.0166	-	0.9625	0.9789	-
	3	1.0055	1.0049	-	0.9909	0.9944	-
90^0	1	1.0037	0.9988	0.9626	0.9895	0.9906	1.0874
	2	1.0042	1.0013	1.1549	0.9878	0.9968	1.0928
	3	1.0021	1.0008	1.0662	0.9969	0.9993	1.0337
180^0	1	0.9658	0.9603	-	1.0334	1.0136	-
	2	0.9873	0.9790	-	1.0072	1.0099	-
	3	0.9980	0.9947	-	1.0016	1.0029	-

b. Vertical penny-shaped crack

Consider, next, a vertical penny-shaped crack of radius *a* contained in a half-space with a depth *h* (measured from the center of the crack to the free surface) as indicated in Figure 5.2(a). The crack front is parameterized by $x_1 = 0$, $x_2 = -a\cos\beta$, $x_3 = h - a\sin\beta$ for $\beta \in [0, 2\pi]$. The crack is subjected only to the self-equilibrated uniform normal traction $t_1^+ = -t_1^- = \sigma_0$, $t_2^+ = -t_2^- = 0$, $t_3^+ = -t_3^- = 0$ (see Figure 5.2(b)) whereas the half-space surface is under all four types of boundary conditions, BC-type-*I*. It is evident from the symmetry of the crack-face loading with respect to the plane $x_1 = 0$ that the mode-II and mode-III stress intensity factors identically vanish along the boundary of the crack. In the numerical study, four meshes of the penny-shaped crack are exploited as illustrated in Figure 5.2(d) and the aspect ratio $h/a = 1.5$ is considered.

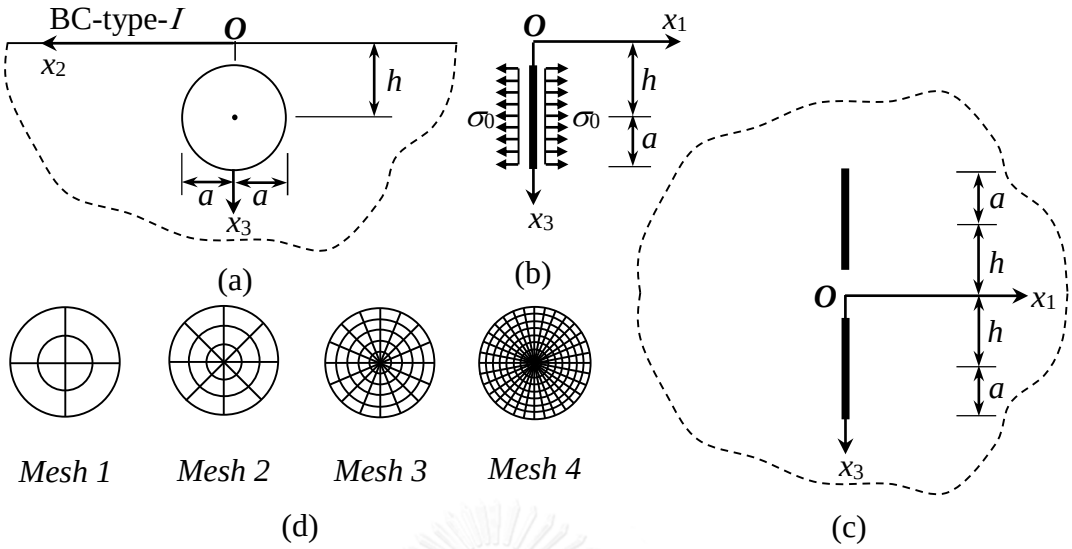

Figure 5.2: (a) Schematic of vertical penny-shaped crack embedded in half-space under BC-type-*I*, (b) uniform normal traction acting to crack surfaces, (c) equivalent whole space problem for BC-type- α, and (d) four meshes adopted in the analysis.

For the first two types of boundary conditions, BC-type-α, the computed stress intensity factors and the T-stress components are first normalized by the reference solution (generated from an equivalent whole space containing a pair of geometrically symmetric cracks with respect to the surface $x_3 = 0$ shown in Figure 5.2(c) and subjected to the symmetric loading condition for BC-type-1 and the anti-symmetric loading condition for BC-type-2 by using the SGBEM with the Mesh 4) and then reported in Table 5.4 and Table 5.5, respectively. Results for the stress intensity factors for the last two boundary conditions (i.e., BC-type-3 and BC-type-4) normalized by $K_I^{ref} = 2\sigma_0\sqrt{a/\pi}$ are compared with those obtained by Hrylyts'kyi *et al.* (2003) in Table 5.6. As indicated by results shown in Table 5.4, the stress intensity factors generated from the first three meshes for BC-type-1 and BC-type-2 are only slightly different from those obtained from the equivalent whole space problem. The discrepancy between the two solutions is small even though the coarsest mesh is utilized in the analysis. However, as shown in Table 5.5, results of the T-stress components indicate that the discrepancy between T_{13} generated by the Mesh 1 and the reference solution is larger than the case of the stress intensity factors. Again, the reduction of accuracy results directly from that the derivatives of the sum of the crack-face displacement are required in the calculation of the T-stress components. For BC-type-3 and BC-type-4, numerical solutions for the mode-I stress intensity factors are in good agreement with those presented by Hrylyts'kyi *et al.* (2003) and the weak dependence

on the level of refinement is also observed for this case. Only coarse meshes with few elements can be utilized to generate reasonably accurate results. This high quality of the computed solutions is due primarily to the application of special crack-tip elements to capture the near-front field.

Table 5.4: Normalized stress intensity factors at $\beta = \{0^0, 90^0\}$ for vertical penny-shaped crack embedded in half-space under BC-type-1 or BC-type-2 and $h/a = 1.5$.

β	Mesh	BC-type-1	BC-type-2
		K_I / K_I^{ref}	K_I / K_I^{ref}
0^0	1	0.9909	0.9918
	2	0.9997	0.9998
	3	1.0001	1.0001
90^0	1	0.9916	0.9912
	2	1.0000	0.9996
	3	1.0002	1.0001

Table 5.5: Normalized T-stress components at $\beta = \{0^0, 90^0\}$ for vertical penny-shaped crack embedded in half-space under BC-type-1 or BC-type-2 and $h/a = 1.5$.

β	Mesh	BC-type-1			BC-type-2		
		T_{11} / T_{11}^{ref}	T_{33} / T_{33}^{ref}	T_{13} / T_{13}^{ref}	T_{11} / T_{11}^{ref}	T_{33} / T_{33}^{ref}	T_{13} / T_{13}^{ref}
0^0	1	1.0033	0.9970	1.1834	1.0084	0.9992	1.1848
	2	1.0024	1.0009	1.0287	1.0025	1.0000	1.0264
	3	1.0014	1.0006	1.0029	1.0013	1.0003	1.0029
90^0	1	1.0038	0.9904	-	1.0078	1.0060	-
	2	1.0016	1.0011	-	1.0033	0.9998	-
	3	1.0015	1.0012	-	1.0012	0.9996	-

Table 5.6: Normalized stress intensity factors at $\beta = \{0^0, 90^0\}$ for vertical penny-shaped crack embedded in half-space under BC-type-3 or BC-type-4 and $h/a = 1.5$.

β	Mesh	Present results		Hrylyts'kyi	
		BC-type-3	BC-type-4	BC-type-3	BC-type-4
0^0	1	1.0114	0.9763	1.0200†	0.9790†
	2	1.0209	0.9838		
	3	1.0213	0.9841		
90^0	1	1.0440	0.9477	1.0500†	0.9530†
	2	1.0524	0.9560		
	3	1.0524	0.9567		

†Results obtained by means of extraction from certain figures reported by Hrylyts'kyi *et al.* (2003)

c. Elliptical crack perpendicular to half-space surface

Consider, next, an elliptical crack oriented vertically within the half-space as indicated in Figure 5.3(a). The semi-major and semi-minor axes of the crack are denoted by *a* and *b*, respectively; the orientation of the major axis relative to the free surface is denoted by the angle α; the depth of the crack measured from the free surface to its center is denoted by h; and $\beta \in [0, 2\pi]$ is an angle used for parameterizing the position along the crack boundary. The crack is loaded by uniformly distributed pressure σ_0 whereas the half-space surface is under the traction-free condition (i.e., BC-type-3). In the analysis, two scenarios of the crack are considered: type A associated with $\alpha = 0$, $a/b = 2$ and type B corresponding to $\alpha \neq 0$, $a/b = 2$, $h/b = 1.8$, and three meshes as depicted in Figure 5.3(b) are used.

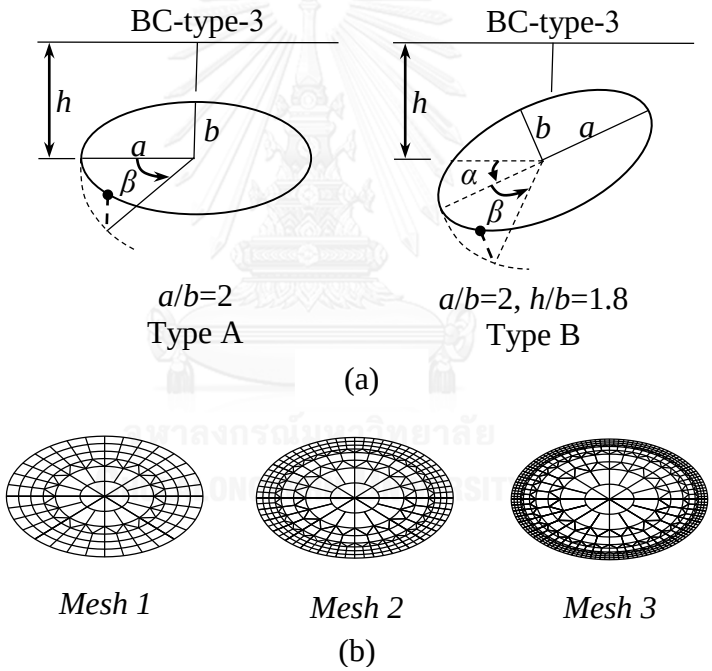

Figure 5.3: (a) Elliptical crack oriented vertically within the half-space and (b) three meshes used in analysis (Mesh 1 containing 168 elements and 32 crack-tip elements; Mesh 2 containing 392 elements and 64 crack-tips elements; and Mesh 3 containing 840 elements and 128 crack-tip elements).

Computed stress intensity factors for both type A and type B are first normalized by $K_I^{ref} = \sigma_0 \sqrt{\pi b}$ and then compared with those obtained by Noguchi *et al.* (1997) as reported in Figure 5.4(a) and Figure 5.4(b), respectively. It can be concluded from these results that numerical solutions computed from the proposed technique are highly

accurate and in good agreement with the reference solution for both type A and type B. In particular, the stress intensity factors in the current study are weakly dependent on the meshes used. Again, this high quality of numerical solutions results directly from the use of special interpolation functions to approximate the near-front jump in the crack-face displacement.

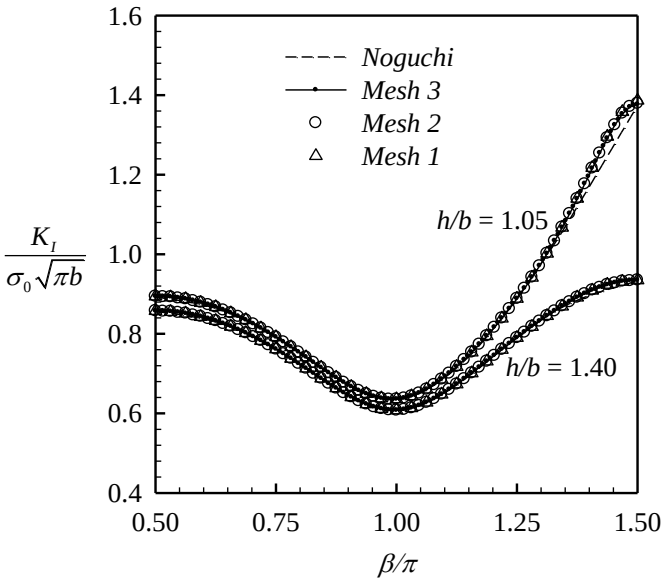

(a)

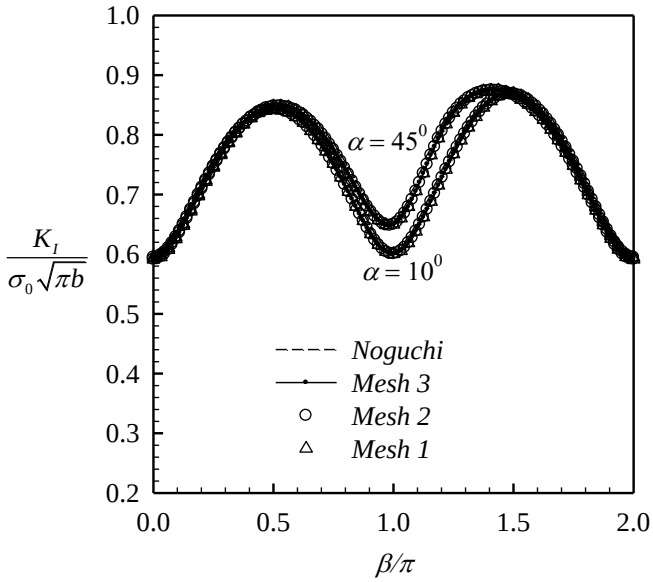

(b)

Figure 5.4: Normalized mode-I stress intensity factors for vertical elliptical crack of (a) type A and (b) type B, in half-space under BC-type-3.

d. Surface-breaking crack

Consider another example associated with a semi-circular surface breaking crack of radius *a* and oriented vertically in a half-space as shown in Figure 5.5(a). The crack front is parameterized by $x_1 = -a\cos\beta$, $x_2 = 0$, $x_3 = a\sin\beta$ for $\beta \in [0, \pi]$. The half-space is subjected to three cases of loading and boundary conditions: (i) half-space under BC-type-1 and crack subjected to uniform normal traction $t_1^+ = 0$, $t_2^+ = -\sigma_0$, $t_3^+ = 0$; (ii) half-space under BC-type-2 and crack subjected to linear normal traction $t_1^+ = 0$, $t_2^+ = -\sigma_0(x_3/a)$, $t_3^+ = 0$; and (iii) half-space under BC-type-3 and crack subjected to three types of loading conditions: uniform distributed pressure (denoted by **0**), linear distributed pressure (denoted by **1**), and quadratic distributed pressure (denoted by **2**) as shown in Figure 5.5(b). In the numerical simulations, three different meshes are adopted as shown in Figure 5.5(c).

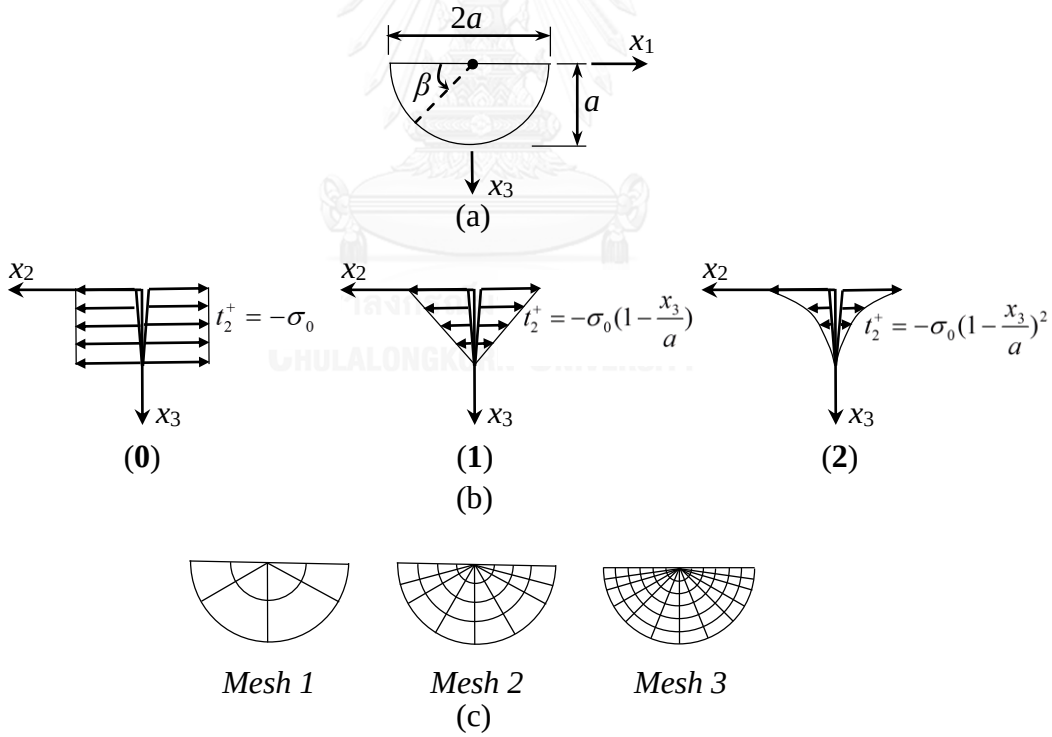

Figure 5.5: (a) Schematic of semi-circular surface-breaking crack in half-space under BC-type-3, (b) crack under three loading conditions, and (c) three meshes used in analysis.

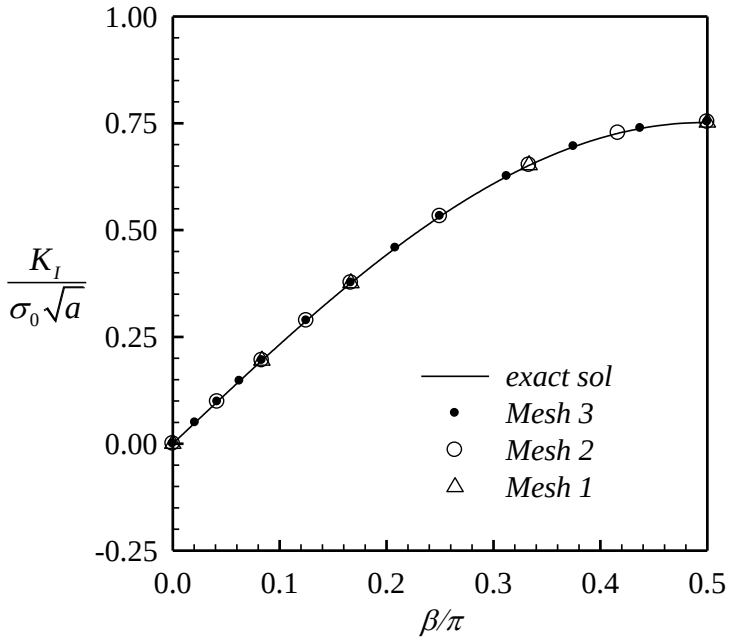

(a)

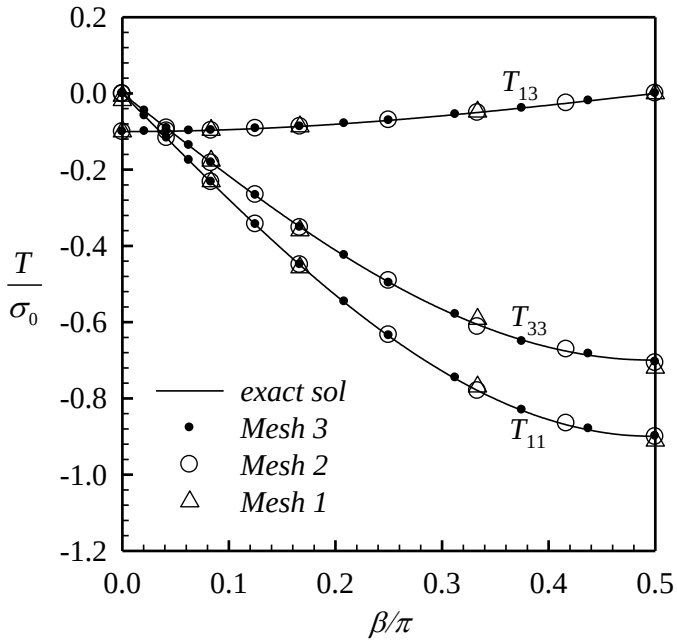

(b)

Figure 5.6: (a) Normalization of mode-I stress intensity factor and (b) normalized T-stress for semi-circular surface-braking crack in half-space under BC-type-2 and subjected to linear normal traction.

For the first two cases, the computed stress intensity factors and the non-zero T-stress components are compared with the existing analytical solutions. As indicated in Table 5.7, numerical results obtained for the uniform normal traction under BC-type-1 are normalized by $K_I^{exact} = 2\sigma_0\sqrt{a/\pi}$ for the mode-I stress intensity factor and those proposed by Wang (2004) for the non-zero T-stress components. Clearly, the present results agree with the analytical solutions. The maximum difference is less than 0.2% for the stress intensity factor and 0.57% for the T-stress components. For the case of linear normal traction under BC-type-2, the normalized mode-I stress intensity factor and T-stress components are compared with the benchmark solution obtained from Shah and Kobayashi (1971) and Rungamornrat and Pinitpanich (2015) (also found in Wang, 2004), respectively, and reported in Figure 5.6. It is clear that the obtained numerical results are nearly indistinguishable from the reference solution.

For the last case, as shown in Table 5.8, the computed stress intensity factors normalized by $K_I^{ref} = \sigma_0\sqrt{\pi a}$ at the intersection point between the crack boundary and the free surface (a surface breaking point) and the deepest point are compared with those obtained by Noguchi and Smith (1995) and Murakami (1985). It is seen that results generated by the proposed technique exhibit good agreement with the benchmark solutions. In particular, the discrepancy between the computed stress intensity factors and the solution reported by Noguchi and Smith (1995) and Murakami (1985) at the surface-breaking point is larger than that at the deepest point. In additkb8yannhion, results obtained from the coarse and intermediate meshes are nearly indistinguishable from those generated by the Mesh 3 (with the maximum discrepancy less than 2%).

Table 5.7: Normalized mode-I stress intensity factors and T-stresses at $\beta = \{0^0, 90^0\}$ for semi-circular surface-breaking crack within half-space under BC-type-1 and subjected to uniform normal traction.

β	Mesh	Stress intensity factor	T-stress	
		K_I / K_I^{exact}	T_{11} / T_{11}^{exact}	T_{33} / T_{33}^{exact}
0^0	1	0.9995	0.9989	0.9944
	2	1.0004	0.9971	0.9989
	3	1.0005	0.9964	0.9989
30^0	1	0.9992	1.0018	1.0013
	2	1.0011	0.9970	0.9993
	3	1.0009	0.9954	0.9987
90^0	1	0.9981	1.0023	1.0006
	2	1.0010	0.9965	0.9990
	3	1.0011	0.9951	0.9987

Table 5.8: Normalized mode-I stress intensity factors for semi-circular surface-breaking crack within half-space under BC-type-3 and subjected to three types of loading conditions.

Loading condition	Mesh	$\beta = 0^0$			$\beta = 90^0$		
		Present results	Noguchi	Murakami	Present results	Noguchi	Murakami
0	1	0.783	0.760	0.748	0.660	0.656	0.666
	2	0.777			0.659		
	3	0.772			0.659		
1	1	0.662	0.644		0.193	0.191	
	2	0.658			0.192		
	3	0.655			0.192		
2	1	0.588	0.573		0.111	0.111	
	2	0.585			0.113		
	3	0.583			0.113		

5.1.2 Anisotropic Cracked Half-Space under BC-type-α

In this particular sub-section, the integral formulation and the implemented numerical procedure are verified for the case of an anisotropic cracked half space under symmetric boundary condition (BC-type-1) and anti-symmetric boundary condition (BC-type-2). Results are reported for a selected representative material which is transversely isotropic with the elastic constants shown in Table 5.1 and compared with the reference solution generated from an equivalent whole space problem (obtained from invoking the symmetrical and anti-symmetrical conditions) by the weakly singular SGBEM proposed by Rungamornrat and Mear (2008b).

a. Horizontal penny-shaped crack

Consider the same problem corresponding to a horizontal penny-shaped crack indicated in Figure 5.1(a) except that the half-space is made of the transversely isotropic, linearly elastic material. The normalized stress intensity factors and the T-stress components along the crack boundary are reported and compared with the reference solutions in Figure 5.8 and Figure 5.9 for BC-type-1 and BC-type-2, respectively. As can be observed from these results, the computed stress intensity factors and T-stress components for both BC-type-1 and BC-type-2 are highly accurate when compared

with the reference solutions and weakly dependent on the meshes used. Similar convergence behavior and the high quality of numerical solutions can also be observed for other types of anisotropic materials such as cubic and orthotropic solids (see Appendix C).

b. Vertical penny-shaped crack

Next, consider the same problem of a vertical penny-shaped crack under the uniform normal traction as shown in Figure 5.2 with the material being replaced by one that is transversely isotropic. In the analysis, the ratio $h/a = 1.25$ is utilized and the same three meshes are employed. The computed stress intensity factors and the T-stress components are normalized and compared with the reference solutions in the same manner as the case of the horizontal penny-shaped crack.

As can be observed from numerical results shown in Figure 5.10, the computed mode-I stress intensity factor show very good agreement with the reference solution for all three meshes and both types of boundary conditions. Similarly, numerical solutions for the T-stress components shown in Figure 5.11 also indicate the good convergence behavior and the slight dependence on the level of refinement. Clearly, results generated by the coarsest, intermediate and finest meshes are almost indistinguishable from the benchmark solution. The high quality of the numerical solutions results directly, again, from using special crack-tip elements to capture the near-front relative crack-face displacement. It should also be remarked that, for this particular case, the symmetric and anti-symmetric boundary conditions have only weak influence on both the value and distribution of the stress intensity factor and the T-stress components along the crack front. Results for cubic and orthotropic materials are also generated for this particular crack problem and reported in Appendix C.

c. Surface-breaking crack

As a final example, consider a semi-circular, surface-breaking crack of radius *a* and oriented vertically in a half-space as shown in Figure 5.7(a) and (b). The crack front is parameterized by $x_1 = -a\cos\beta$, $x_2 = 0$, $x_3 = a\sin\beta$ for $\beta \in [0, \pi]$. The surface $x_3 = 0$ of the half-space is subjected to the boundary conditions BC-type-1 and BC-type-2 whereas the crack is subjected to three types of loading conditions: the non-uniform normal traction $t_1^+ = t_3^+ = 0,\ t_2^+ = -\sigma_0 (x_3/a)^2$, the non-uniform horizontal shear traction $t_2^+ = t_3^+ = 0,\quad t_1^+ = \sigma_0 (x_3/a)^2$, and the non-uniform vertical shear traction $t_1^+ = t_2^+ = 0,$

$t_3^+ = \sigma_0 (x_3/a)^2$. Three meshes as depicted in Figure 5.7(d) are exploited in the simulations and the reference solution obtained from the Mesh 4 in Figure 5.2(d) is constructed based on an equivalent whole space containing a vertical penny-shaped crack of radius a with the plane $x_3 = 0$ passing through its center and subjected to symmetric and anti-symmetric tractions on the crack surface (see Figure 5.7(c)).

For the first loading condition, the mode-II and mode-III stress intensity factors vanish whereas the mode-I stress intensity factor and the T-stress components vary along the fracture boundary. The computed mode-I stress intensity factor and the non-zero T-stress components are reported in Figures 5.12 and 5.13, respectively. In addition to the good agreement between the computed numerical results and the benchmark solution and the weak dependence on the mesh refinement, it is also observed that the discrepancy between mode-I stress intensity factor and all T-stress components for BC-type-1 and BC-type-2 are insignificant.

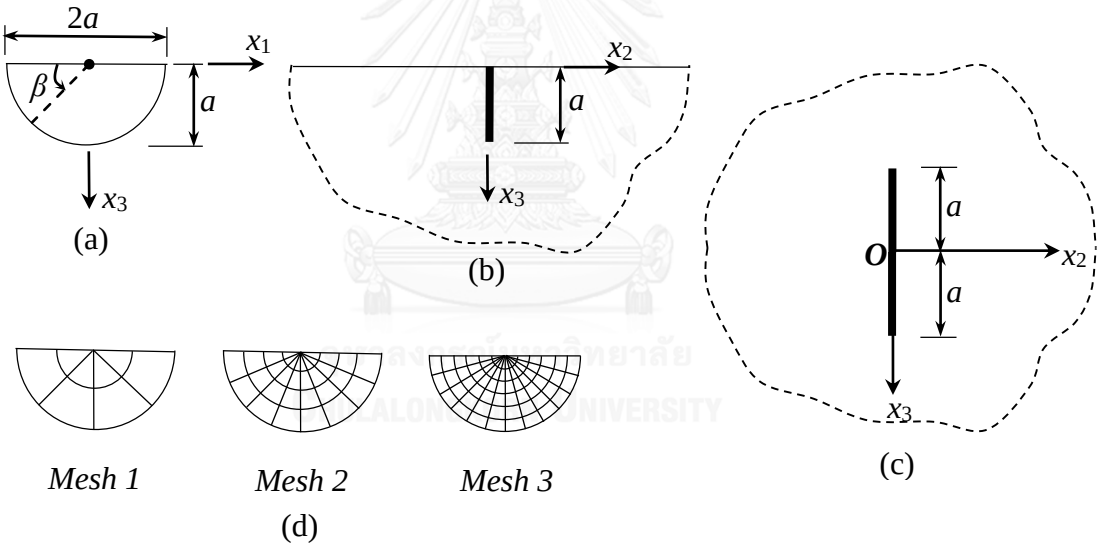

Figure 5.7: (a) Schematic semi-circular surface breaking crack, (b) semi-circular surface-breaking crack in half-space, (c) equivalent whole space problem, and (d) three meshes used in analysis.

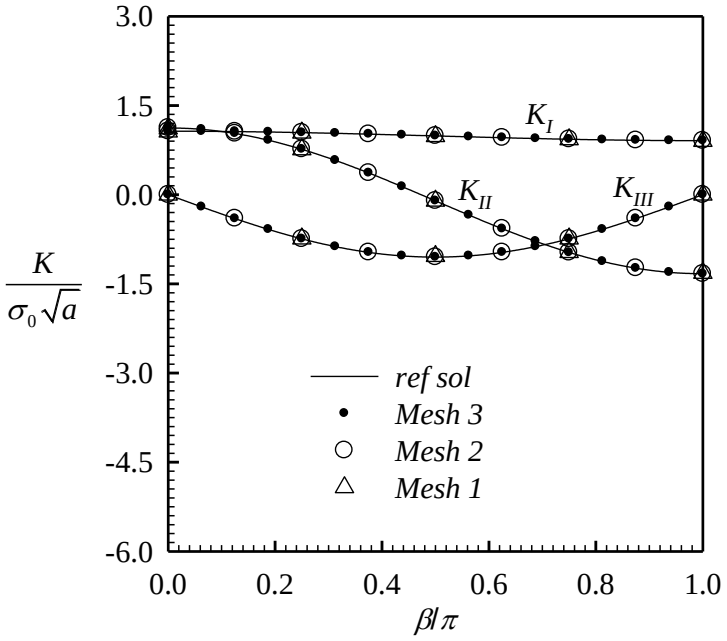

(a)

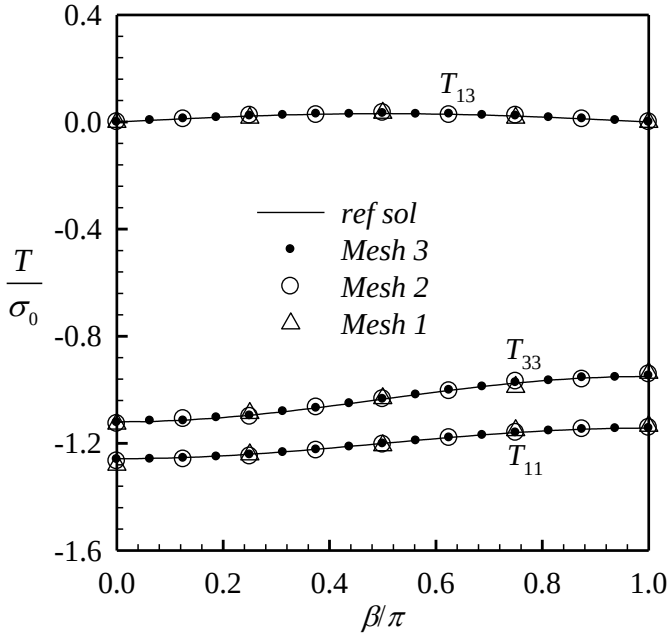

(b)

Figure 5.8: (a) Normalized stress intensity factors and (b) normalized T-stress components for horizontal penny-shaped crack in transversely isotropic half-space under BC-type-1.

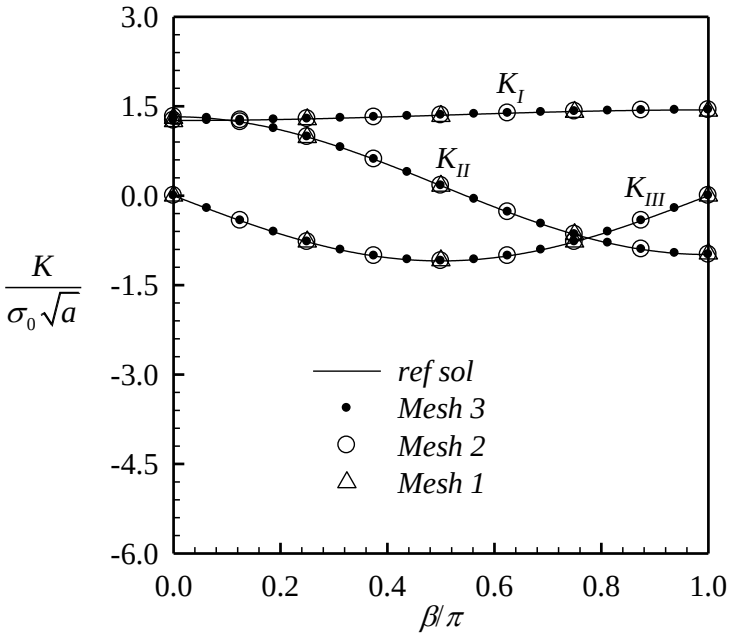

(a)

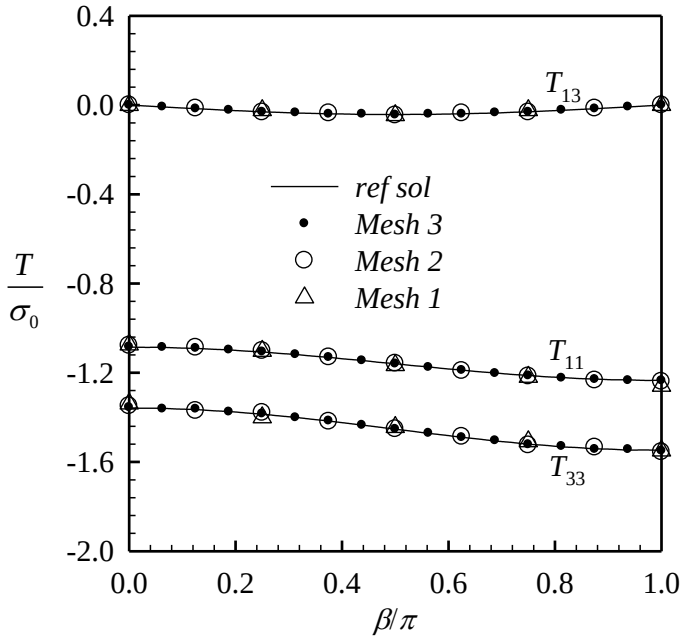

(b)

Figure 5.9: (a) Normalized stress intensity factors and (b) normalized T-stress components for horizontal penny-shaped crack in transversely isotropic half-space under BC-type-2.

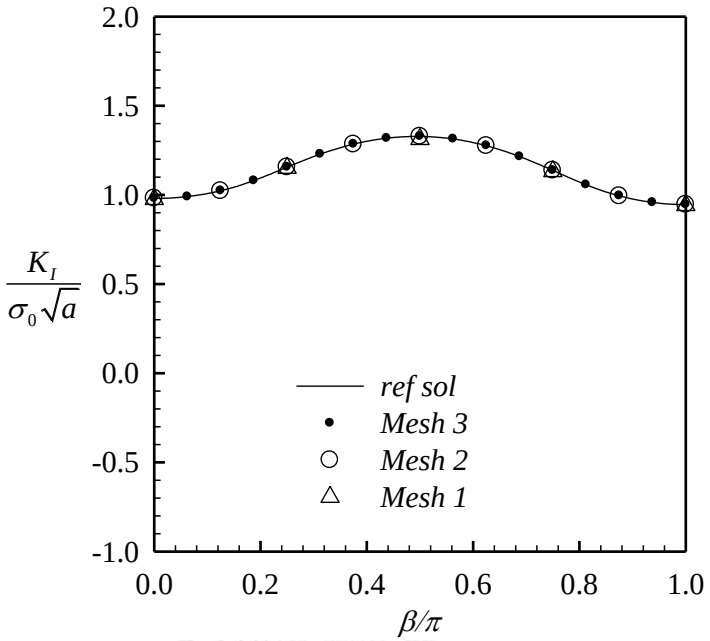

(a)

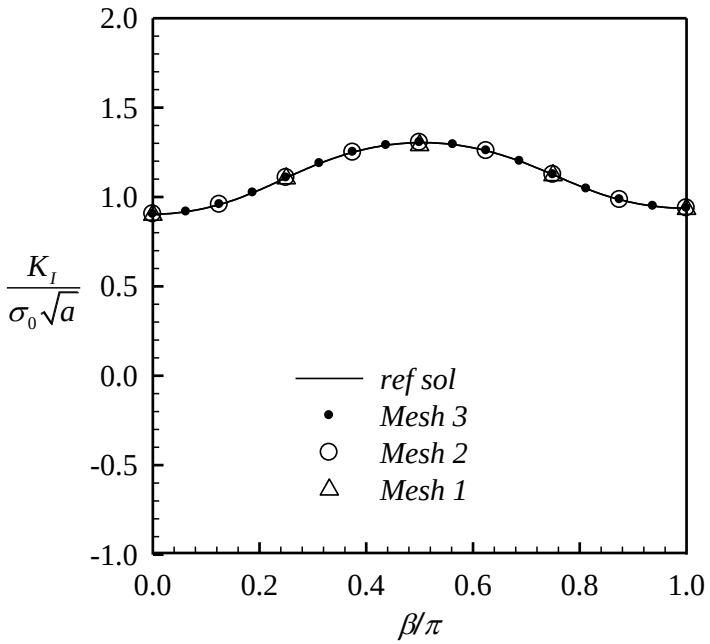

(b)

Figure 5.10: Normalized mode-I stress intensity factor for vertical penny-shaped crack in transversely isotropic half-space under (a) BC-type-1 and (b) BC-type-2.

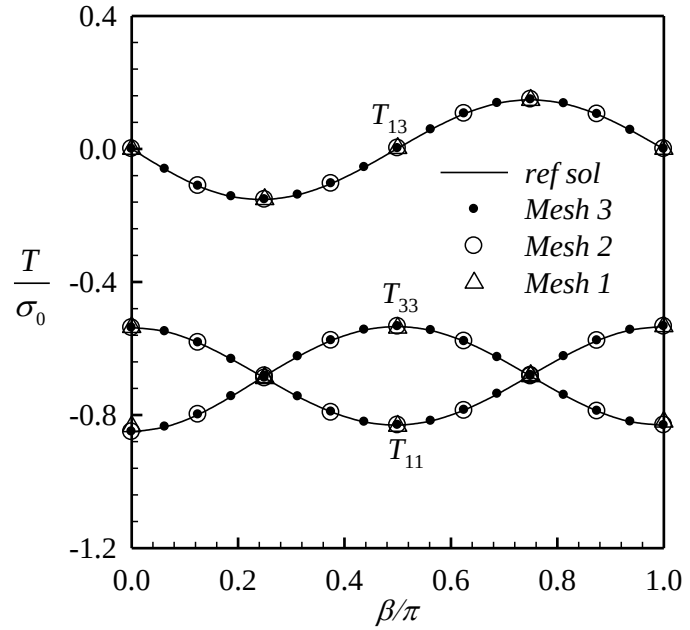

(a)

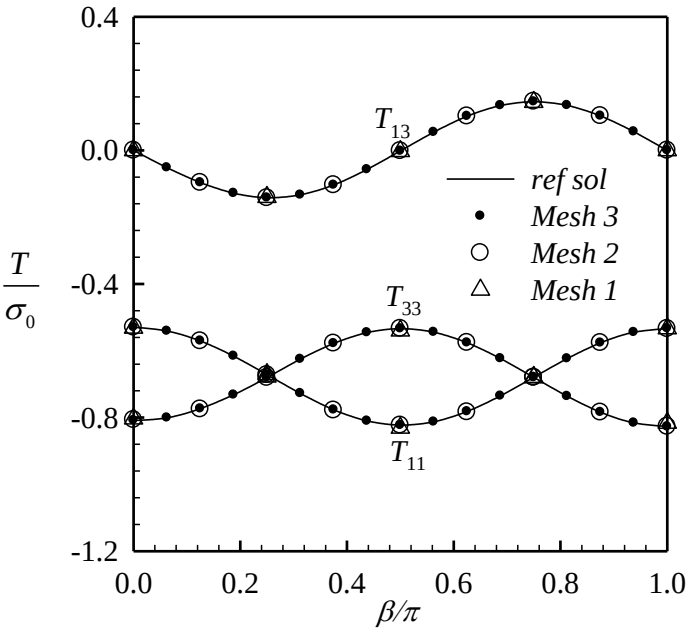

(b)

Figure 5.11: Normalized T-stress components for vertical penny-shaped crack in transversely isotropic half-space under (a) BC-type-1 and (b) BC-type-2.

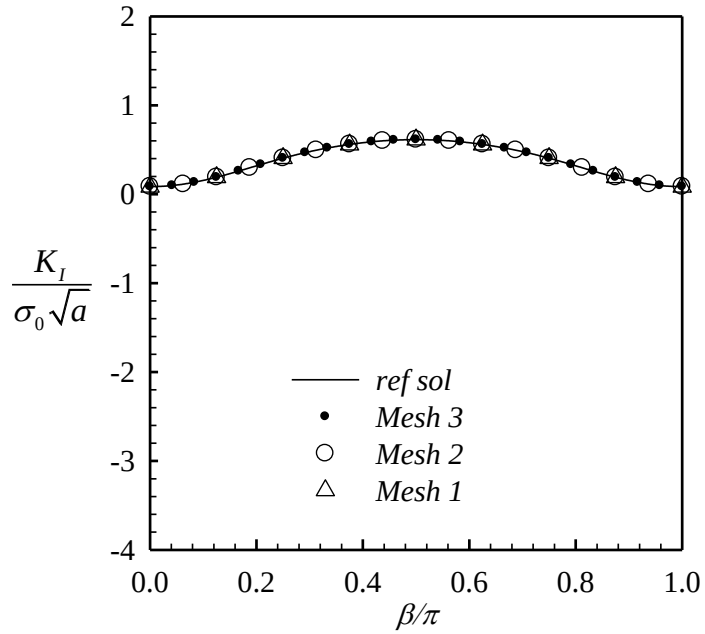

(a)

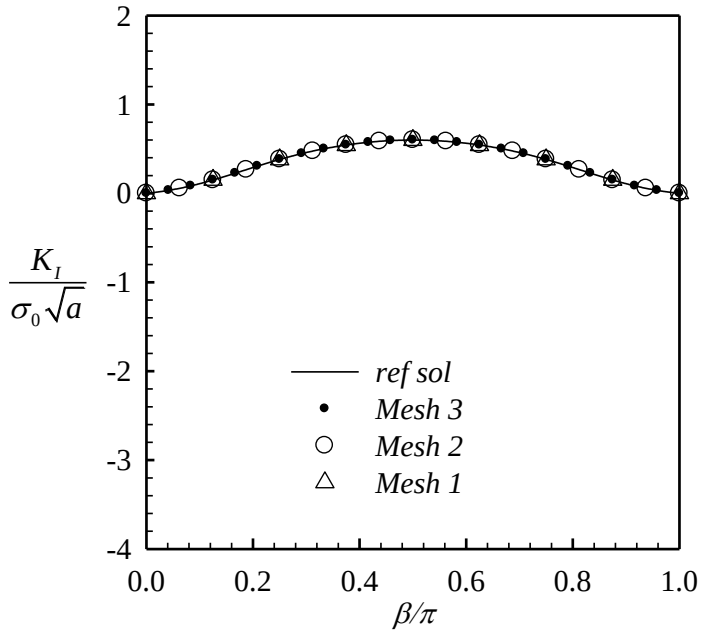

(b)

Figure 5.12: Normalized mode-I stress intensity factors for semi-circular surface-breaking crack subjected to non-uniform normal traction in transversely isotropic half-space under (a) BC-type-1 and (b) BC-type-2.

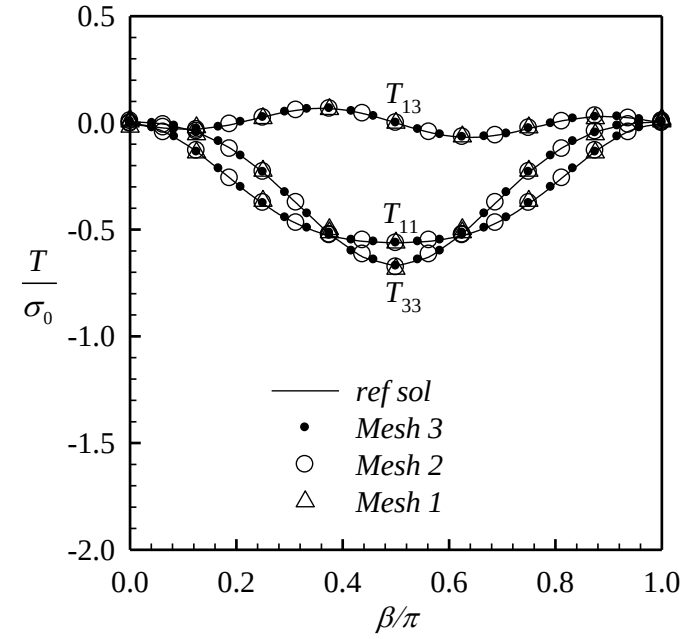

(a)

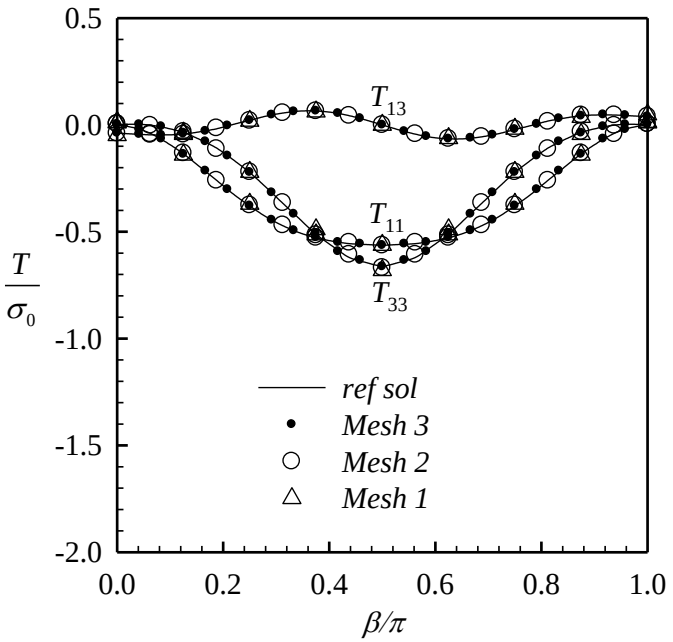

(b)

Figure 5.13: Normalized T-stress components for semi-circular surface-breaking crack subjected to non-uniform normal traction in transversely isotropic half-space under (a) BC-type-1 and (b) BC-type-2.

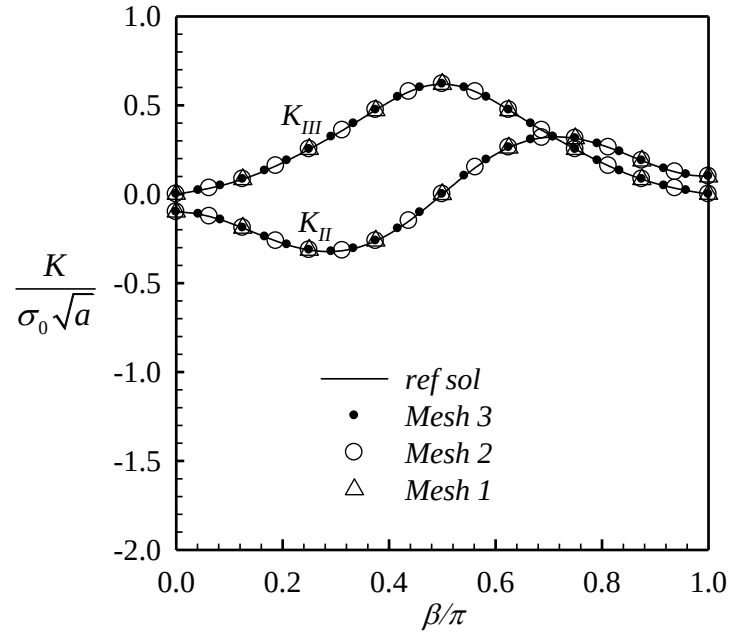

(a)

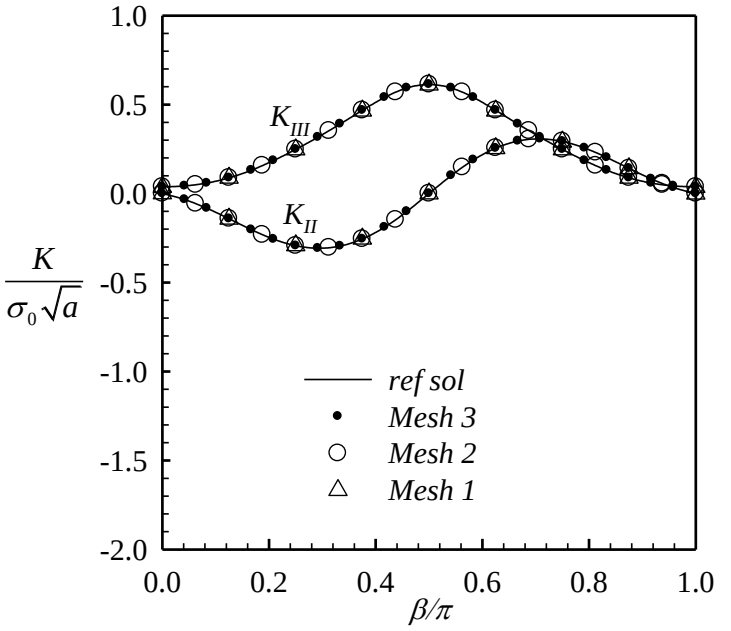

(b)

Figure 5.14: Normalized stress intensity factors for semi-circular surface-breaking crack subjected to non-uniform shear traction in x_1-direction in transversely isotropic half-space under (a) BC-type-1 and (b) BC-type-2.

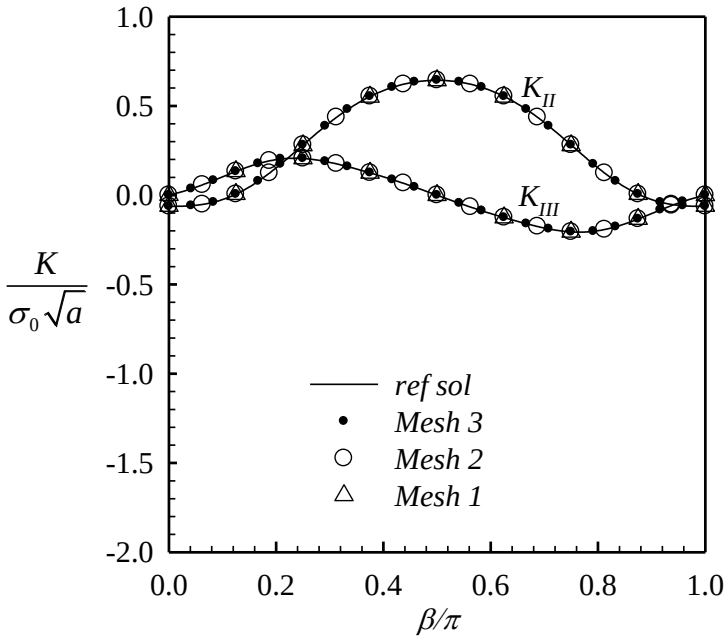

(a)

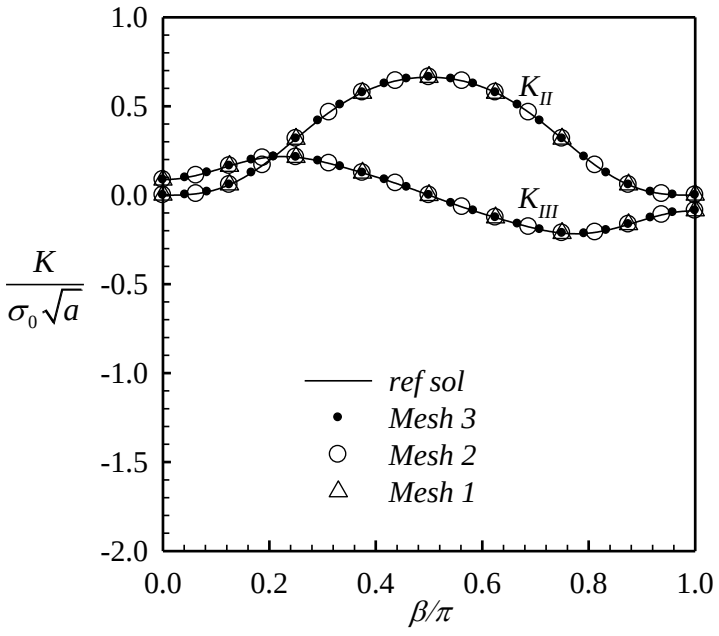

(b)

Figure 5.15: Normalized stress intensity factors for semi-circular surface-breaking crack subjected to non-uniform shear traction in x_3-direction in transversely isotropic half-space under (a) BC-type-1 and (b) BC-type-2.

Unlike the first loading case, the applied shear traction in either x_1- or x_3-direction yields zero mode-I stress intensity factor and the T-stress components along the fracture front. The non-zero mode-II and mode-III stress intensity factors for the second and third loading conditions are reported for all three meshes along with the reference solution in Figures 5.14 and 5.15, respectively. Similar to all previous cases, it is apparent that the proposed technique yields highly accurate numerical solutions which are comparable to the benchmark results for all three meshes employed. In addition, obtained results also suggest that both the value and distribution of the stress intensity factors are weakly dependent on the boundary condition posed on the half-space surface.

Additional results for both cubic and orthotropic materials for all three types of crack-face loading are also reported in Appendix C.

5.2 Investigation for complex problems

Once the integral formulation and implemented solution procedure are fully tested, more complex boundary value problems involving multiple and non-flat cracks are presented here to additionally demonstrate both the robustness and capability of the proposed technique. The convergence behavior of numerical results is investigated by performing the simulations using a series of meshes.

5.2.1. Embedded Spherical Cap Crack

Consider a linearly elastic half-space containing a spherical cap crack of radius *a* and a half-subtended angle α as depicted in Figure 5.16(a). The orientation of the crack is such that its surface can be parameterized by $x_1 = a\sin\theta\cos\beta$, $x_2 = -a\sin\theta\sin\beta$, $x_3 = h + a - a\cos\theta$ where $\theta \in [0,\alpha]$, $\beta \in [0,2\pi]$ and h is the distance from the half-space surface to the top of the spherical cap crack. The half-space is subjected to the remote uniform biaxial tensions $\sigma_{11} = \sigma_{33} = \sigma_0$ as indicated in Figure 5.16(b). In the simulations, the half-subtended angle is taken as $\alpha = 45^0$; the depth is taken as $h/a = 0.5$; and four meshes indicated in Figure 5.16(c) are exploited. Similar to the previous section, two types of materials (e.g., isotropic and transversely isotropic materials with the elastic constants shown in Table 5.1) are chosen in the simulations. Additional results generated for other types of anisotropic materials (e.g., cubic and orthotropic materials) are provided in Appendix C.

For isotropic case, the computed stress intensity factors and T-stress components under all four types of boundary conditions are first normalized by $K_{ref} = \sigma_0\sqrt{a}$ and

$T_{ref} = \sigma_0$, respectively, and then reported in Figure 5.17 and Figure 5.20 for all the first three meshes. It can be observed that the numerical results generated from the coarsest and intermediate meshes are nearly identical to that generated by the Mesh 3 for all cases. Similarly, the computed stress intensity factors and T-stress components for the transversely isotropic elastic half-space under the boundary conditions BC-type-1 and BC-type-2 are first normalized by $K_{ref} = \sigma_0\sqrt{a}$ and $T_{ref} = \sigma_0$, respectively, and then reported in Figure 5.21 and Figure 5.22 for all the first three meshes. It can be seen, again, for this relatively complex boundary value problem posed by the material anisotropy and non-planar crack geometry that results obtained from the three different meshes are still in excellent agreement. This good convergence behavior and the requirement of using relatively coarse meshes to accurately capture the numerical solutions should result directly from the selection of suitable shape functions for crack-tip elements to approximate the near-front relative crack face displacement. Besides, results from the first two boundary conditions are also compared with the reference solutions generated from an equivalent whole space containing a pair of geometrically symmetric cracks with respect to the plane $x_3 = 0$ using the SGBEM with the Mesh 4. The good agreement between obtained results and the reference solution is observed for both the stress intensity factors and the T-stress components (see Figure 5.17-5.18 and Figure 5.21-5.22).

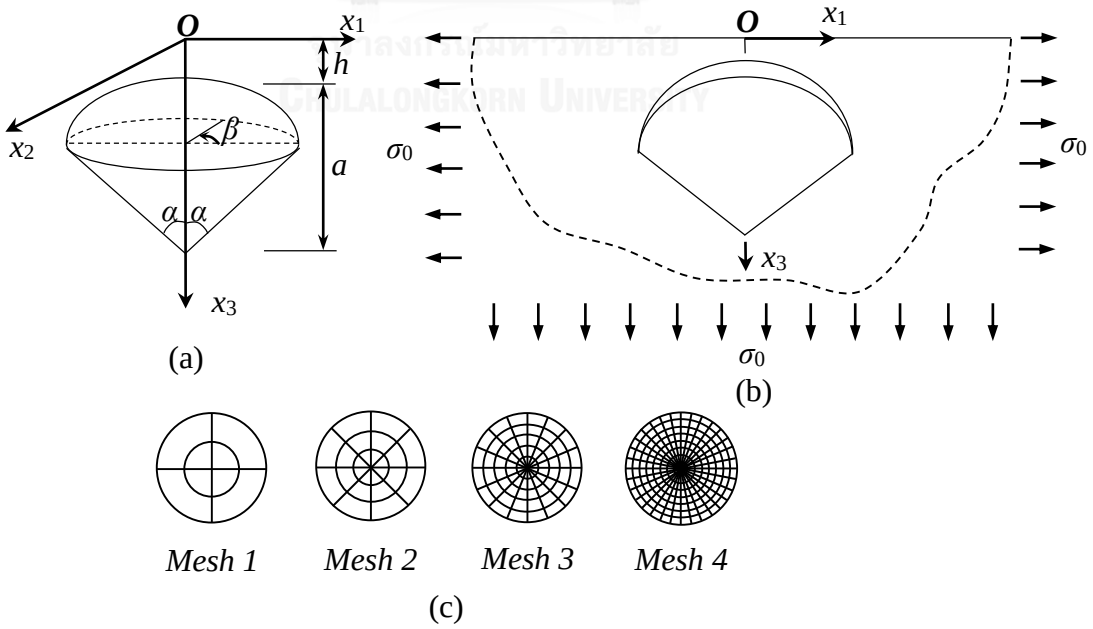

Figure 5.16: (a) Schematic of spherical cap crack embedded in an elastic half-space, (b) remote uniform biaxial tensions, and (c) three meshes adopted in analysis.

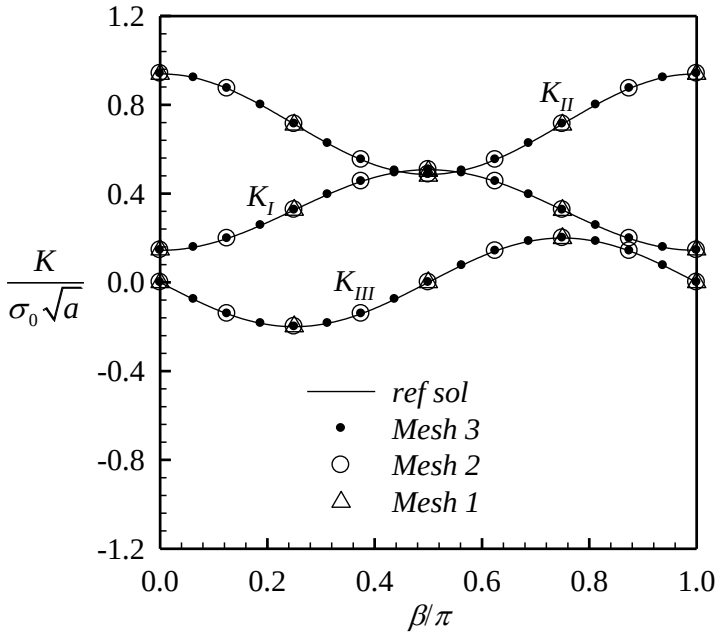

(a)

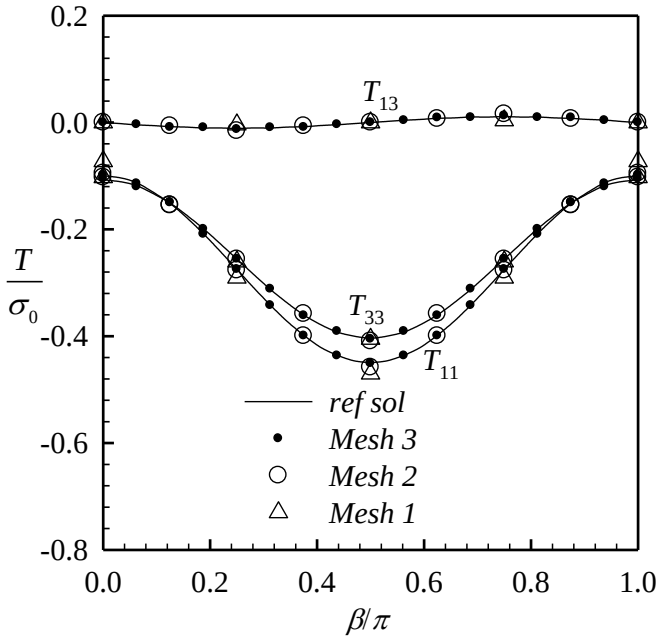

(b)

Figure 5.17: (a) Normalized stress intensity factors and (b) normalized T-stress components for spherical cap crack in isotropic half-space under BC-type-1.

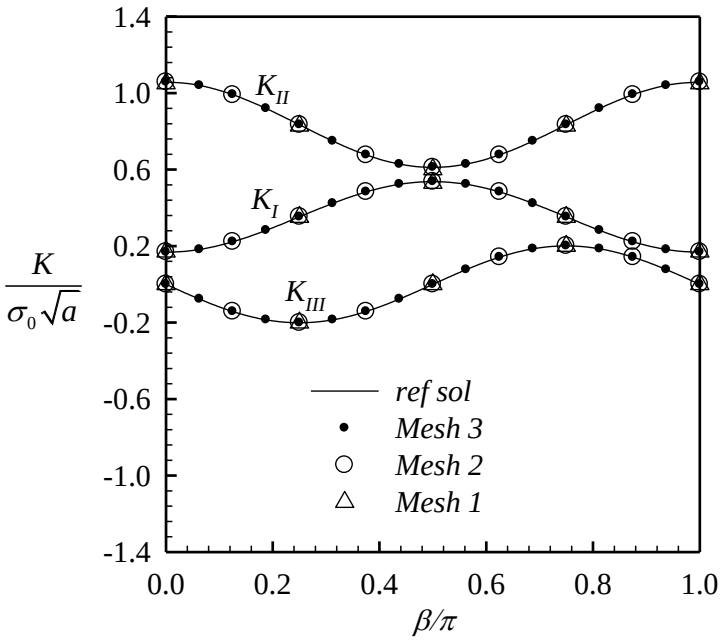

(a)

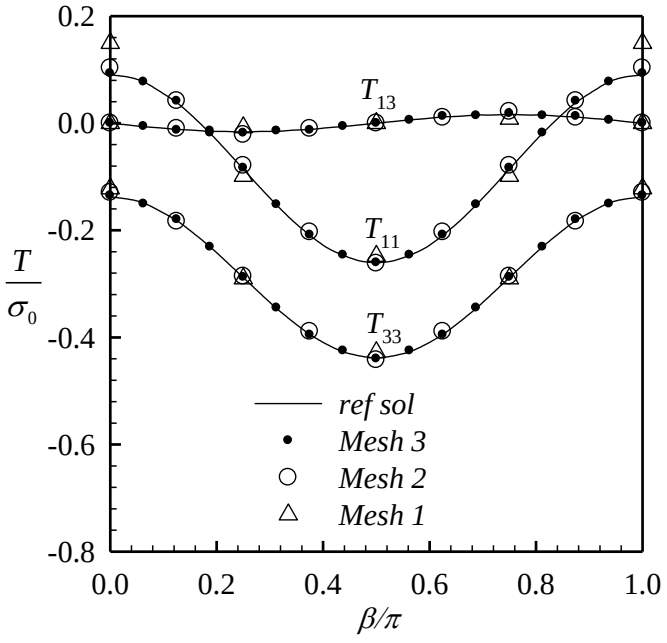

(b)

Figure 5.18: (a) Normalized stress intensity factors and (b) normalized T-stress components for spherical cap crack in isotropic half-space under BC-type-2.

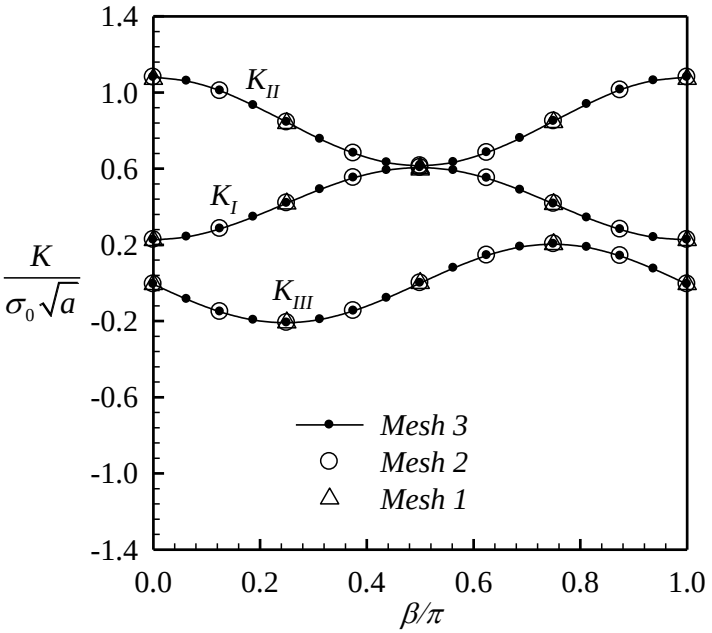

(a)

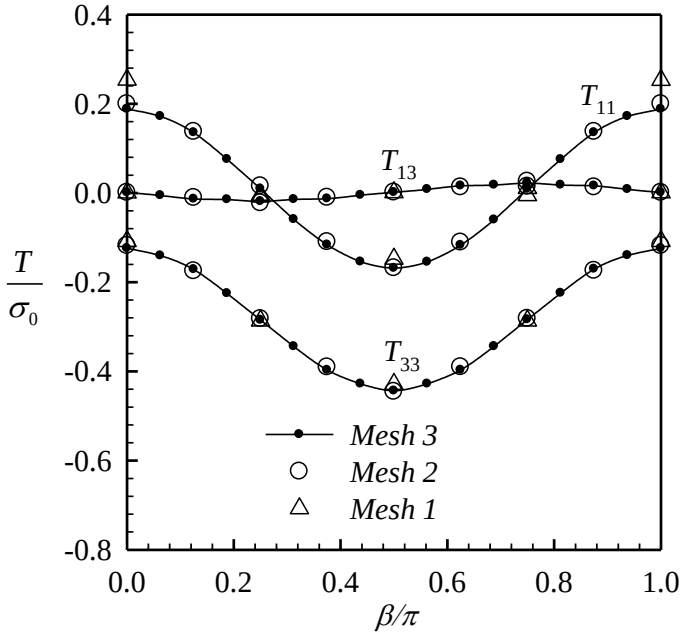

(b)

Figure 5.19: (a) Normalized stress intensity factors and (b) normalized T-stress components for spherical cap crack in isotropic half-space under BC-type-3.

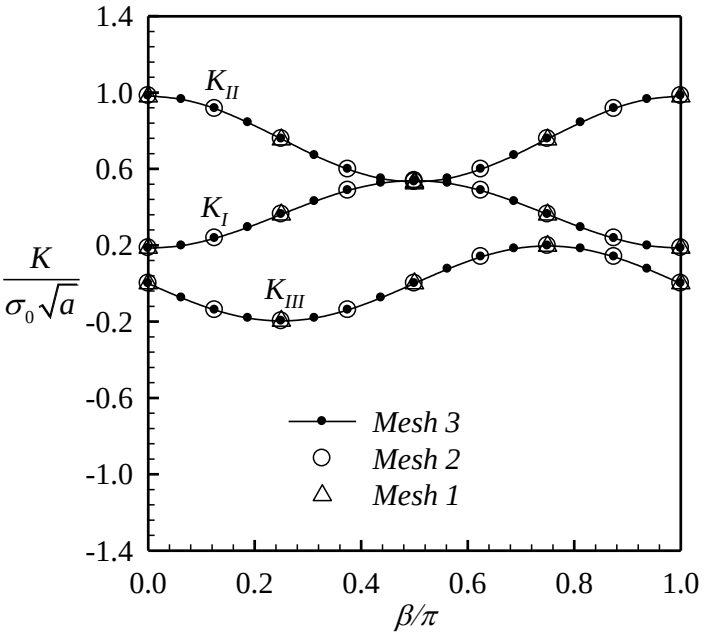

(a)

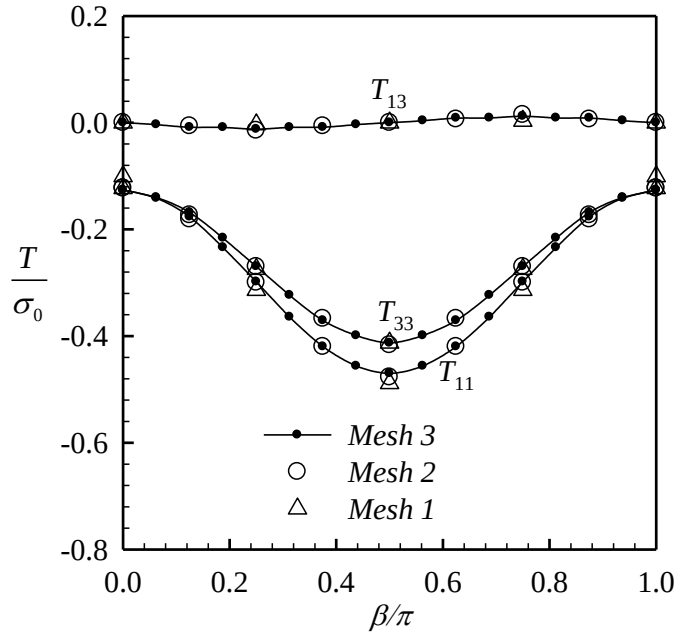

(b)

Figure 5.20: (a) Normalized stress intensity factors and (b) normalized T-stress components for spherical cap crack in isotropic half-space under BC-type-4.

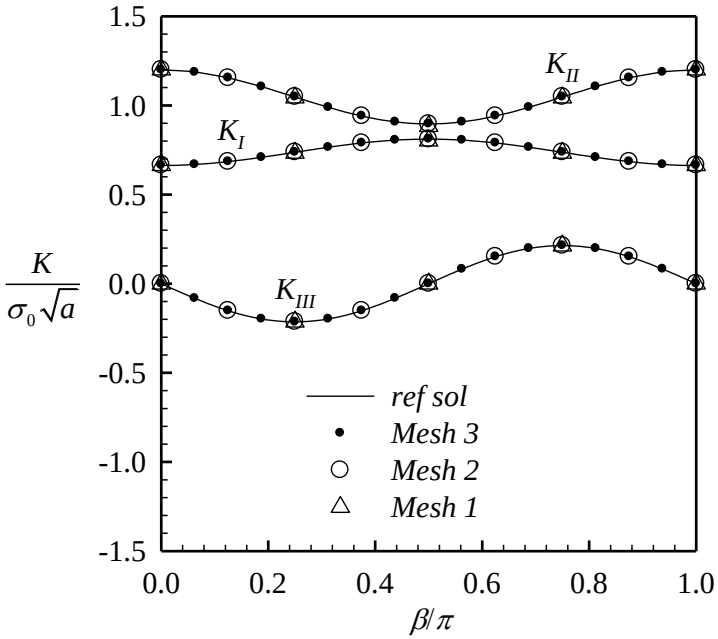

(a)

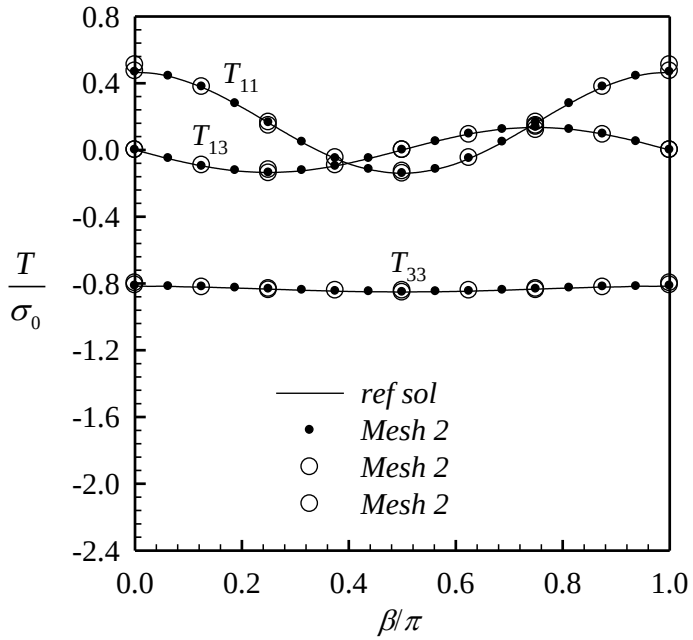

(b)

Figure 5.21: (a) Normalized stress intensity factors and (b) normalized T-stress components for spherical cap crack in transversely isotropic half-space under BC-type-1.

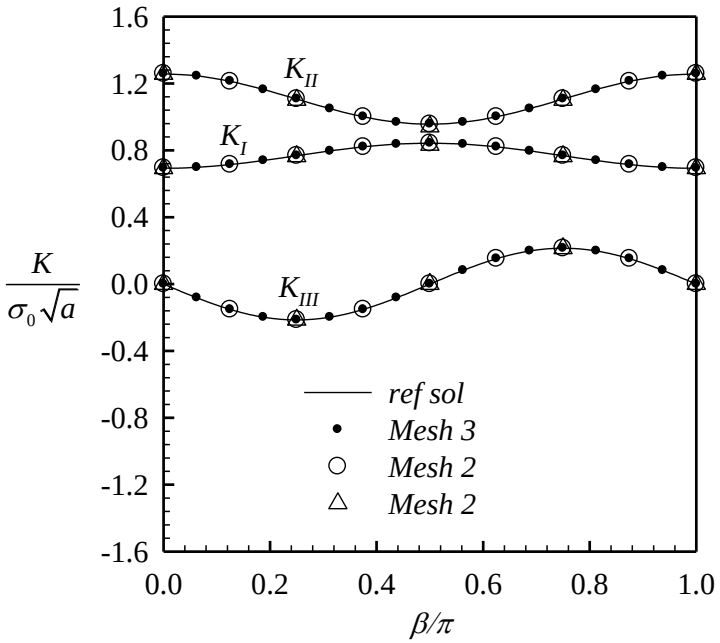

(a)

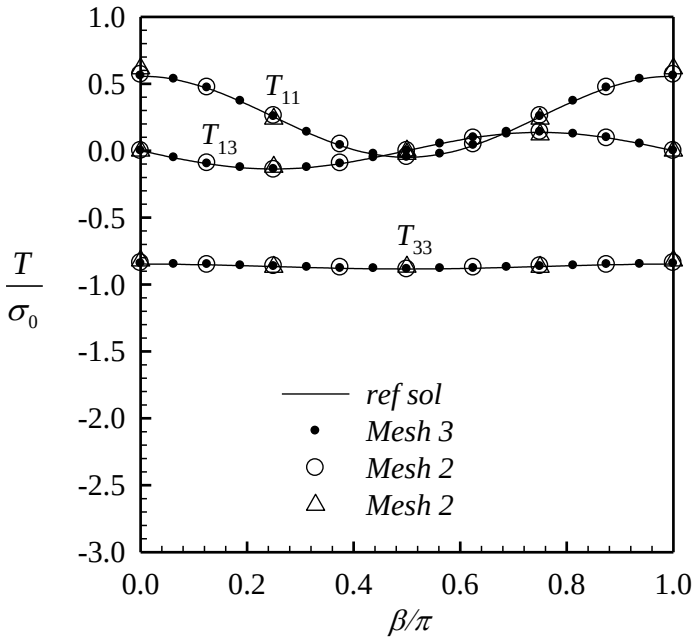

(b)

Figure 5.22: (a) Normalized stress intensity factors and (b) normalized T-stress components for spherical cap crack in transversely isotropic half-space under BC-type-2.

5.2.2. Two Embedded Elliptical Cracks

Consider an elastic half-space containing two identical, vertical elliptical cracks as indicated in Figure 5.23(a). The half-space is subjected to a uniform remote uniaxial tension σ_0 as shown in Figure 5.23(b). The crack front of both is parameterized by

$$\text{Crack 1:}\quad x_1 = 0;\quad x_2 = d - a\sin\beta;\quad x_3 = h + b\cos\beta \tag{5.1}$$

$$\text{Crack 2:}\quad x_1 = 0;\quad x_2 = -d - a\sin\beta;\quad x_3 = h + b\cos\beta \tag{5.2}$$

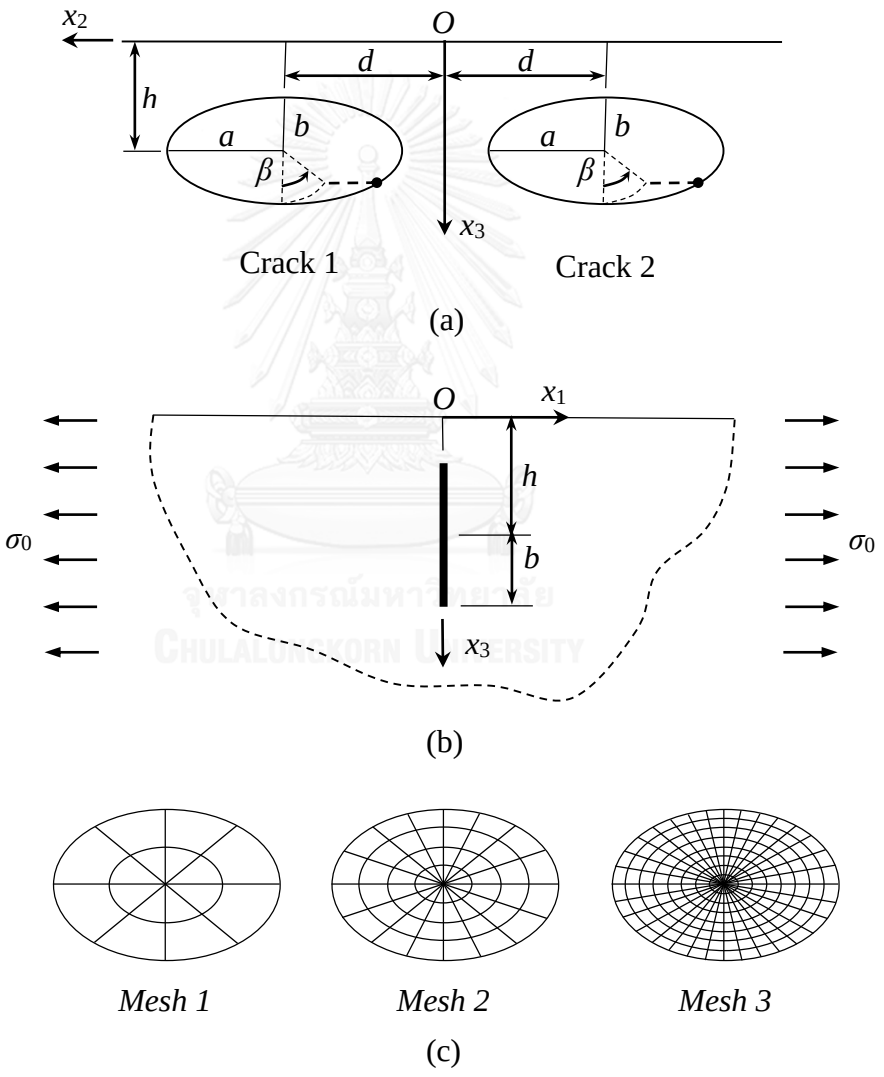

Figure 5.23: (a) Schematic of two identical elliptical cracks embedded in elastic half-space, (b) half-space under remote uniaxial tension in x_1-direction, and (c) three meshes adopted in analysis.

where d is the distance between the center of each crack and x_3-axis; a and b are the major and minor semi-axes of the elliptical cracks; and $\beta \in [0, 2\pi]$. In the simulations, the aspect ratio $a/b = 1.5$ and $d/a = 1.1,\ 2.0$ and two types of materials including isotropic and transversely isotropic solids are considered and three meshes shown in Figure 5.23(c) are employed. Due to the symmetry, the computed stress intensity factors and the T-stress components are reported only for the crack 1.

The stress intensity factors and the T-stress components generated from the three meshes for all four types of boundary conditions along the front of the crack 1 are reported in Figures 5.24-5.31. It is evident that the numerical solutions for the stress intensity factors and the T-stress components exhibit the good convergence behavior; in particular, the discrepancy between results obtained from the Mesh 1 and Mesh 2 and that from the Mesh 3 is insignificant for the two crack depths $d/a = 1.1$ and $d/a = 2.0$ considered in the simulations. In addition, the dependence of results along the crack front on the ratio d/a is also investigated. It is observed that the variation of both the stress intensity factors and the T-stress components at points on the crack front relatively close to those on the other crack is significant and strongly dependent on the ratio d/a. Clearly, the higher value of the ratio d/a, the less variation of the stress intensity factors and the T-stress components.

The normalized stress intensity factors and T-stress components obtained from the transversely isotropic half-space under BC-type-1 and BC-type-2 along the front of the crack 1 are reported in Figures 5.32-5.35. Similar to results of the isotropic case, the good convergence of both the stress intensity factors and the T-stress components for $d/a = 1.1$ and 2.0 are observed. In particular, results obtained from the coarse and intermediate meshes are almost indistinguishable from those computed from the fine mesh. Results shown in Figures 5.32-5.35 also indicate that the interaction of the two elliptical cracks and its influence on the stress intensity factors and the T-stress components is obviously dependent on the ratio d/a. The variation of the stress intensity factors and the T-stress components is found significant along the region of the crack front where the two cracks are relatively close. In particular, this variation is more rapid when the value of d is close to a.

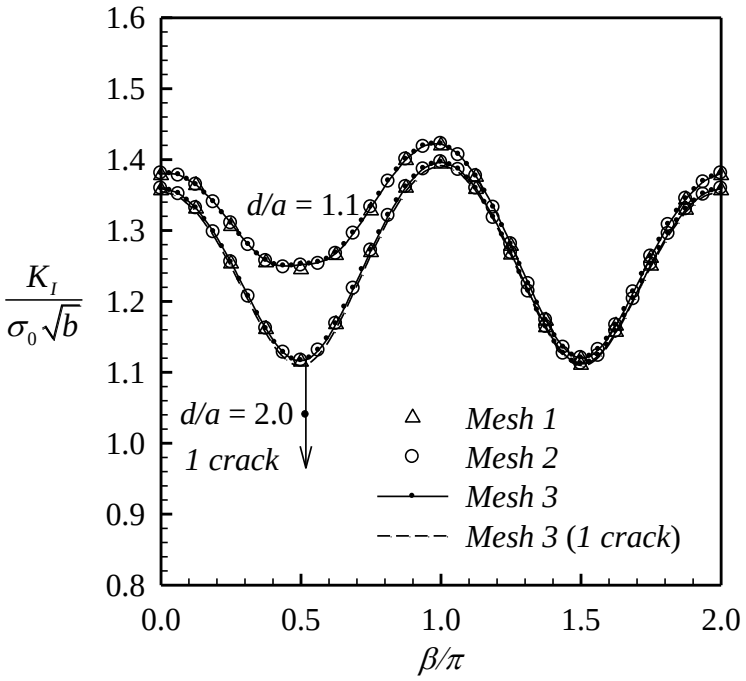

(a)

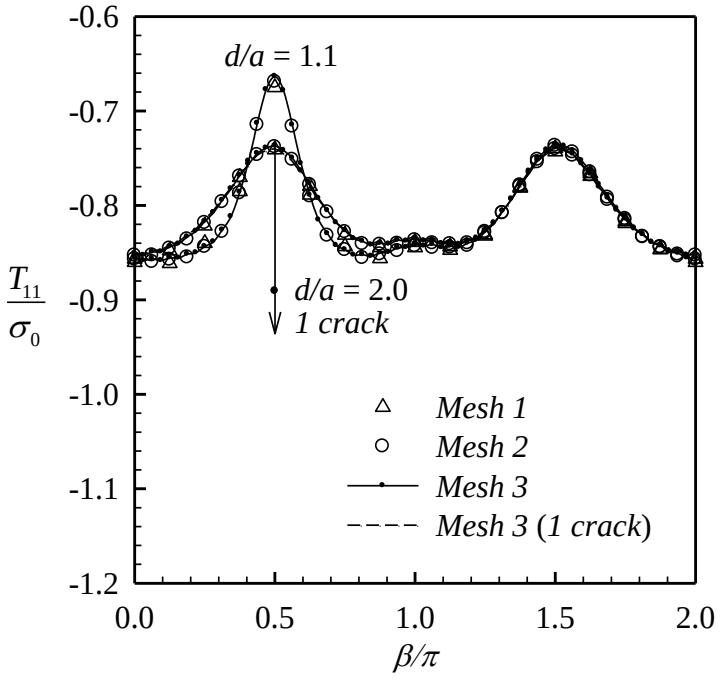

(b)

Figure 5.24: (a) Normalized mode-I stress intensity factor and (b) normalized T-stress component T_{11} for elliptical crack 1 in isotropic half-space under BC-type-1.

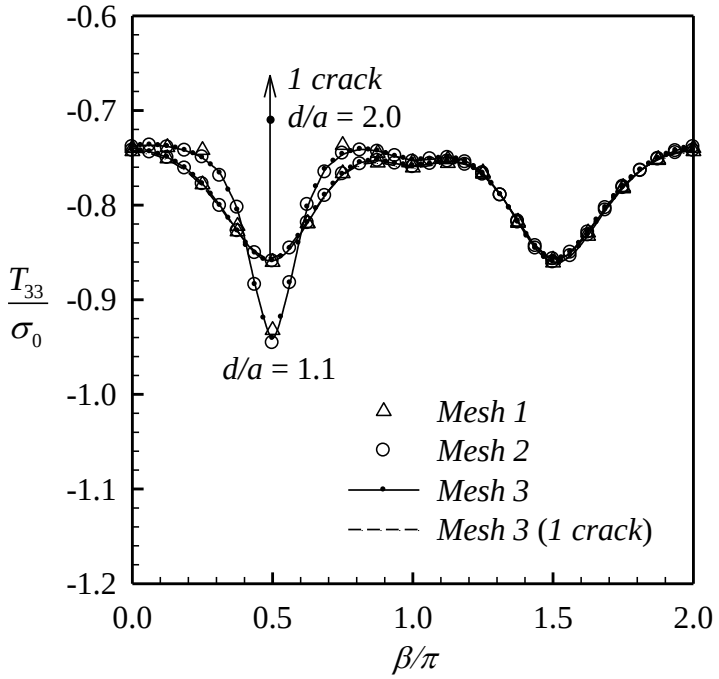

(a)

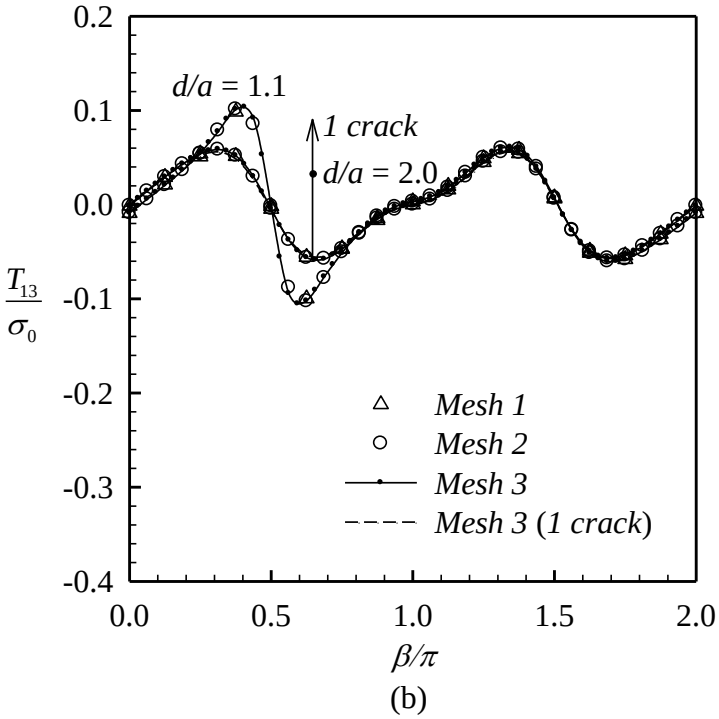

(b)

Figure 5.25: (a) Normalized T-stress component T_{33} and (b) normalized T-stress component T_{13} for elliptical crack 1 in isotropic half-space under BC-type-1.

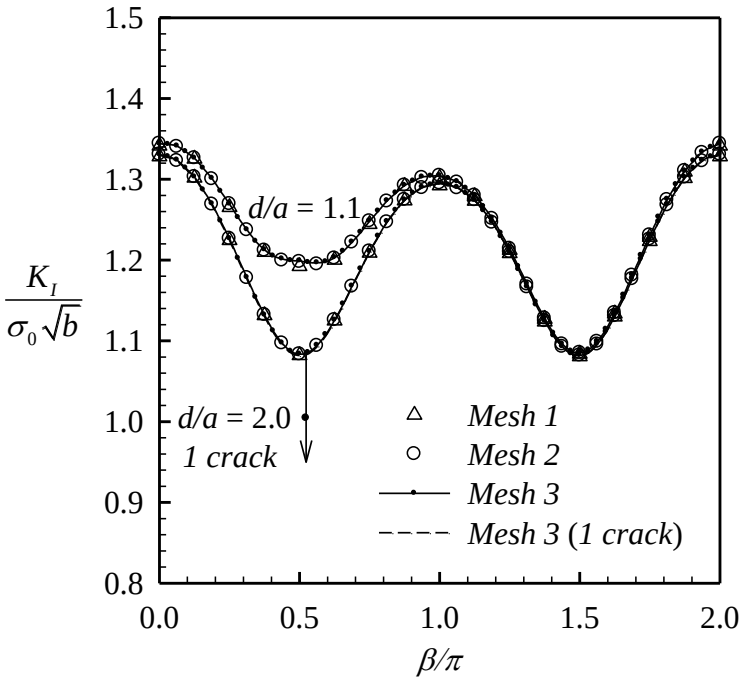

(a)

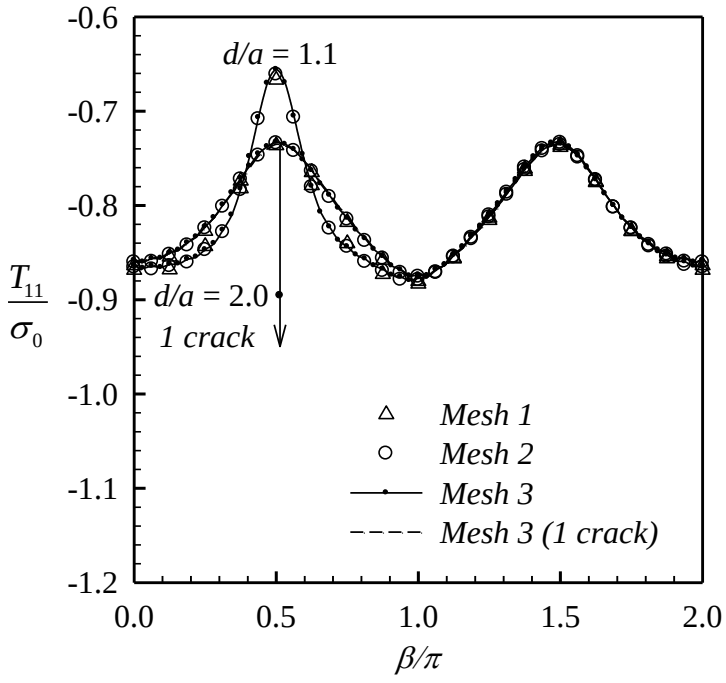

(b)

Figure 5.26: (a) Normalized mode-I stress intensity factor and (b) normalized T-stress component T_{11} for elliptical crack 1 in isotropic half-space under BC-type-2.

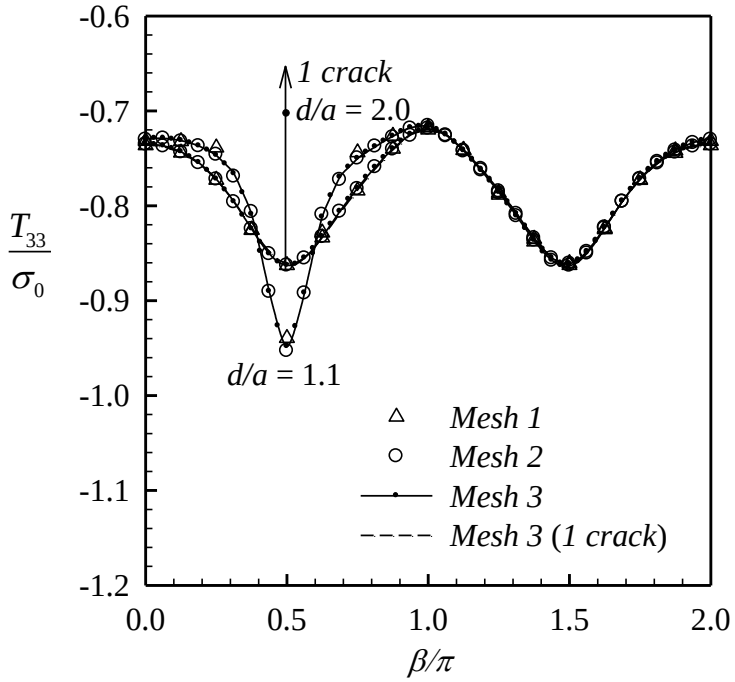

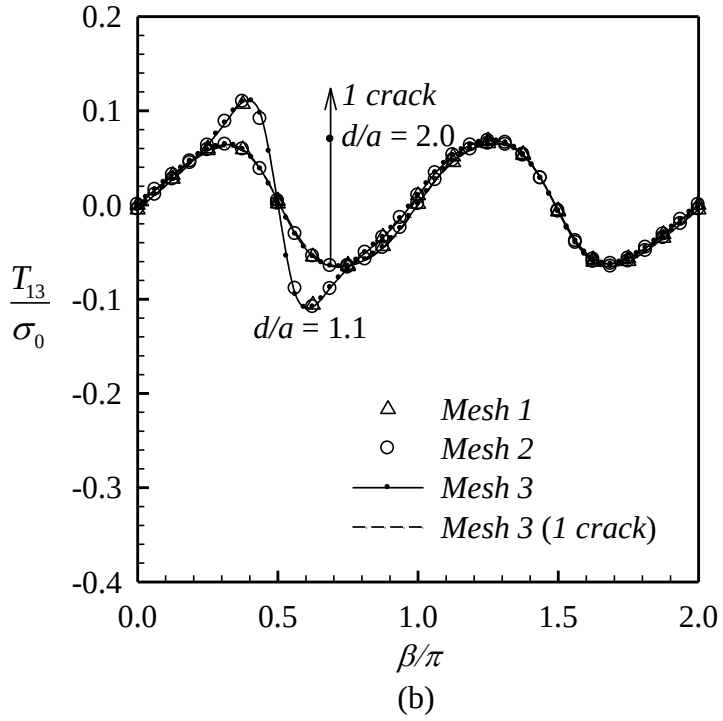

Figure 5.27: (a) Normalized T-stress component T_{33} and (b) normalized T-stress component T_{13} for elliptical crack 1 in isotropic half-space under BC-type-2.

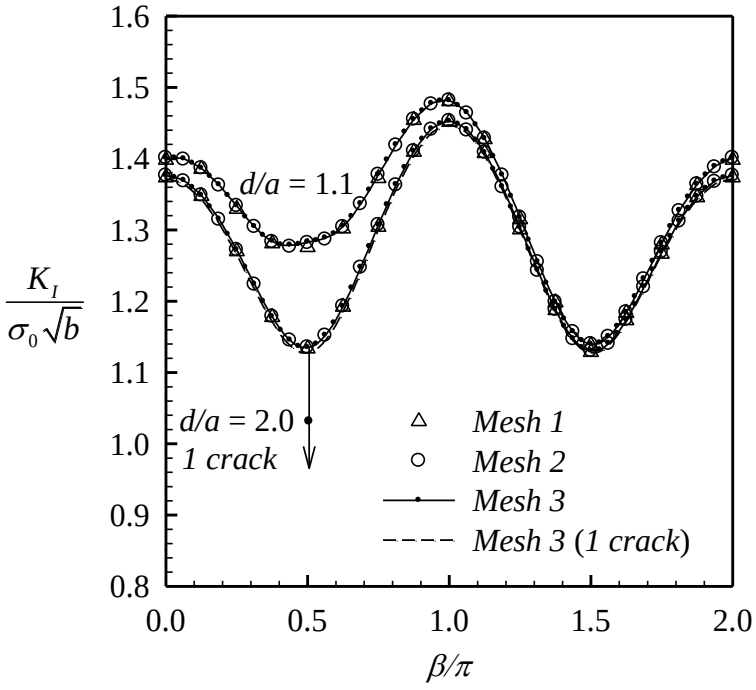

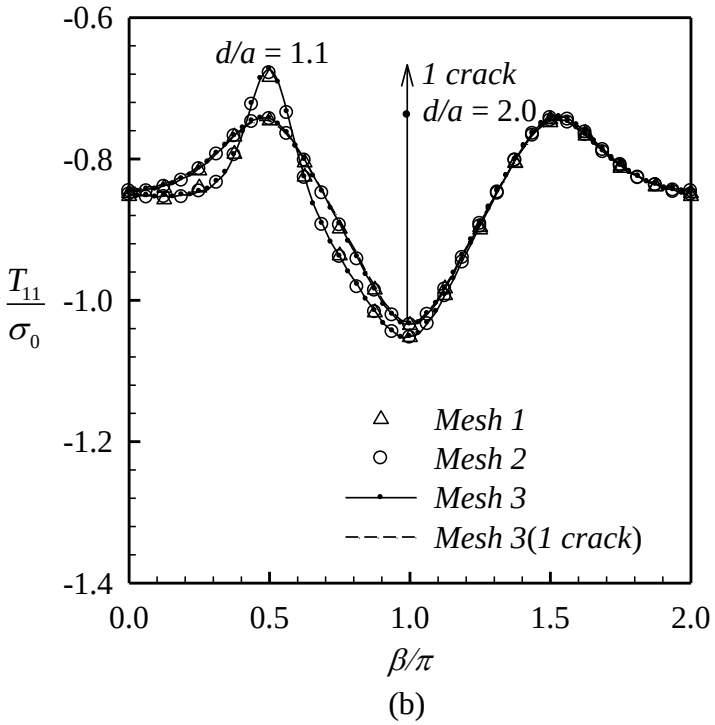

Figure 5.28: (a) Normalized mode-I stress intensity factor and (b) normalized T-stress component T_{11} for elliptical crack 1 in isotropic half-space under BC-type-3.

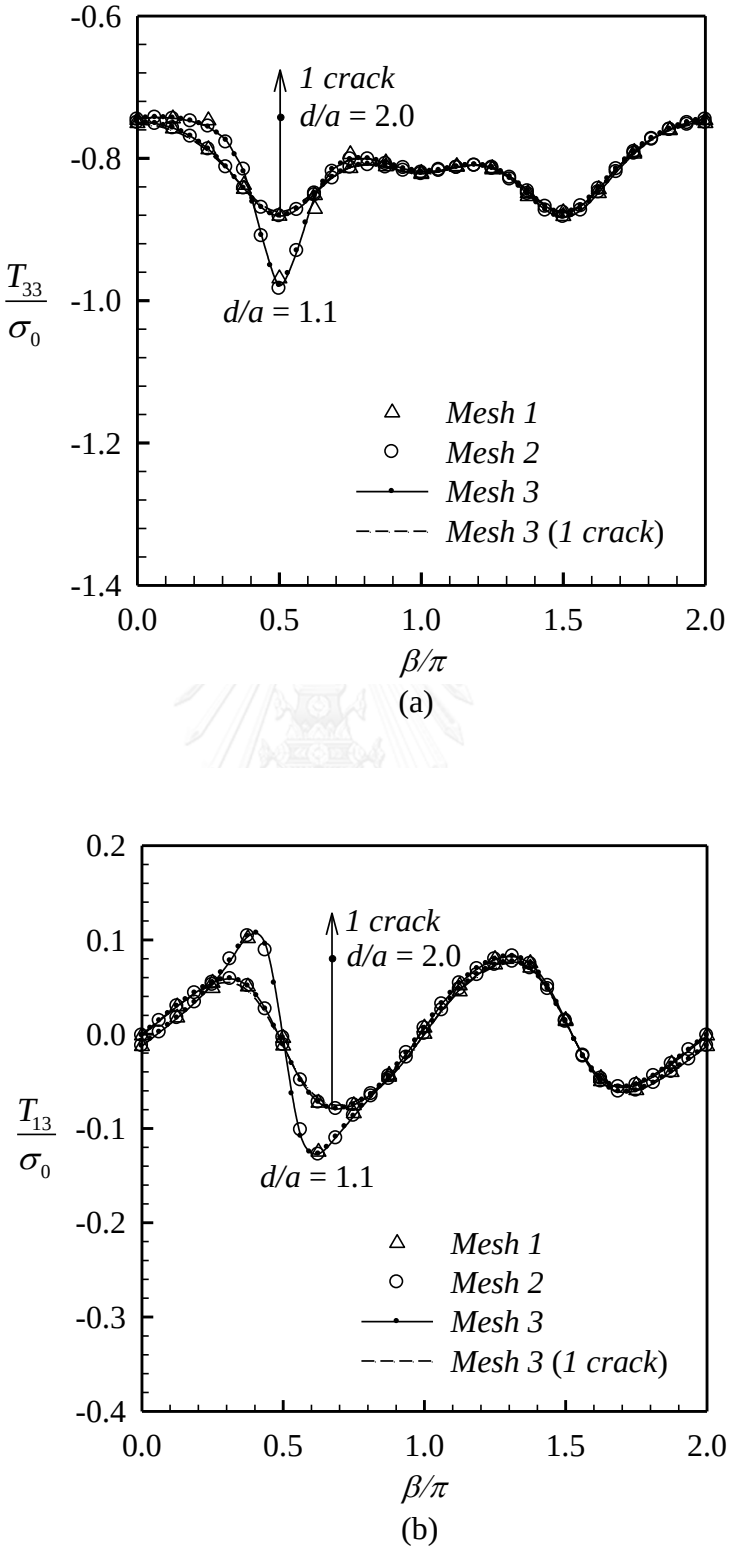

Figure 5.29: (a) Normalized T-stress component T_{33} and (b) normalized T-stress component T_{13} for elliptical crack 1 in isotropic half-space under BC-type-3.

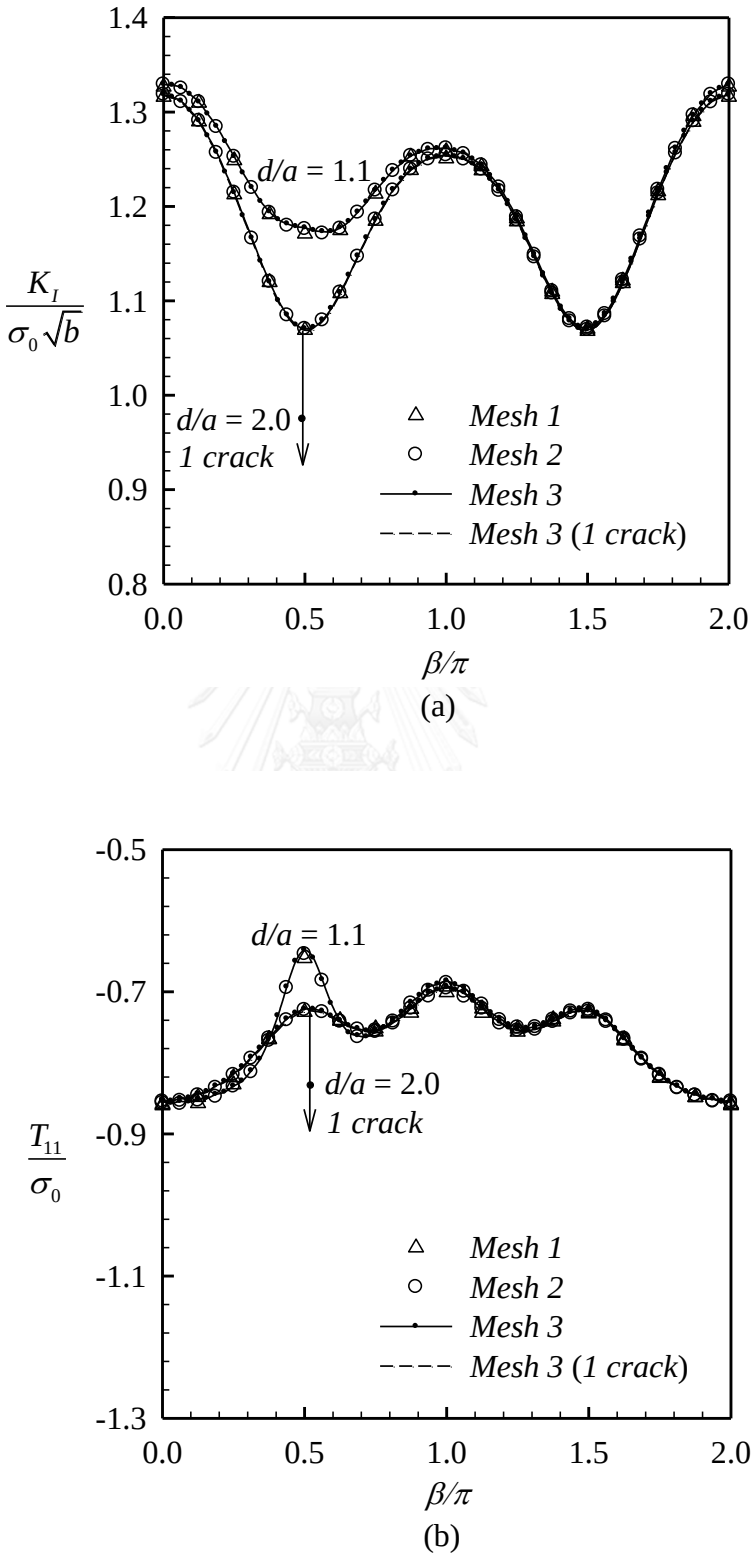

Figure 5.30: (a) Normalized mode-I stress intensity factor and (b) normalized T-stress component T_{11} for elliptical crack 1 in isotropic half-space under BC-type-4.

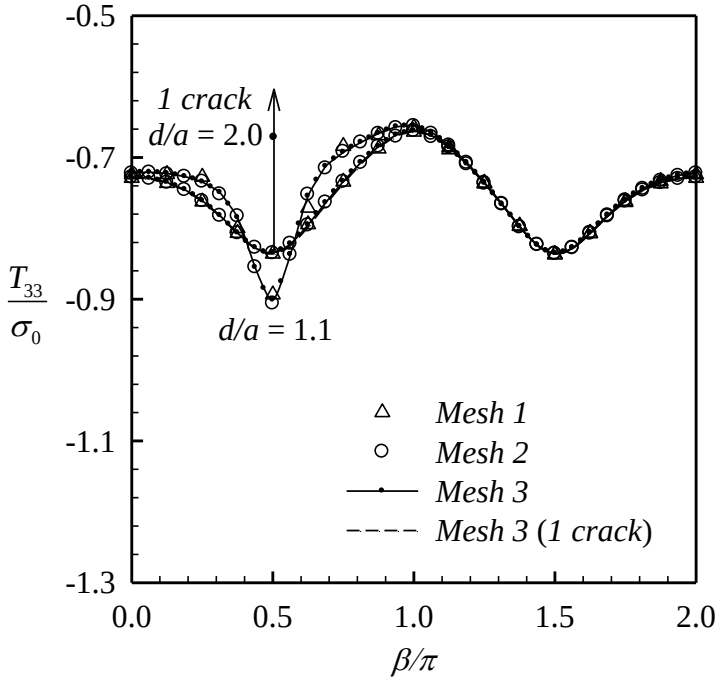

(a)

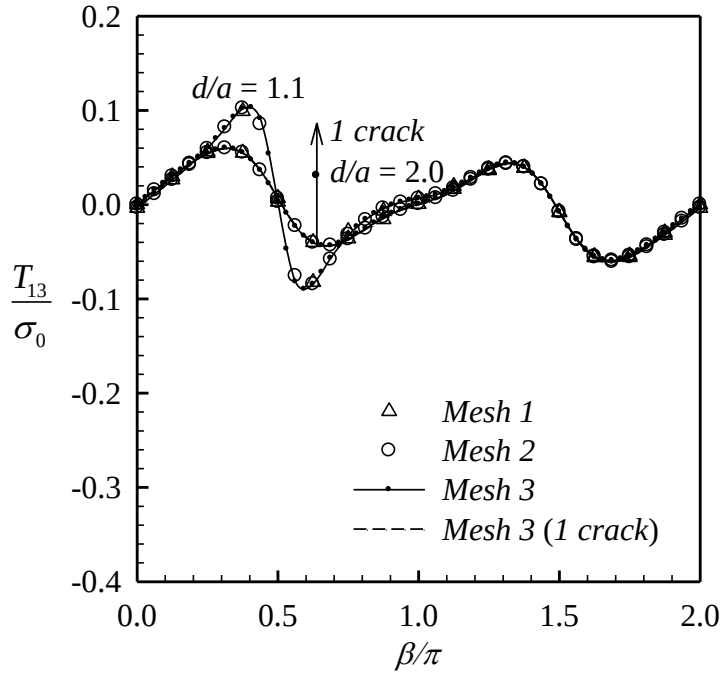

(b)

Figure 5.31: (a) Normalized T-stress component T_{33} and (b) normalized T-stress component T_{13} for elliptical crack 1 in isotropic half-space under BC-type-4.

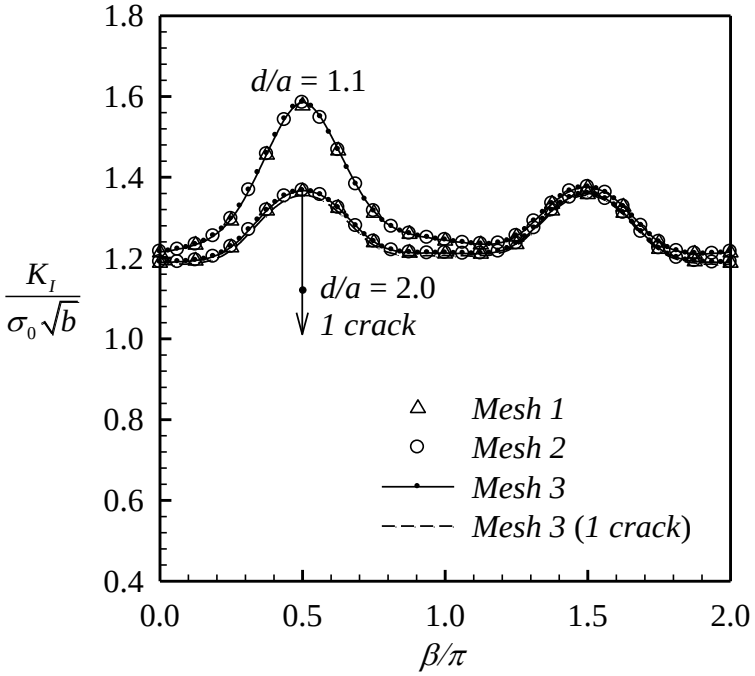

(a)

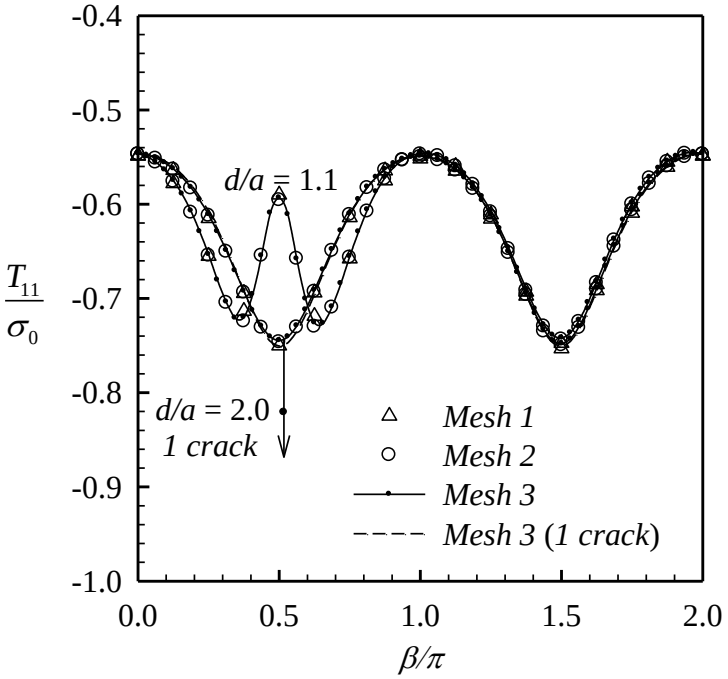

(b)

Figure 5.32: (a) Normalized mode-I stress intensity factor and (b) normalized T-stress component T_{11} for elliptical crack 1 in transversely isotropic half-space under BC-type-1.

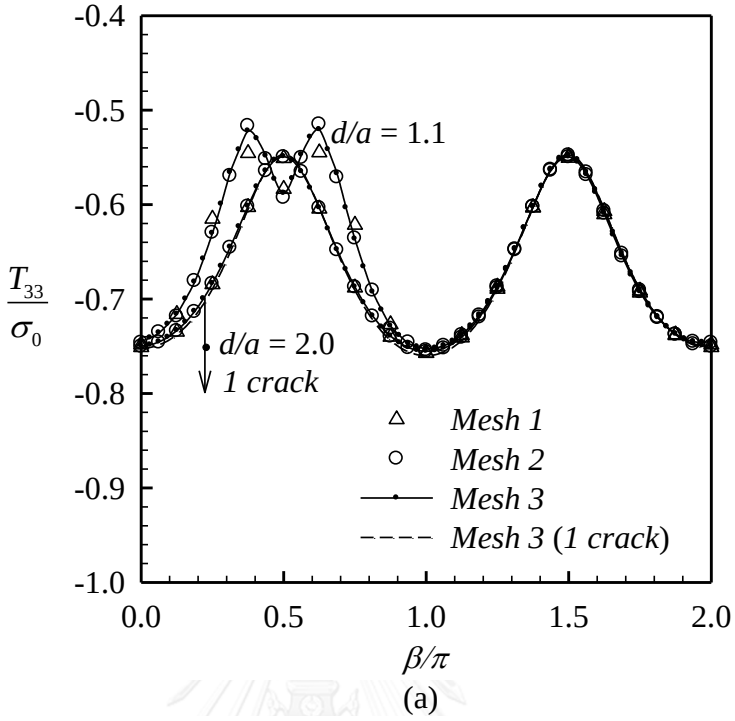

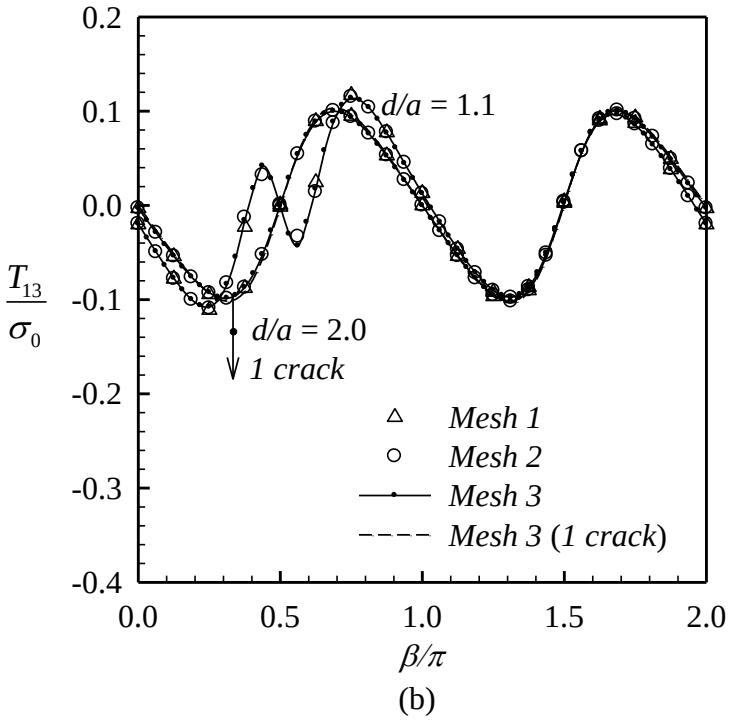

Figure 5.33: (a) Normalized T-stress component T_{33} and (b) normalized T-stress component T_{13} for elliptical crack 1 in transversely isotropic half-space under BC-type-1.

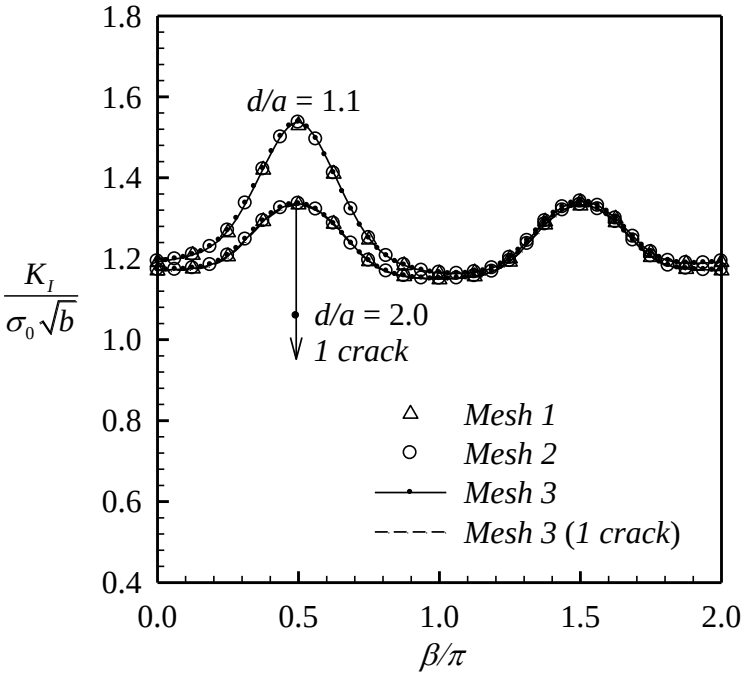

(a)

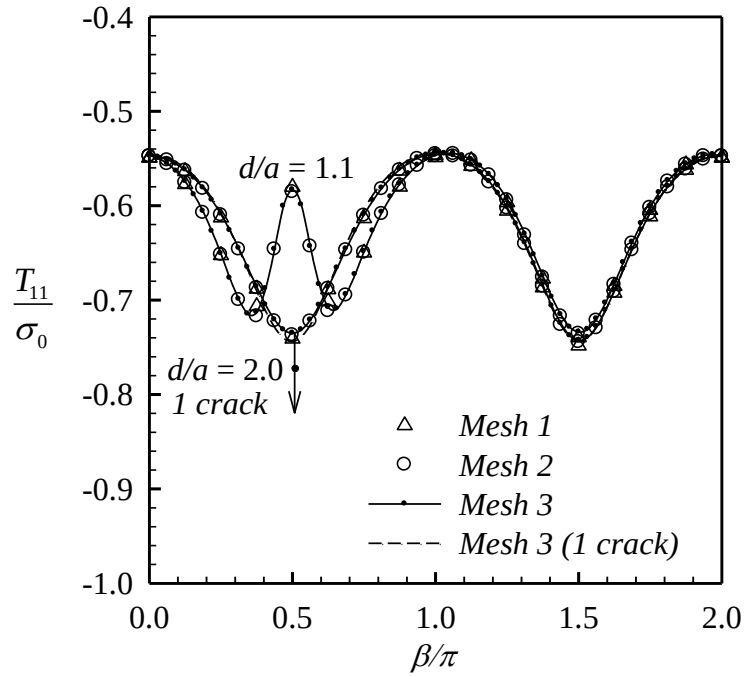

(b)

Figure 5.34: (a) Normalized mode-I stress intensity factor and (b) normalized T-stress component T_{11} for elliptical crack 1 in transversely isotropic half-space under BC-type-2.

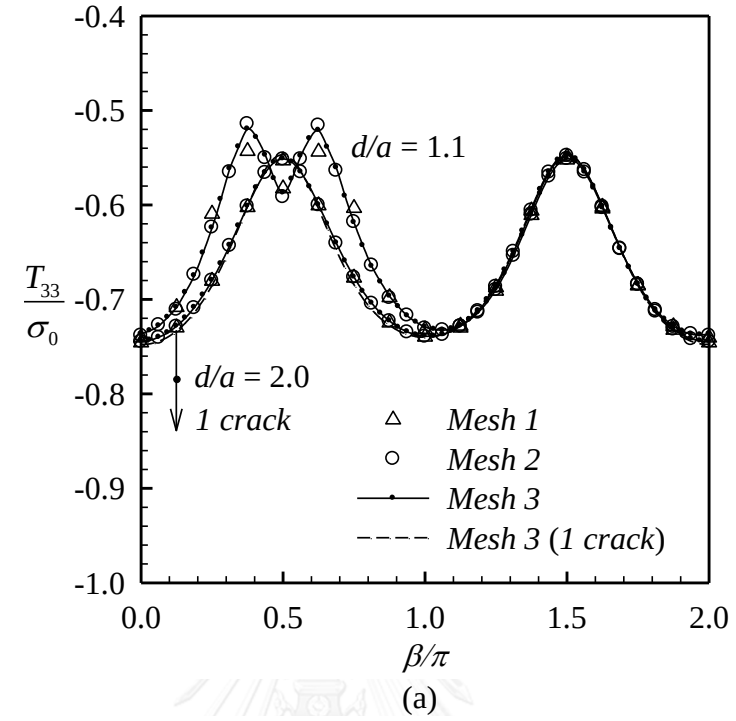

(a)

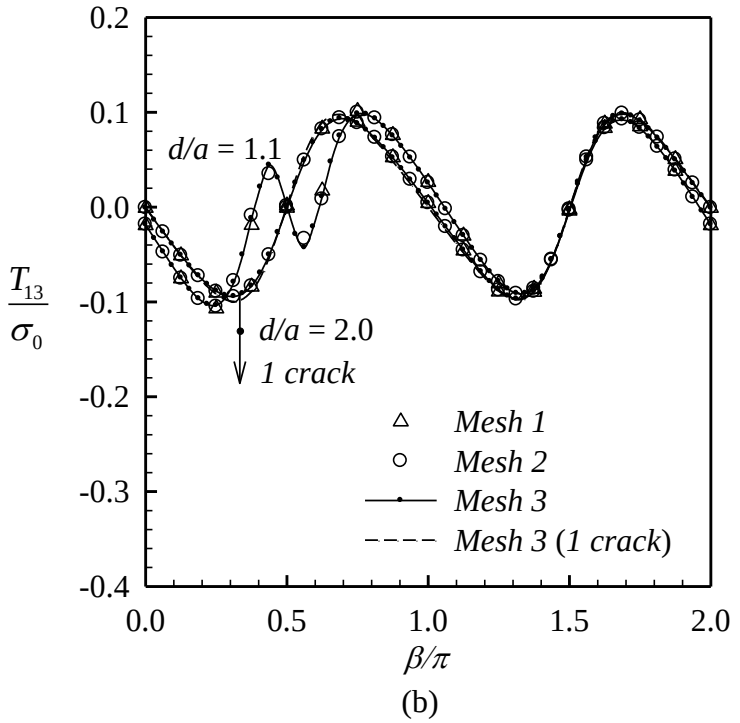

(b)

Figure 5.35: (a) Normalized T-stress component T_{33} and (b) normalized T-stress component T_{13} for elliptical crack 1 in transversely isotropic half-space under BC-type-2.

CHAPTER 6
CONCLUSIONS

6.1. Summary

A set of singularity-reduced integral relations and equations has been established for a generally anisotropic, linearly elastic half-space containing arbitrary shaped cracks with the free surface subjected to symmetrical and anti-symmetrical boundary conditions on the free surface. The systematic regularization procedure based upon the integration by parts through Stokes' theorem and special representations for both hypersingular kernels and strongly singular kernels has been developed and the final regularized integral equations containing only weakly singular kernels have been established. In addition, results proposed by Li (1996) has been adopted to form a set of singularity-reduced boundary integral relations/equations for an isotropic, linearly elastic half-space subjected to the traction-free boundary condition and the fully-restrained boundary condition on the half-space surface. Another key feature of the developed integral equations is the automatic treatment of the free surface via the use of the fundamental solutions of the half-space with the same type of boundary conditions. This therefore avoids the discretization of the half-space surface in the solution procedure. A weakly singular, symmetric Galerkin boundary element method has been successfully implemented to numerically solve the weak-form crack-face traction boundary integral equation for the jump in the crack-face displacement and such information has then been utilized as the known data to determine the sum of the crack-face displacement from the weak-form crack-face displacement integral equation by standard Galerkin method. Special crack-tip elements have also been exploited to enhance the approximation of the near-front field. The fracture data along the crack boundary such as the stress intensity factors and the T-stress components has been directly extracted from the relative and sum of crack-face displacement using the explicit formula.

Results from extensive numerical experiments and the comparison with several benchmarked cases have revealed that the proposed numerical procedure is highly accurate and computationally robust for the analysis of anisotropic cracked half-spaces under symmetric and anti-symmetric boundary conditions and isotropic cracked half-space under various types of boundary conditions. Applying the special crack-tip elements along the crack boundary has indicated that the stress intensity factors and the T-stress components can be accurately captured using relatively very coarse meshes

and this therefore renders the technique more suitable for linear fracture analysis than the standard finite element method which generally requires sufficiently fine mesh to capture the near-front field and experiences difficulty in the treatment of an unbounded domain.

6.2. Limitation and Essential Future Studies

While the proposed technique has been successfully implemented, it is still restricted, for an anisotropic cracked half-space, to symmetric and anti-symmetric boundary conditions and the material must possess the plane of material symmetry parallel to the free surface. The potential extension of the current work to treat other types of boundary conditions such as the traction-free and rigid surfaces and other types of materials such as multi-field and smart solids is considered essential. It is important to emphasize that besides the reduction of the computational cost directly gained from using the half-space model instead of the full treatment of a cracked whole space under symmetric and anti-symmetric conditions, the key ingredients and results established in the present study also form the useful and essential basis for such nontrivial generalization.

REFERENCES

Bogdanov, V. L. (2011), Nonaxisymmetric problem of the stress-strain state of an elastic half-space with a near-surface circular crack under the action of loads along it, *Journal of Mathematical Sciences*, **174**(3): 341-366.

Bonnet, M. and Bui, H. D. (1993), Regularization of the displacement and traction BIE for 3D elastodynamics using indirect methods, *Advances in Boundary Element Techniques*, Kane, J. H., Maier, G., Tosaka, N. and Atluri, S. N., Springer Berlin Heidelberg**:** 1-29.

Bui, H. D. (1977), An integral equations method for solving the problem of a plane crack of arbitrary shape, *Journal of the Mechanics and Physics of Solids*, **25**(1): 29-39.

Cruse, T. A. (1988), *Boundary element analysis in computational fracture mechanics*, Kluwer Academic Publishers.

Dhondt, G. (1995), Green functions for a half circular crack in half infinite space under normal loading, *International Journal of Solids and Structures*, **32**(13): 1807-1857.

Eskandari-Ghadi, M., Ardeshir-Behrestaghi, A. and Navayi Neya, B. (2013), Mathematical analysis for an axissymmetric disc-shaped crack in transversely isotropic half-space, *International Journal of Mechanical Sciences*, **68**: 171-179.

Feng, X. Q., Xu, M., Wang, X. and Gu, B. (2007), Fracture mechanics analysis of three-dimensional ion cut technology, *Journal of Mechanics of Materials and Structures*, **2**(9): 1831-1852.

Ghajar, R. and Alizadeh, K. J. (2013), Mixed mode stress intensity factors for elliptical subsurface cracks in an elastic half-space subjected to a uniform normal loading, *Fatigue & Fracture of Engineering Materials & Structures*, **36**(11): 1199-1208.

Gordeliy, E. and Detournay, E. (2011), Displacement discontinuity method for modeling axisymmetric cracks in an elastic half-space, *International Journal of Solids and Structures*, **48**(19): 2614-2629.

Gray, L. J., Martha, L. F. and Ingraffea, A. R. (1990), Hypersingular integrals in boundary element fracture analysis, *International Journal for Numerical Methods in Engineering*, **29**(6): 1135-1158.

Gu, H. and Yew, C. H. (1988), Finite element solution of a boundary integral equation for mode I embedded three-dimensional fractures, *International Journal for Numerical Methods in Engineering*, **26**(7): 1525-1540.

Guiggiani, M., Krishnasamy, G., Rizzo, F. J. and Rudolphi, T. J. (1991), Hypersingular boundary integral equations: A new approach to their numerical treatment, *Boundary integral methods*, Morino, L. and Piva, R., Springer Berlin Heidelberg**:** 211-220.

Hayashi, K. and Abé, H. (1980), Stress intensity factors for a semi-elliptical crack in the surface of a semi-infinite solid, *International Journal of Fracture*, **16**(3): 275-285.

Hrylyts'kyi, M. D., Laushnyk, I. P. and Stankevych, O. M. (2003), Reduction of the problem of interaction of cracks in a restrained half space to boundary integral equations, *Materials Science*, **39**(1): 79-85.

Kassir, M. K. and Sih, G. C. (1975), *Three-dimensional crack problems: a new selection of crack solutions in three-dimensional elasticity, Vol. 2*, Noordhoff International Publishing.

Katsikadelis, J. T. (2002), *Boundary elements: Theory and applications*, Elsevier Science Ltd.

Keat, W. D., Larson, M. C. and Verges, M. A. (1998), Inverse method of identification for three-dimensional subsurface cracks in a half-space, *International Journal of Fracture*, **92**(3): 253-286.

Khaj, M. V. and Sushko, O. P. (1994), Interaction of coplanar surface cracks in a half-space, *Strength of Materials*, **26**(10): 720-724.

Khaj, M. V. and Sushko, O. P. (1996), A study of the influence of the orientation of a planar surface crack in the shape of a limaçon of pascal on the stress concentration in a half-space, *Journal of Mathematical Sciences*, **81**(6): 3069-3072.

Kit, H. S., Khaj, M. V. and Sushko, O. P. (2000), Investigation of the interaction of flat surface cracks in a half-space by BIEM, *International Journal of Engineering Science*, **38**(14): 1593-1616.

Li, S. (1996), Singularity-reduced integral equations for discontinuities in three dimensional elastic media, *Ph.D. Dissertation*, The University of Texas at Austin.

Li, S. and Mear, M. (1998), Singularity-reduced integral equations for displacement discontinuities in three-dimensional linear elastic media, *International Journal of Fracture*, **93**(1-4): 87-114.

Li, S., Mear, M. E. and Xiao, L. (1998), Symmetric weak-form integral equation method for three-dimensional fracture analysis, *Computer Methods in Applied Mechanics and Engineering*, **151**(3–4): 435-459.

Lo, K. K. (1979), Three-dimensional crack in the interior of a half-space, *Journal of Elasticity*, **9**(4): 435-439.

Martin, P. A., Päivärinta, L. and Rempel, S. (1993), A normal crack in an elastic half-space with stress-free surface, *Mathematical Methods in the Applied Sciences*, **16**(8): 563-579.

Martin, P. A. and Rizzo, F. J. (1996), Hypersingular integrals: how smooth must the density be?, *International Journal for Numerical Methods in Engineering*, **39**(4): 687-704.

Mayrhoffer, K. and Fischer, F. D. (1989), Stress intensity factor variation of a penny-shaped crack situated close to the free surface of a half space, *7th International Conference on Fracture, Houston (USA)*: 83-89.

Monastyrskyy, B. and Kaczyński, A. (2010), On the problem of a transversely isotropic half-space weakened by a penny-shaped crack filled with a gas, *Journal of Theoretical and Applied Mechanics*, **48(2)**: 435-451.

Movchan, N. V. and Willis, J. R. (2000), Surface-breaking crack in an elastic half-space, *Journal of Engineering Mathematics*, **37**(1-3): 143-154.

Murakami, Y. (1985), Analysis of stress intensity factors of modes I, II and III for inclined surface cracks of arbitrary shape, *Engineering Fracture Mechanics*, **22**(1): 101-114.

Noguchi, H. and Smith, R. A. (1995), An analysis of a semi-infinite solid with three-dimensional cracks, *Engineering Fracture Mechanics*, **52**(1): 1-14.

Noguchi, H., Smith, R. A., Carruthers, J. J. and Gilchrist, M. D. (1997), Stress intensity factors of embedded elliptical cracks and an assessment of the ASME XI defect recharacterisation criteria, *International Journal of Pressure Vessels and Piping*, **70**(1): 69-76.

Rungamornrat, J. and Mear, M. E. (2008a), Weakly-singular, weak-form integral equations for cracks in three-dimensional anisotropic media, *International Journal of Solids and Structures*, **45**(5): 1283-1301.

Rungamornrat, J. and Mear, M. E. (2008b), A weakly-singular SGBEM for analysis of cracks in 3D anisotropic media, *Computer Methods in Applied Mechanics and Engineering*, **197**(49–50): 4319-4332.

Rungamornrat, J. and Pinitpanich, M. (2015), T-stress solution of penny-shaped crack in transversely isotropic elastic media, *Engineering Fracture Mechanics,* (*under review*).

Rungamornrat, J. and Senjuntichai, T. (2009), Regularized boundary integral representations for dislocations and cracks in smart media, *Smart Materials and Structures*, **18**(7): 074010.

Shah, R. C. and Kobayashi, A. S. (1971), Stress intensity factor for an elliptical crack under arbitrary normal loading, *Engineering Fracture Mechanics*, **3**: 71-96.

Shah, R. C. and Kobayashi, A. S. (1973), Stress intensity factors for an elliptical crack approaching the surface of a semi-infinite solid, *International Journal of Fracture*, **9**(2): 133-146.

Skalsky, V., Stankevych, O. M. and Serhiyenko, O. (2013), Wave displacement field at a half-space surface caused by an internal crack under twisting load, *Wave Motion*, **50**(2): 326-333.

Sládek, V. and Sládek, J. (1982), Three dimensional crack analysis for an anisotropic body, *Applied Mathematical Modelling*, **6**(5): 374-380.

Smith, F. W. and Alavi, M. J. (1971), Stress intensity factors for a penny shaped crack in a half space, *Engineering Fracture Mechanics*, **3**(3): 241-254.

Srivastava, K. N. and Singh, K. (1969), The effect of penny-shaped crack on the distribution of stress in a semi-infinite solid, *International Journal of Engineering Science*, **7**(5): 469-490.

Subsathaphol, T. (2014), Analysis of T-stress for cracks in 3D linear piezoelectric media, *Master Thesis*, Chulalongkorn University.

Sushko, O. P. and Khaj, M. V. (1996), Solution of problems of the theory of elasticity for a half-space with planar boundary cracks, *Journal of Mathematical Sciences*, **79**(6): 1434-1438.

Ting, T. C. T. and Lee, V.-G. (1997), The three-dimensional elastostatic green's function for general anisotropic linear elastic solids, *The Quarterly Journal of Mechanics and Applied Mathematics*, **50**(3): 407-426.

Wang, C. Y. (1997), Elastic fields produced by a point source in solids of general anisotropy, *Journal of Engineering Mathematics*, **32**(1): 41-52.

Wang, X. (2004), Elastic *T*-stress solutions for penny-shaped cracks under tension and bending, *Engineering Fracture Mechanics*, **71**: 2283-2298.

Weaver, J. (1977), Three-dimensional crack analysis, *International Journal of Solids and Structures*, **13**(4): 321-330.

Xiao, L. (1998), Symmetric weak-form integral equation method for three-dimensional fracture analysis, *Ph.D. Dissertation*, The University of Texast Austin.

Xu, G. (2000), A variational boundary integral method for the analysis of three-dimensional cracks of arbitrary geometry in anisotropic elastic solids, *Journal of Applied Mechanics*, **67**: 403–408.

Xu, G. and Ortiz, M. (1993), A variational boundary integral method for the analysis of 3-D cracks of arbitrary geometry modelled as continuous distributions of dislocation loops, *International Journal for Numerical Methods in Engineering*, **36**(21): 3675-3701.

APPENDIX A

FORMULATIONS OF $M_{mj}(\boldsymbol{\xi}, \boldsymbol{x})$ AND $N_{mj}(\boldsymbol{\xi}, \boldsymbol{x})$

$$M_{\alpha\beta}(\boldsymbol{\xi},\boldsymbol{x}) = \frac{4\beta}{3}\mu\xi_3\varepsilon_{3\gamma\alpha}\frac{\partial^2}{\partial x_\gamma \partial x_\beta}\bar{h}_2 \tag{A.1}$$

$$N_{\alpha\beta}(\boldsymbol{\xi},\boldsymbol{x}) = 4\alpha\mu\xi_3\varepsilon_{3\gamma\alpha}\frac{\partial^2}{\partial x_\gamma \partial x_\beta}\bar{h}_3 \tag{A.2}$$

$$M_{\alpha 3}(\boldsymbol{\xi},\boldsymbol{x}) = -\frac{4\beta}{3}\mu\varepsilon_{3\beta\alpha}\frac{\partial}{\partial x_\beta}(\xi_3\bar{h}_1 - \bar{h}_2) \tag{A.3}$$

$$N_{\alpha 3}(\boldsymbol{\xi},\boldsymbol{x}) = -4\alpha\mu\varepsilon_{3\beta\alpha}\frac{\partial}{\partial x_\beta}(-\bar{h}_3 + \xi_3\bar{h}_2) \tag{A.4}$$

$$M_{3\alpha}(\boldsymbol{\xi},\boldsymbol{x}) = 4(\alpha - \frac{\beta}{3})\mu\varepsilon_{3\beta\alpha}\frac{\partial}{\partial x_\beta}\bar{h}_2 \tag{A.5}$$

$$N_{3\alpha}(\boldsymbol{\xi},\boldsymbol{x}) = 4(\alpha - \frac{\beta}{3})(1-2\nu)\mu\varepsilon_{3\beta\alpha}\frac{\partial}{\partial x_\beta}\bar{h}_3 \tag{A.6}$$

$$M_{33}(\boldsymbol{\xi},\boldsymbol{x}) = N_{33}(\boldsymbol{\xi},\boldsymbol{x}) = 0 \tag{A.7}$$

where the constants α and β are defined by

$$\alpha = -\frac{(1-2\nu)}{8\pi(1-\nu)} \tag{A.8}$$

$$\beta = -\frac{3}{8\pi(1-\nu)} \tag{A.9}$$

and $\bar{h}_i$ (i = 1, 2, and 3) are harmonic functions defined in the domain $x_3 > 0$ as follows

$$\bar{h}_1 = \frac{1}{\bar{r}} \tag{A.10}$$

$$\bar{h}_{i+1} = \int \bar{h}_i dx_3 \tag{A.11}$$

with

$$\bar{r} = \sqrt{(\xi_\alpha - x_\alpha)(\xi_\alpha - x_\alpha) + (\xi_3 + x_3)(\xi_3 + x_3)} \tag{A.12}$$

APPENDIX B

FORMULATIONS OF $P_{mj}(\boldsymbol{\xi}, \boldsymbol{x})$ AND $Q_{mj}(\boldsymbol{\xi}, \boldsymbol{x})$

$$P_{\alpha\beta}(\boldsymbol{\xi},\boldsymbol{x}) = \frac{4\mu}{(3-4\nu)}[(\alpha-\frac{\beta}{3})\varepsilon_{\alpha\beta 3}\bar{h}_1 + \frac{\beta}{3}\varepsilon_{\alpha\gamma 3}(-\bar{h}_{3,\gamma\beta} + \xi_3\bar{h}_{2,\gamma\beta})] \tag{B.1}$$

$$Q_{\alpha\beta}(\boldsymbol{\xi},\boldsymbol{x}) = \frac{4\mu}{(3-4\nu)}[(\alpha-\frac{\beta}{3})\varepsilon_{\alpha\beta 3}\bar{h}_2 - \frac{\beta}{3}\varepsilon_{\alpha\gamma 3}(\bar{h}_{4,\gamma\beta} - \xi_3\bar{h}_{3,\gamma\beta})] \tag{B.2}$$

$$P_{\alpha 3}(\boldsymbol{\xi},\boldsymbol{x}) = \frac{4\mu}{(3-4\nu)}\varepsilon_{\alpha\gamma 3}[(\alpha+\frac{\beta}{3})\bar{h}_{2,\gamma} - \frac{\beta}{3}\xi_3\bar{h}_{1,\gamma}] \tag{B.3}$$

$$Q_{\alpha 3}(\boldsymbol{\xi},\boldsymbol{x}) = \frac{4\mu}{(3-4\nu)}\varepsilon_{\alpha\gamma 3}[(\alpha+\frac{\beta}{3})\bar{h}_{3,\gamma} - \frac{\beta}{3}\xi_3\bar{h}_{2,\gamma}] \tag{B.4}$$

$$P_{3j}(\boldsymbol{\xi},\boldsymbol{x}) = Q_{3j}(\boldsymbol{\xi},\boldsymbol{x}) = 0 \tag{B.5}$$

where α, β and $\bar{h}_i$ are defined in Appendix A

APPENDIX C
ADDITIONAL RESULTS

This Appendix shows additional results of a half-space made of cubic and orthotropic materials and subjected to BC-type-α.

Table C.1: Independent, relative elastic constants for cubic Gnaupel-Herold *et al.*, 1998 and orthotropic materials Kaw, 2006. The plane $x_3 = 0$ is taken as a plane of material symmetry.

Materials	E_{1111}	E_{1122}	E_{1133}	E_{2222}	E_{2233}	E_{3333}	E_{1212}	E_{1313}	E_{2323}
Cubic	114.100	65.300	65.300	114.100	65.300	114.100	28.500	28.500	28.500
Orthotropic	185.000	7.269	7.204	16.380	9.938	16.370	7.168	6.998	3.000

C.1 Results for Cubic and Orthotropic Materials under BC-type-α

C.1.1 Horizontal Penny-Shaped Crack

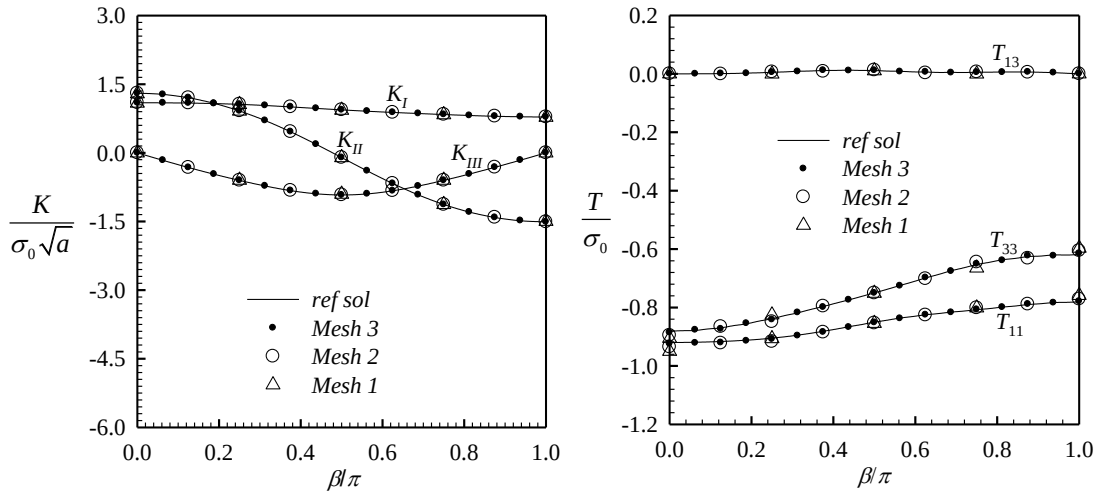

(a) (b)

Figure C.1: (a) Normalized stress intensity factors and (b) normalized T-stress components for horizontal penny-shaped crack in cubic half-space under BC-type-1.

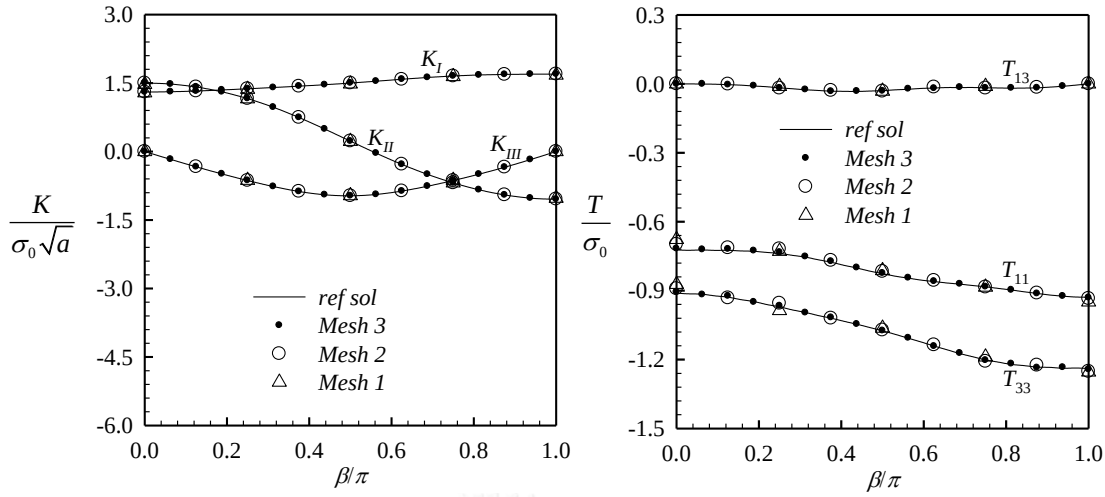

(a) (b)

Figure C.2: (a) Normalized stress intensity factors and (b) normalized T-stress components for horizontal penny-shaped crack in cubic half-space under BC-type-2.

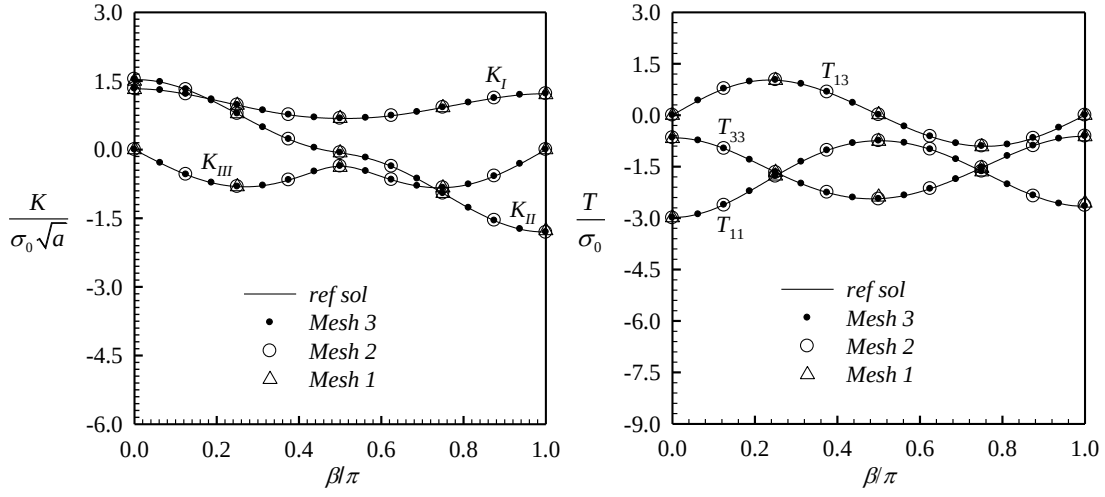

(a) (b)

Figure C.3: (a) Normalized stress intensity factors and (b) normalized T-stress components for horizontal penny-shaped crack in orthotropic half-space under BC-type-1.

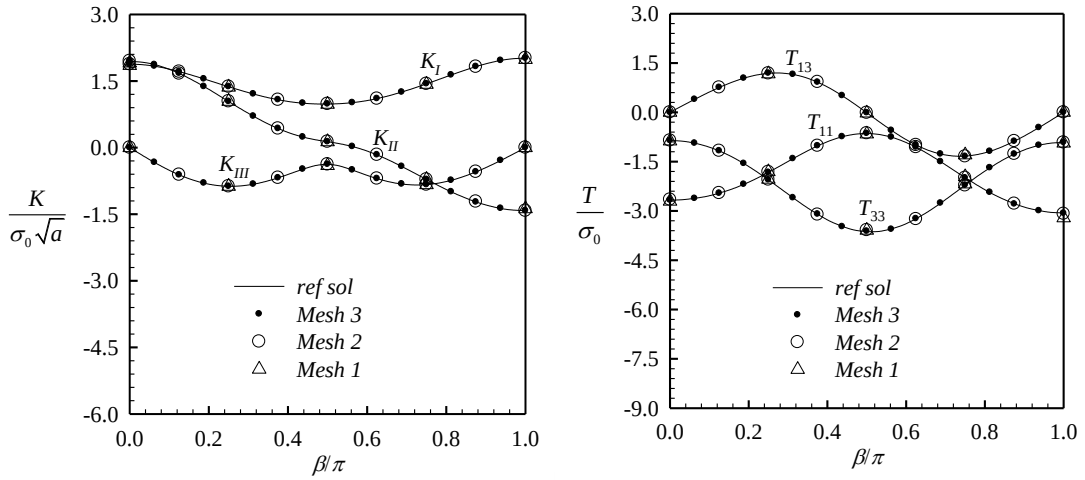

(a) (b)

Figure C.4: (a) Normalized stress intensity factors and (b) normalized T-stress components for horizontal penny-shaped crack in orthotropic half-space under BC-type-2.

C.1.2 Vertical Penny-Shaped Crack

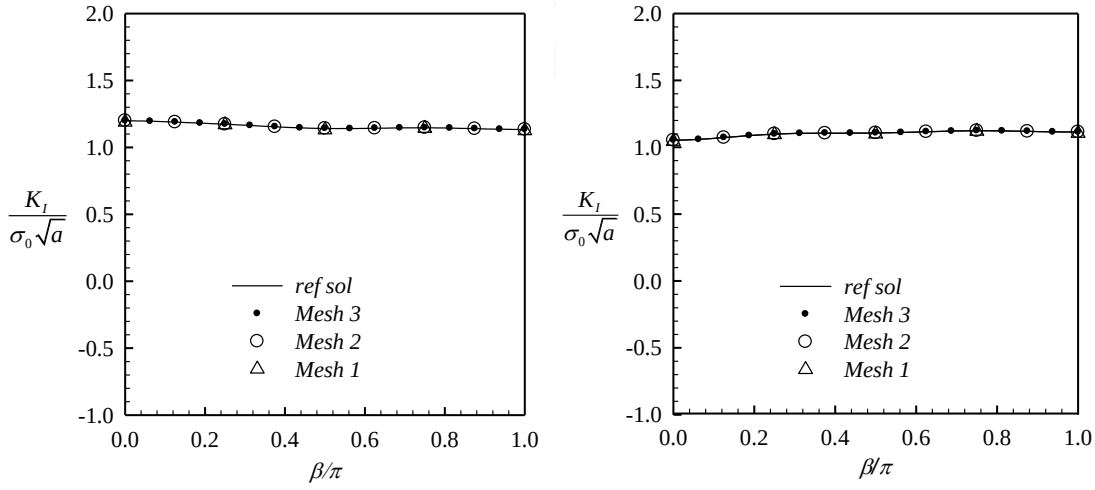

(a) (b)

Figure C.5: Normalized mode-I stress intensity factors for vertical penny-shaped crack in cubic half-space under (a) BC-type-1 and (b) BC-type-2.

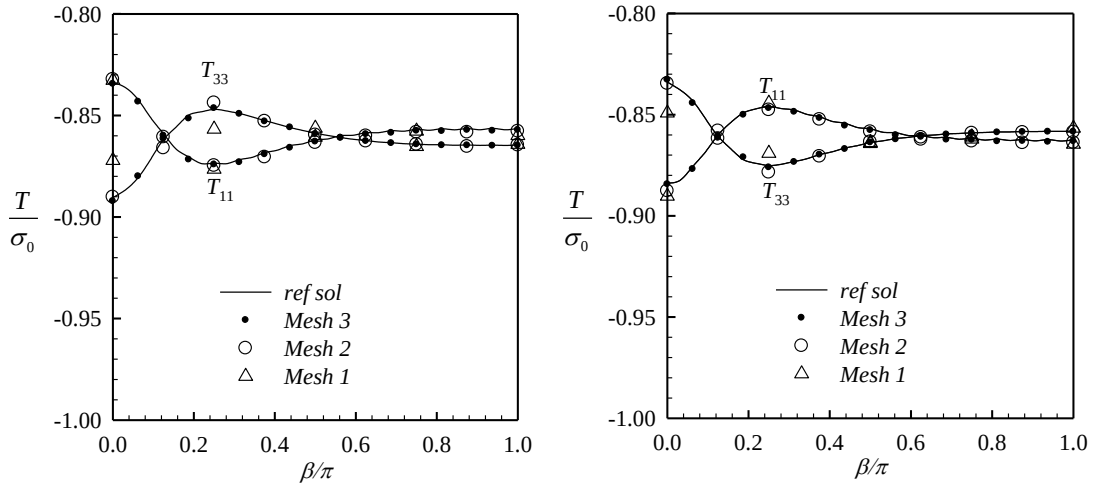

Figure C.6: Normalized T-stress components for vertical penny-shaped crack in cubic half-space under (a) BC-type-1 and (b) BC-type-2.

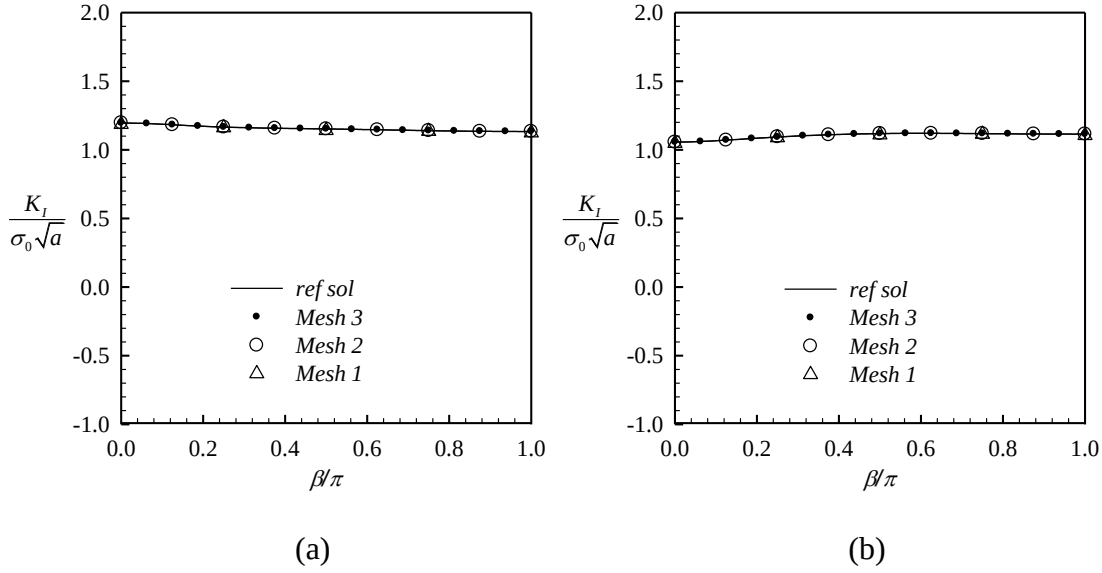

Figure C.7: Normalized mode-I stress intensity factors for vertical penny-shaped crack in orthotropic half-space under (a) BC-type-1 and (b) BC-type-2.

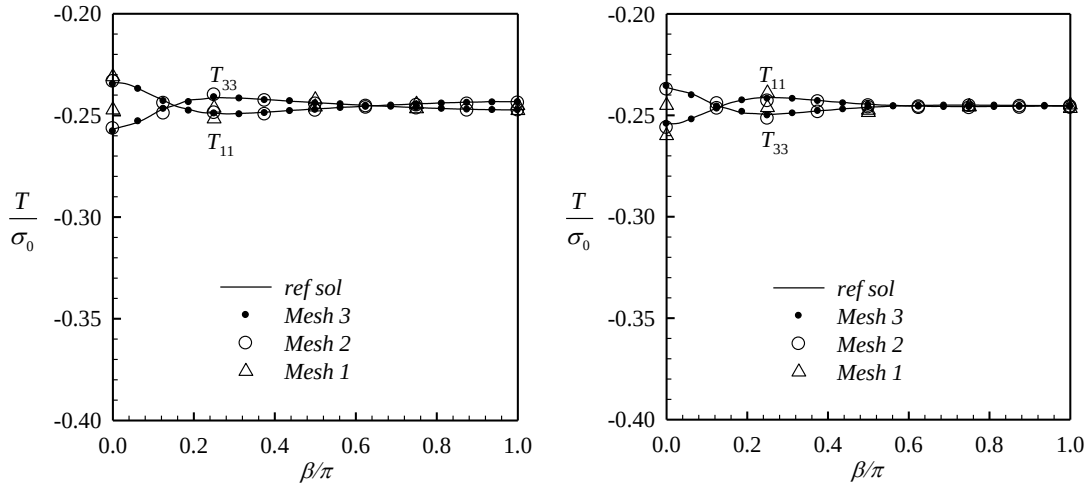

(a) (b)

Figure C.8: Normalized T-stress components for vertical penny-shaped crack in orthotropic half-space under (a) BC-type-1 and (b) BC-type-2.

C.13 Surface-Breaking Crack

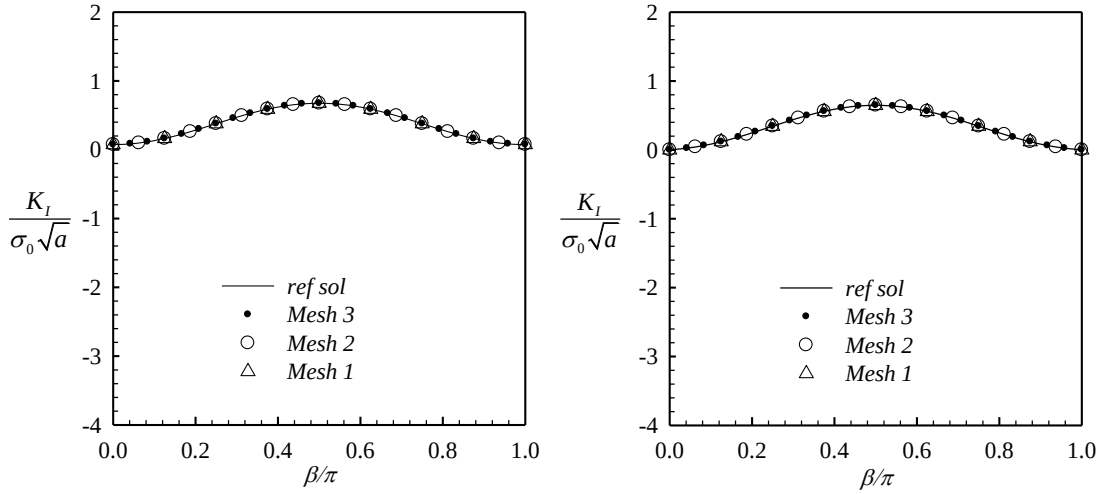

(a) (b)

Figure C.9: Normalized mode-I stress intensity factors for surface-breaking crack subjected to non-uniform normal traction in cubic half-space under (a) BC-type-1 and (b) BC-type-2.

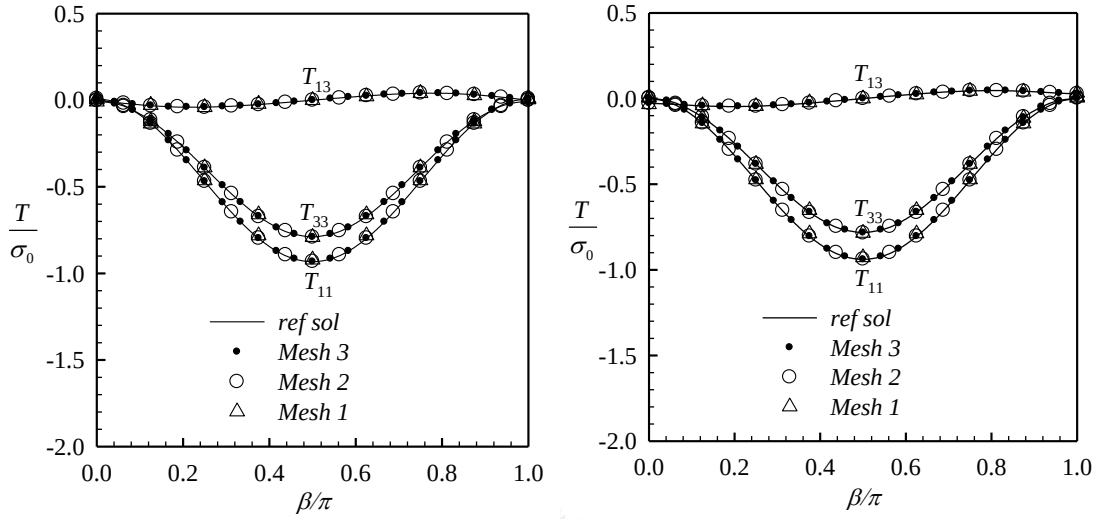

(a) (b)

Figure C.10: Normalized T-stress components for surface-breaking crack subjected to non-uniform normal traction in cubic half-space under (a) BC-type-1 and (b) BC-type-2.

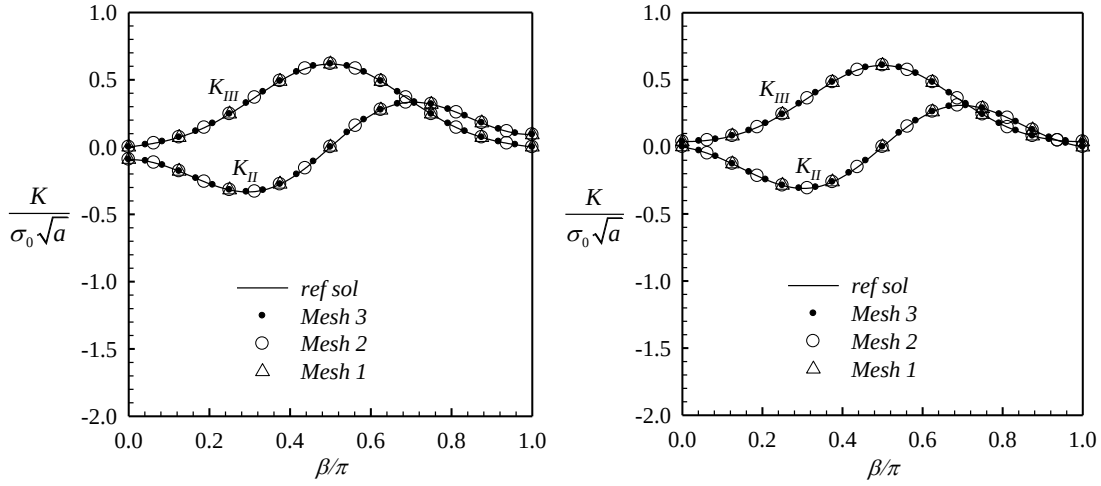

(a) (b)

Figure C.11: Normalized stress intensity factors for surface-breaking crack subjected to non-uniform shear traction in x_1-direction in cubic half-space under (a) BC-type-1 and (b) BC-type-2.

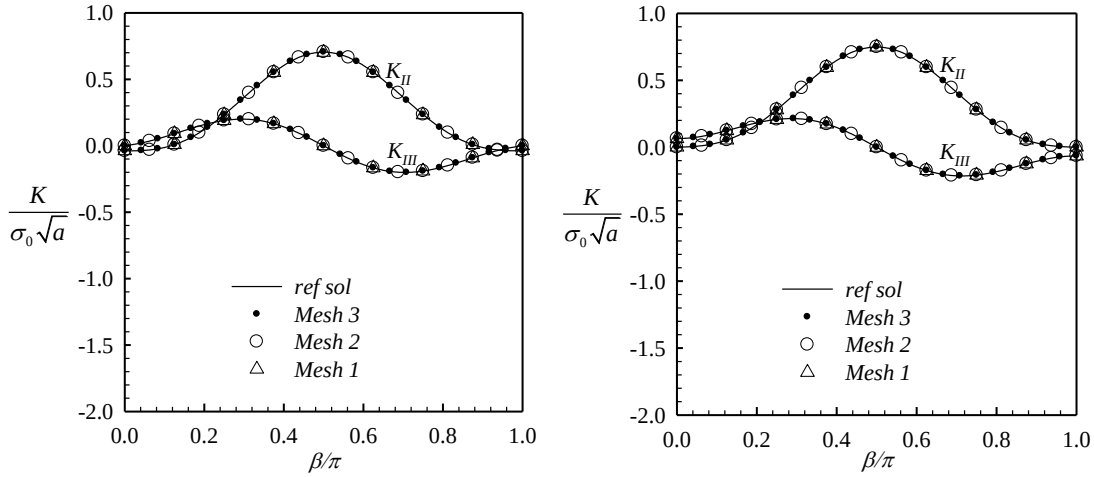

Figure C.12: Normalized stress intensity factors for surface-breaking crack subjected to non-uniform shear traction in x_3-direction in cubic half-space under (a) BC-type-1 and (b) BC-type-2.

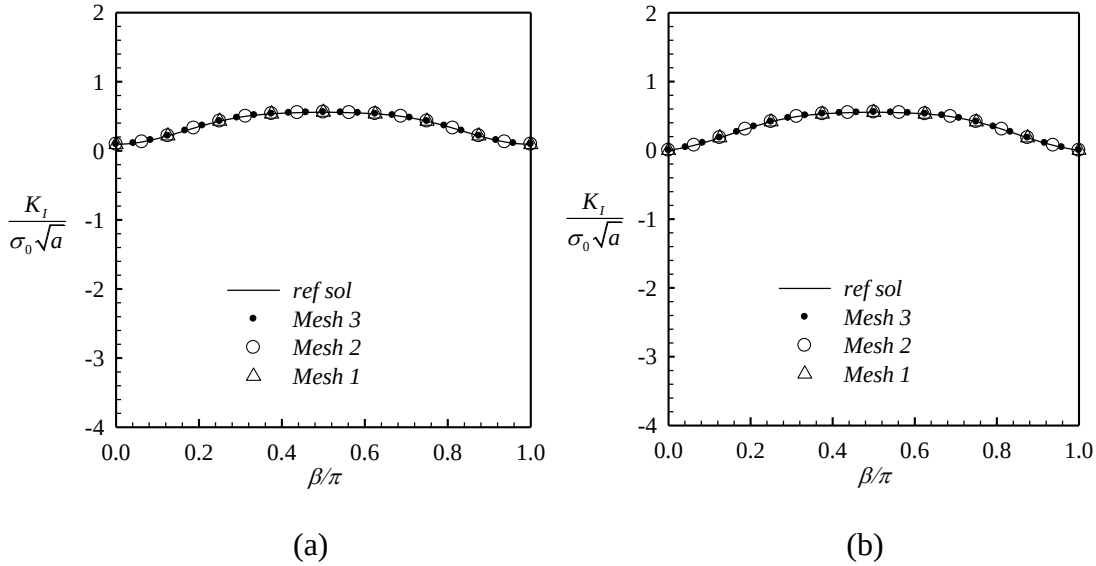

Figure C.13: Normalized mode-I stress intensity factors for surface-breaking crack subjected to non-uniform normal traction in orthotropic half-space under (a) BC-type-1 and (b) BC-type-2.

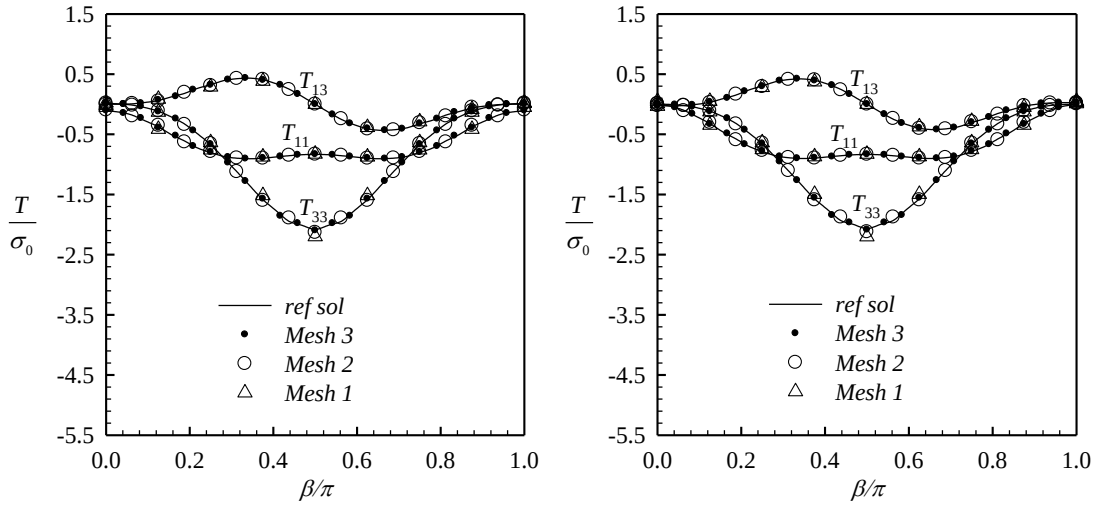

Figure C.14: Normalized T-stress components for surface-breaking crack subjected to non-uniform normal traction in orthotropic half-space under (a) BC-type-1 and (b) BC-type-2.

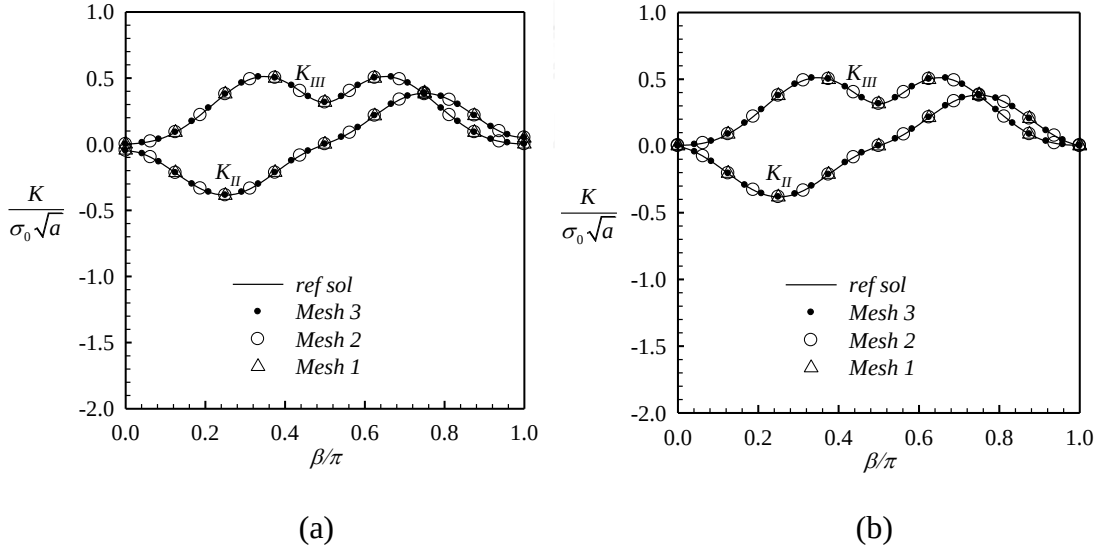

Figure C.15: Normalized stress intensity factors for surface-breaking crack subjected to non-uniform shear traction in x_1-direction in orthotropic half-space under (a) BC-type-1 and (b) BC-type-2.

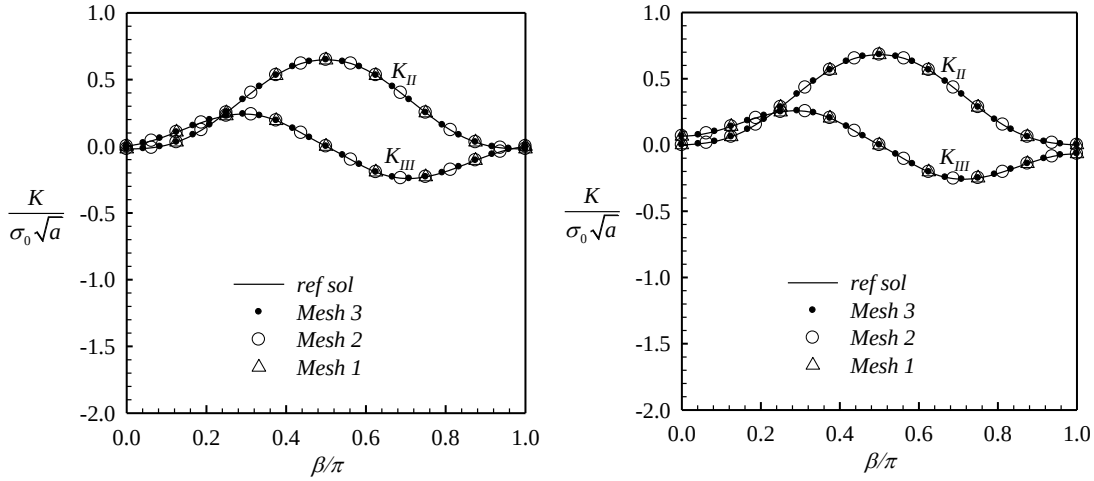

Figure C.16: Normalized stress intensity factors for surface-breaking crack subjected to non-uniform shear traction in x_3-direction in orthotropic half-space under (a) BC-type-1 and (b) BC-type-2.

C.2 Results for More Complex Problems

C.2.1 Spherical Cap Crack

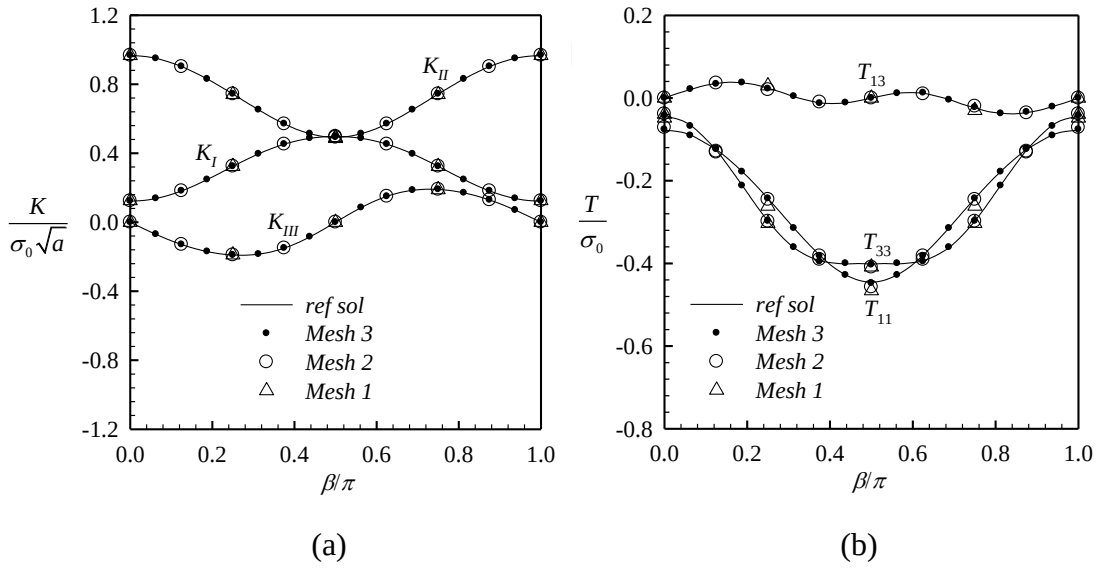

Figure C.17: (a) Normalized stress intensity factors and (b) normalized T-stress components for spherical cap crack in cubic half-space under BC-type-1.

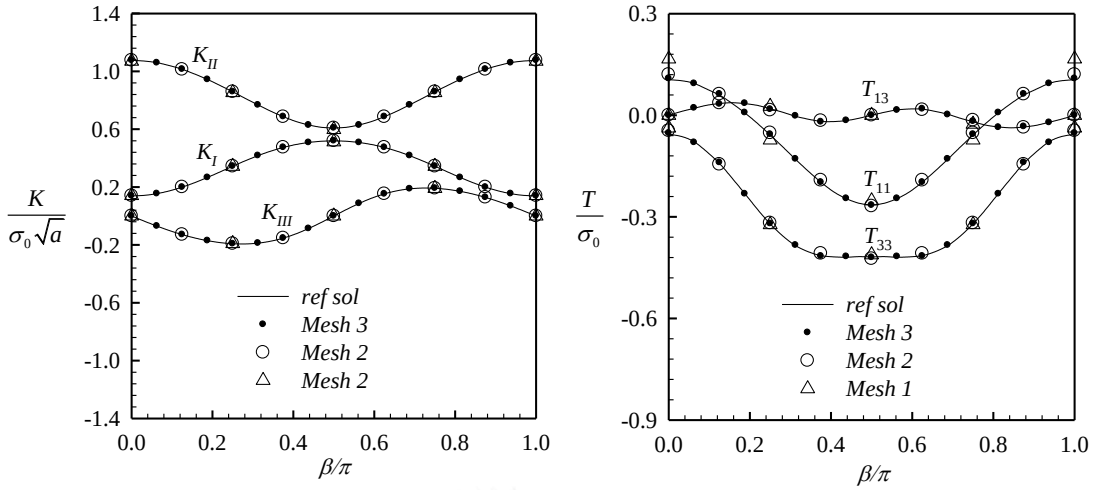

(a) (b)

Figure C.18: (a) Normalized stress intensity factors and (b) normalized T-stress components for spherical cap crack in cubic half-space under BC-type-2.

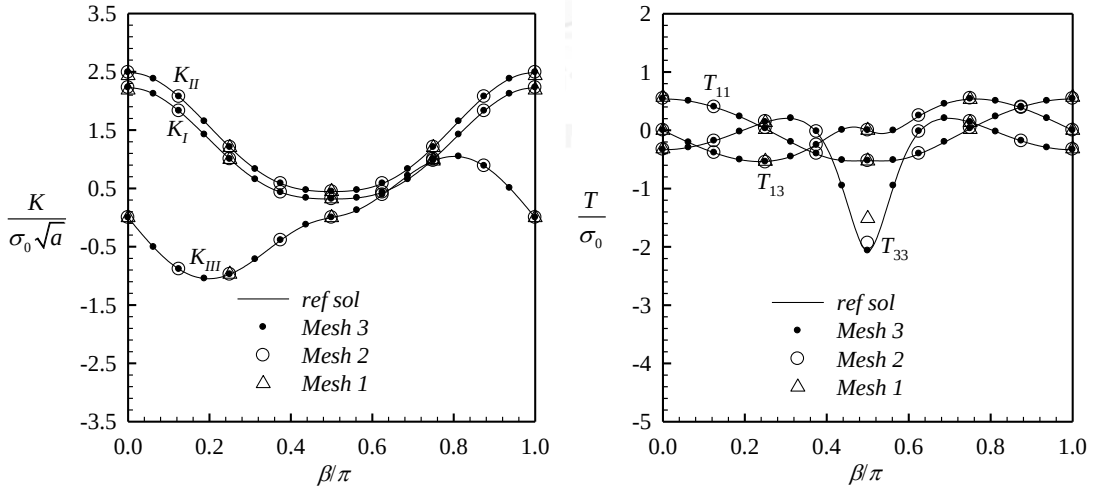

(a) (b)

Figure C.19: (a) Normalized stress intensity factors and (b) normalized T-stress components for spherical cap crack in orthotropic half-space under BC-type-1.

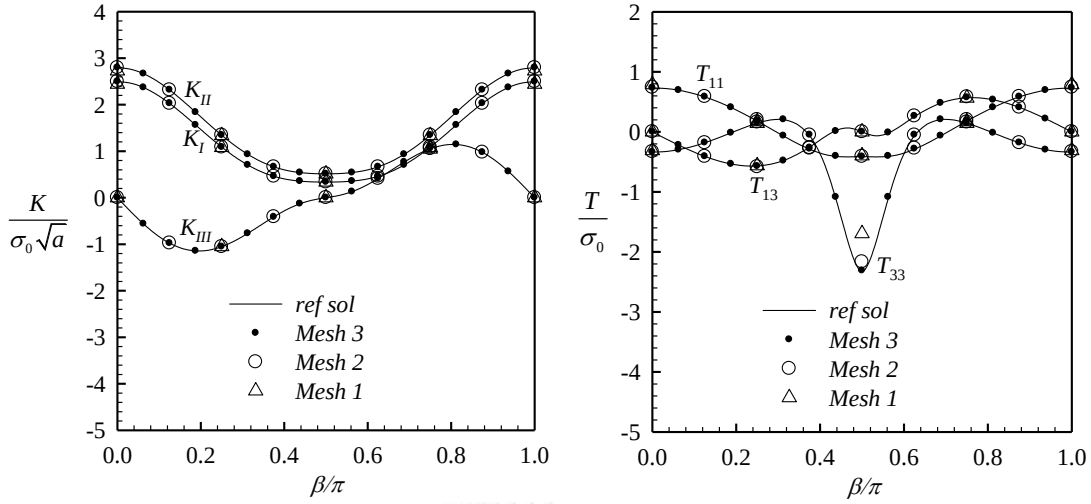

(a) (b)

Figure C.20: (a) Normalized stress intensity factors and (b) normalized T-stress components for spherical cap crack in orthotropic half-space under BC-type-2.

C.2.2 Two Embedded Elliptical Cracks

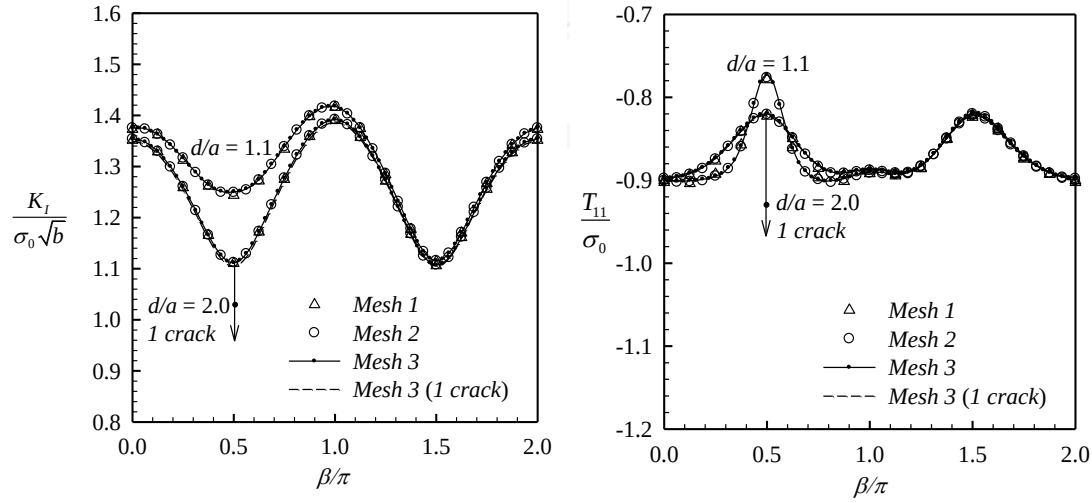

(a) (b)

Figure C.21: (a) Normalized mode-I stress intensity factor and (b) normalized T-stress component T_{11} for elliptical crack 1 in cubic half-space under BC-type-1.

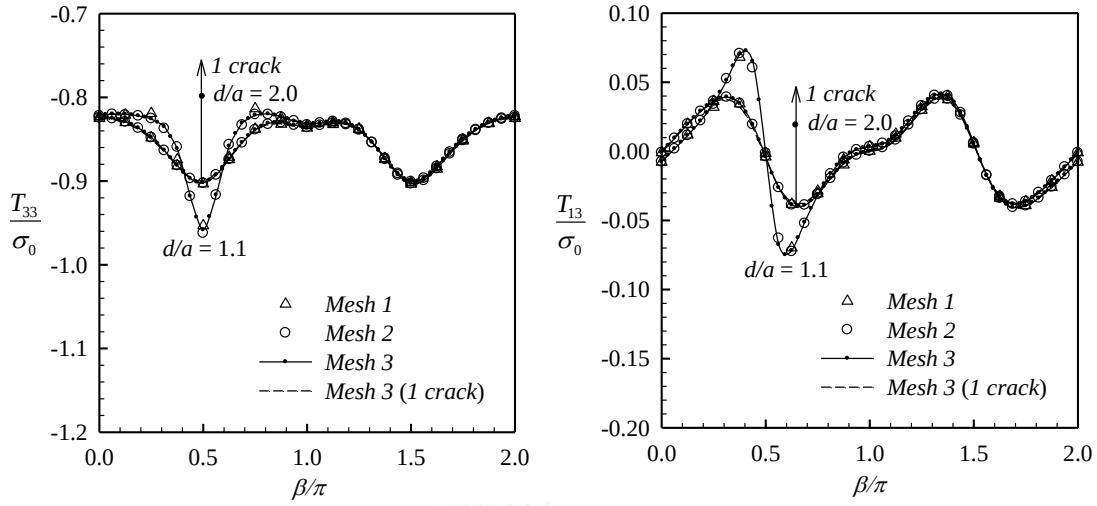

(a) (b)

Figure C.22: (a) Normalized T-stress component T_{33} and (b) normalized T-stress component T_{13} for elliptical crack 1 in cubic half-space under BC-type-1.

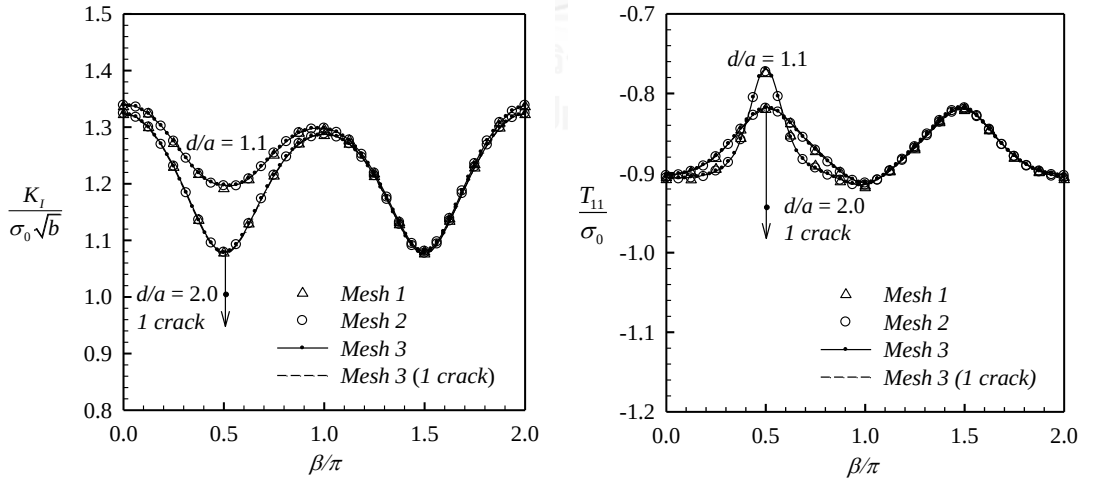

(a) (b)

Figure C.23: (a) Normalized mode-I stress intensity factor and (b) normalized T-stress component T_{11} for elliptical crack 1 in cubic half-space under BC-type-2.

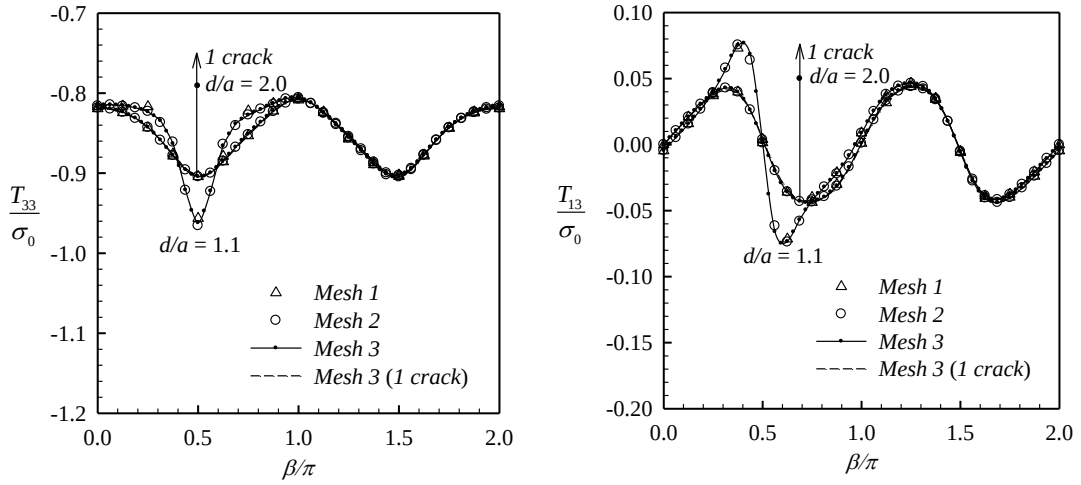

(a) (b)

Figure C.24: (a) Normalized T-stress component T_{33} and (b) normalized T-stress component T_{13} for elliptical crack 1 in cubic half-space under BC-type-2.

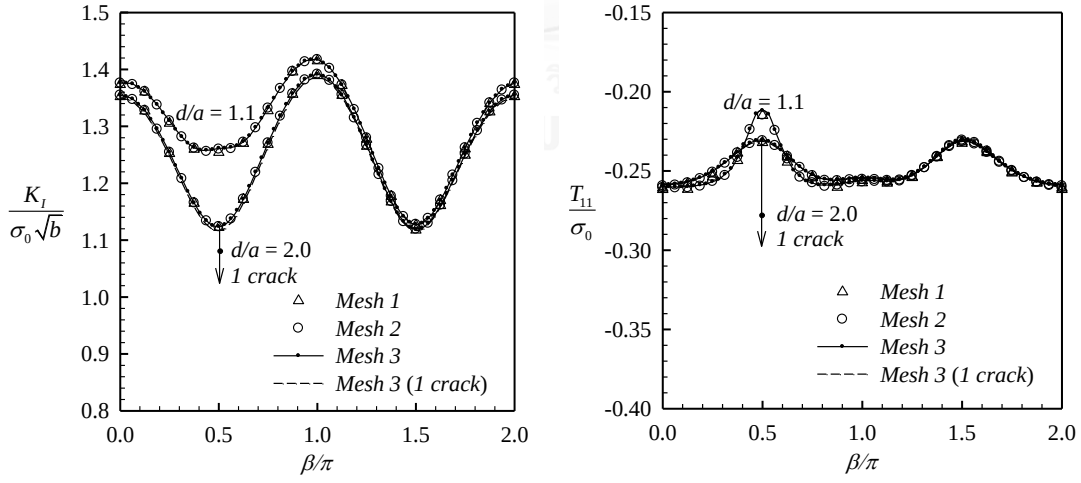

(a) (b)

Figure C.25: (a) Normalized mode-I stress intensity factor and (b) normalized T-stress component T_{11} for elliptical crack 1 in orthotropic half-space under BC-type-1.

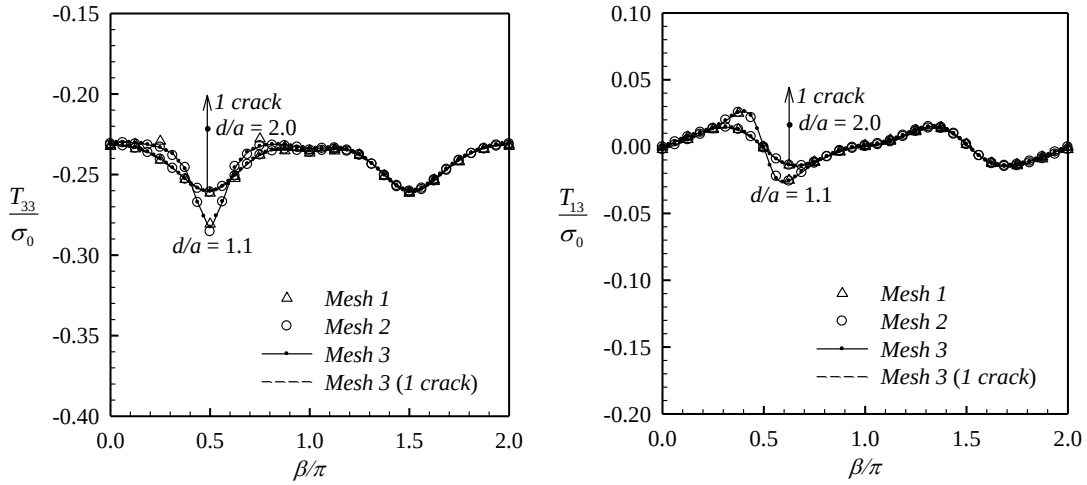

(a) (b)

Figure C.26: (a) Normalized T-stress component T_{33} and (b) normalized T-stress component T_{13} for elliptical crack 1 in orthotropic half-space under BC-type-1.

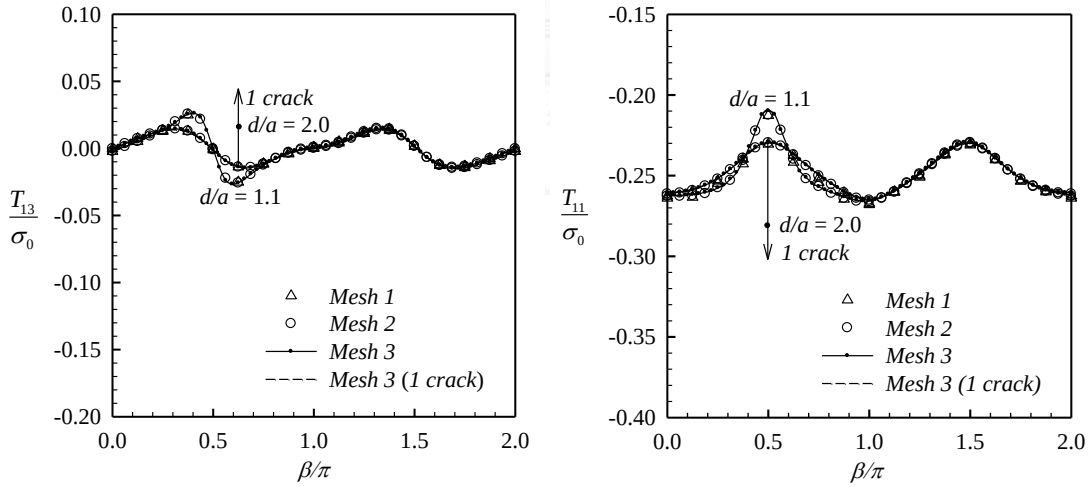

(a) (b)

Figure C.27: (a) Normalized mode-I stress intensity factor and (b) normalized T-stress component T_{11} for elliptical crack 1 in orthotropic half-space under BC-type-2.

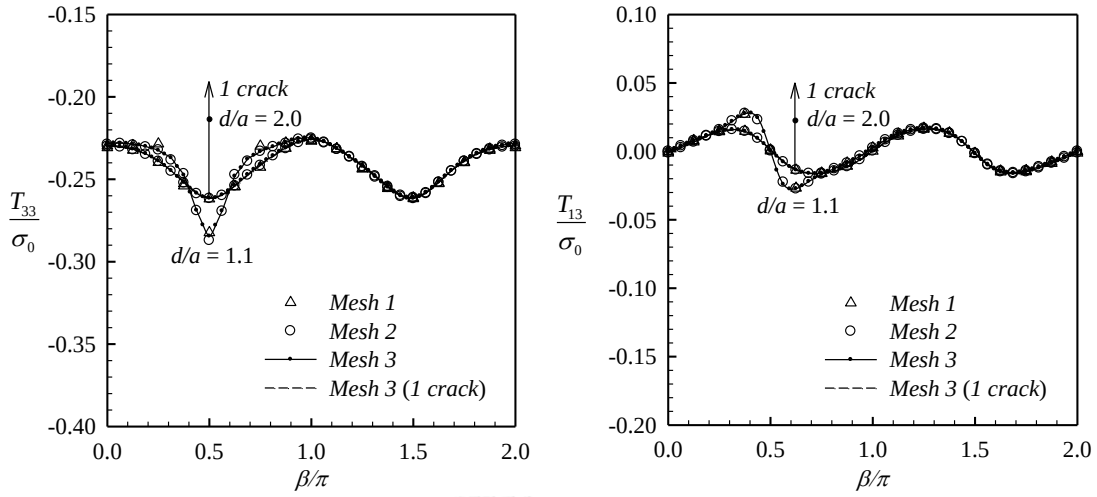

(a) (b)

Figure C.28: (a) Normalized T-stress component T_{33} and (b) normalized T-stress component T_{13} for elliptical crack 1 in orthotropic half-space under BC-type-2.

VITA

Tien Ngoc Pham was born in Binh Dinh, Vietnam on August 21, 1977. The son of Binh Ngoc Pham and Bay Thi Vo. After obtaining the degree of Bachelor of Engineering from Ho Chi Minh City University of Technology in 2001, he joined Nam Thanh Co. Ltd. in Ho Chi Minh City until 2002. He has been employed by Mientrung University of Civil Engineering since 2003. In 2007, he also received his degree of Master of Engineering from the same university where he earned his degree of Bachelor of Engineering. In 2012, he was admitted to study at Civil Engineering Department of Chulalongkorn University.